Master's thesis

NTNU
Norwegian University of Science and Technology
Faculty of Natural Sciences
Department of Chemistry

Kristine Wiik

Unimolecular Decomposition Reactions of Picric Acid and its Methylated Derivatives

A DFT Study

Master's thesis in Chemical Engineering and Biotechnology
Supervisor: Ida-Marie Høyvik
Co-supervisor: Ole Swang and Erik Unneberg
June 2021

NTNU
Norwegian University of
Science and Technology

Kristine Wiik

Unimolecular Decomposition Reactions of Picric Acid and its Methylated Derivatives

A DFT Study

Master's thesis in Chemical Engineering and Biotechnology
Supervisor: Ida-Marie Høyvik
Co-supervisor: Ole Swang and Erik Unneberg
June 2021

Norwegian University of Science and Technology
Faculty of Natural Sciences
Department of Chemistry

NTNU
Norwegian University of
Science and Technology

ABSTRACT

Although energetic materials such as explosives have been used and studied for more than a hundred years, fundamental understanding of the underlying processes that govern energetic material sensitivity is yet to be established. Theoretical sensitivity models with high predictive power could significantly improve the efficiency, safety, and sustainability of the production and use of energetic materials, and are thus highly desired. Recent years have seen an increase in the use of density functional theory in research on energetic materials. In this thesis, the theory is employed for the study of thermal unimolecular decomposition of picric acid (2,4,6-trinitrophenol, abbreviated to PA), (mono)methyl picric acid (mPA), and dimethyl picric acid (dmPA). While the molecular structures of these species only differ by one to two methyl substituents, their sensitivities to impact are drastically different. This anomalous sensitivity behaviour has been observed for more than 40 years, but its cause is nevertheless still unclear.

In this thesis, three unimolecular reaction pathways believed important for the initiation of ortho-nitrophenols and ortho-nitrotoluenes are investigated for PA, mPA, and dmPA. The energetics of these reaction pathways are calculated and compared with the objective of rationalising the unexpected sensitivity behaviour of the three explosives. The results reveal few significant differences in the energetics between PA, mPA, and dmPA. In other words, the results do not reflect the large sensitivity differences observed in experiments. There are several possible explanations why this is the case. Firstly, bimolecular reactions may take place to a significant extent in the condensed phases of the studied explosives, altering the reaction energetics. Secondly, the gas phase calculations may not be representative for the studied unimolecular reaction pathways when they occur in the condensed phase, due to twisting and bending of the molecules as they are packed in their crystal structures. Thirdly, solid state effects such as crystal defects, molecular stacking, and particle size may be determining factors for the sensitivity. Hence, more work is needed before firm conclusions can be drawn.

Recommendations for future work include determining the crystal structures of mPA and dmPA and performing molecular dynamics simulations of the initiation reactions. This will be helpful for assessing the feasibility and/or relative dominance of uni- and bimolecular reactions in the condensed phases. Redoing the calculations of this thesis using the molecular geometries from the crystal structures might also be useful in this context. Additionally, the crystal structures might reveal physical properties of the materials that can be determining for their impact sensitivities.

SAMMENDRAG

Til tross for at eksplosiver og andre energetiske materialer har blitt benyttet og studert i over hundre år, er forståelsen av deres følsomhet fremdeles svært begrenset. Gode modeller som forutsier følsomhet, kan gjøre håndteringen av slike materialer sikrere og mer effektiv, både når det gjelder utvikling, produksjon, transport, lagring, bruk og eventuell avhending. Utviklingen av slike modeller er derfor et viktig forskningsmål.

I de senere år har bruken av tetthetsfunksjonalteori vært økende innen forskning på energetiske materialer, og i denne masteroppgaven benyttes teorien til å studere termisk unimolekylær dekomponering av pikrinsyre (2,4,6-trinitrofenol, forkortet til PA), (mono)metylpikrinsyre (mPA) og dimetylpikrinsyre (dmPA). Til tross for at det er kun én eller to metylgrupper som skiller disse molekylenes strukturer fra hverandre, er deres slagfølsomhet drastisk forskjellig. Denne anomale oppførselen har vært kjent i mer enn 40 år, men årsaken fortsatt ukjent.

I arbeidet blir tre unimolekylære reaksjonsveier, som er antatt å være viktige for initiering av orto-nitrofenoler og orto-nitrotoluener, studert for PA, mPA og dmPA. Energetiske forhold til disse reaksjonsveiene beregnes og sammenlignes for å rasjonalisere følsomhetsforskjellene. Resultatene viser få signifikante energidifferanser mellom PA, mPA, og dmPA, og resultatene reflekterer derfor ikke forskjellene i eksperimentelt målt følsomhet. Det kan være flere årsaker til dette. For det første kan bimolekylære reaksjonstrinn være viktigere enn unimolekylære når faste stoffer dekomponerer. For det andre kan energetiske forhold ved de unimolekylære reaksjonsveiene avhenge av om reaksjonene forløper i gassfase eller i fast fase. Dersom de funksjonelle gruppene til PA, mPA og/eller dmPA i stor grad bøyes ut av ringplanet på grunn av krystallpakkingen, kan energiberegningene påvirkes. For det tredje kan faststoffeffekter som krystalldefekter, molekylær stabling og partikkelstørrelse være avgjørende for slagfølsomheten til de studerte stoffene. Mer forskning er derfor nødvendig før klare konklusjoner kan trekkes.

For videre arbeid foreslås karakterisering av krystallstrukturene til mPA og dmPA samt molekyldynamikksimuleringer av initieringsreaksjonene. Det kan gi informasjon som gjør det lettere å fastslå den relative vikigheten av uni- og bimolekylære reaksjoner i kondensert fase. I tillegg kan krystallstrukturene avdekke fysikalske egenskaper ved materialene, noe som er avgjørende for slagfølsomheten. Det kan også være nyttig å gjenta beregningene utført i denne masteroppgaven for de molekylære geometriene som finnes i krystallstrukturene.

PREFACE

This thesis is a work of collaboration between the NTNU Chemistry Department, the Norwegian Defence Research Establishment (FFI), and SINTEF Industry. It represents the conclusion of my study in the Chemical Engineering and Biotechnology integrated master's programme at NTNU.

ACKNOWLEDGEMENTS

First of all, I would like to thank Ida-Marie for being an inspiring lecturer and a fantastic supervisor. Your enthusiasm, support, and feedback have been crucial for both the quality of my work and my general well-being. Next, I would like to thank Ole for sharing his immense knowledge and experience, providing much needed and appreciated help for the transition state optimisations, and always bringing kindness and good stories into the Teams meetings. I would also like to thank Erik for the many interesting discussions and all the amazing opportunities I have received through FFI. An additional huge thanks to Tomas for the quality control and for being central to the task of defining the research question for this thesis. To all the above-mentioned I would like to express my sincerest gratitude for the help and support you have given me throughout this work, both academically and otherwise. You are prime examples of how the academic and personal aspects of guiding a student towards a master's degree should be balanced. Your supporting words, reassurances, and genuine care for my well-being means more to me than words can express.

On an even more personal note, big thanks are directed to my classmates for top-tier cooperation and information sharing, for the festivities, and for making the long days at campus bearable. A special thanks go out to Benedicte and Amalie for all the de-stressing knitting sessions and superb advice on all matters. Furthermore, I would like to thank my parents for always believing in me. Last, but certainly not least, thanks to Martin for the unconditional love and support. I am so glad I chose B1-101 as my go-to study hall.

All molecular graphics presented in this thesis have been constructed with UCSF Chimera [1], developed by the Resource for Biocomputing, Visualization, and Informatics at the University of California, San Francisco, with support from NIH P41-GM103311. All energy plots have been constructed using MechaSVG [2]. The calculations of this thesis have been performed on resources provided by the NTNU IDUN/EPIC computing cluster [3], and on resources provided by UNINETT Sigma2 — the National Infrastructure for High Performance Computing and Data Storage in Norway, using NWChem [4].

CONTENTS

LIST OF FIGURES

LIST OF TABLES

ABBREVIATIONS

MOLECULES TREATED IN THE THESIS

Aci-dmPA-2	*Cis*-aci-3,5-dimethyl-2,4,6-trinitrophenol[1] [2]
Aci-dmPA-3	*Cis*-aci-3,5-dimethyl-2,4,6-trinitrophenol[1] [2]
Aci-dmPA-4	*Cis*-aci-3,5-dimethyl-2,4,6-trinitrophenol[3]
Aci-PA-2	*Cis*-aci-2,4,6-trinitrophenol[1] [2]
Aci-PA-3	*Cis*-aci-2,4,6-trinitrophenol[1] [2]
Aci-mPA-2	*Cis*-aci-3-methyl-2,4,6-trinitrophenol[1] [2]
Aci-mPA-3	*Cis*-aci-3-methyl-2,4,6-trinitrophenol[1] [2]
Aci-mPA-4	*Cis*-aci-3-methyl-2,4,6-trinitrophenol[3]
dmPA	3,5-dimethyl-2,4,6-trinitrophenol
dmPA-aci-TS2	TS connecting dmPA with aci-dmPA-2
dmPA-aci-TS4	TS connecting dmPA and with-dmPA-4
dmPA-anth	5-hydroxy-7-methyl-4,6-dinitro-2,1-benzisoxazole
dmPA-ket	2,4-dimethyl-3,5-dinitrocyclopentaketene
dmPA-H_2Oelim-TS	TS connecting dmPA-hyd-anth with dmPA-anth
dmPA-hyd-anth	Hydro-5-hydroxy-7-methyl-4,6-dinitro-2,1-benzisoxazole[4]
dmPA-ket-TS1	TS connecting dmPA with dmPA-ket and *trans*-HONO
dmPA-ket-TS2	TS connecting aci-dmPA-2 with dmPA-ket and *cis*-HONO

1 The structures Aci-Y-2 and Aci-Y-3, with Y ∈ {PA, mPA, dmPA}, only differ by a rotation about the C – N bond to which the aci-group is connected. To distinguish between the conformers, see Figure 4.3

2 Aci-Y-2 and Aci-Y-3, with Y ∈ {PA, mPA, dmPA}, are constructed upon the transfer of hydrogen from the hydroxyl substituent to a neighbouring nitro group.

3 Aci-Y-4, with Y ∈ {PA, mPA, dmPA}, are constructed upon the transfer of hydrogen from a methyl substituent to a neighbouring nitro group.

4 Following the nomenclature of Cohen *et al.*[5]

dmPA-ket-TS3	TS connecting aci-dmPA-3 with dmPA-ket and *cis*-HONO
dmPA-rad-1	2-hydroxy-4,6-dimethyl-3,5-dinitrophenyl radical[5]
dmPA-rad-2	4-hydroxy-2,6-dimethyl-3,5-dinitrophenyl radical
dmPA-rad-3	2-hydroxy-4,6-dimethyl-3,5-dinitrophenyl radical [5]
mPA	3-methyl-2,4,6-trinitrophenol
mPA-aci-TS2	TS connecting mPA with aci-mPA-2
mPA-aci-TS4	TS connecting mPA with aci-mPA-4
mPA-anth	7-hydroxy-4,6-dinitro-2,1-benzisoxazole
mPA-ket	3-methyl-2,4-dinitrocyclopentaketene
mPA-H_2Oelim-TS	TS connecting mPA-hyd-anth with mPA-anth
mPA-hyd-anth	Hydro-7-hydroxy-4,6-dinitro-2,1-benzisoxazole[6]
mPA-ket-TS1	TS connecting mPA with mPA-ket and *trans*-HONO
mPA-ket-TS2	TS connecting aci-mPA-2 with mPA-ket and *cis*-HONO
mPA-ket-TS3	TS connecting aci-mPA-3 with mPA-ket and *cis*-HONO
mPA-rad-1	2-hydroxy-6-methyl-3,5-dinitrophenyl radical[5]
mPA-rad-2	4-hydroxy-2-methyl-3,5-dinitrophenyl radical
mPA-rad-3	2-hydroxy-6-methyl-3,5-dinitrophenyl radical [5]
PA	2,4,6-trinitrophenol
PA-aci-TS2	TS connecting PA and aci-PA-2
PA-ket	2,4-dinitrocyclopentaketene
PA-ket-TS1	TS connecting PA with PA-ket and *trans*-HONO
PA-ket-TS2	TS connecting aci-PA-2 with PA-ket and *cis*-HONO
PA-ket-TS3	TS connecting aci-PA-3 with PA-ket and *cis*-HONO
PA-rad-1	2-hydroxy-3,5-dinitrophenyl radical[5]
PA-rad-2	4-hydroxy-3,5-dinitrophenyl radical

5 Y-rad-1 and Y-rad-3, with Y $\in$ {PA, mPA, dmPA}, are conformers connected through rotation about the C$-$O bond.

6 Following the nomenclature of Cohen *et al.*[5]

PA-rad-3	2-hydroxy-3,5-dinitrophenyl radical [5]

OTHER

BDE	Bond Dissociation Energy
DFT	Density Functional Theory
GGA	Generalised-Gradient Approximation
GTO	Gaussian Type Orbital
HF	Hartree-Fock
HMX	Octahydro-1,3,5,7-tetranitro-1,3,5,7-tetrazocine
LDA	Local Density Approximation
mGGA	Meta-Generalised Gradient Approximation
PES	Potential Energy Surface
RDS	Rate-Determining Step
STO	Slater Type Orbital
TATB	1,3,5-triamino-2,4,6-trinitrobenzene
TNT	2,4,6-trinitrotoluene
TS	Transition State

1

INTRODUCTION

Energetic materials are substances that undergo exothermic chemical reactions in response to some stimulus and that react in timescales leading to combustion, explosion, or detonation [6]. Such materials are of great interest to the defence sector as they are substantial ingredients in explosives, propellants, and pyrotechnics and they are also important for various industrial applications. In order to ensure safe handling and storage of energetic materials, it is crucial to know how sensitive they are to external stimuli such as impact or shock [7–9].

Although more than a century has passed since detonation phenomena were first observed [10–13], no consistent microscale theory of detonation initiation exists to date. While the literature surrounding energetic material sensitivity is abundant, fundamental understanding of the underlying processes that govern sensitivity is yet to be established [14]. This is due in part to the incredible speed of energetic material decomposition which makes it difficult to determine the specific reaction steps and to capture the underlying phenomena by standard experimental methods [7, 15, 16]. Over the last decades, the incredible advancements of computer technology and quantum chemical methods have provided an alternative path to chemical insight, namely that of computer simulations and molecular modelling. This path has been widely [5, 9, 15, 17–36] employed by modern scientists with the goal of demystifying energetic material sensitivity, and implementations of density functional theory (DFT) are in fact among the most commonly used tools in research on energetic materials today. While these tremendous technological advancements have made it possible to study systems and processes which were previously inaccessible, important questions regarding energetic material sensitivity still remain unanswered.

The impact sensitivity is one of the most common measures of sensitivity in energetic materials. It is usually determined by drop hammer tests [19, 37, 38], in which a mass is dropped upon a sample of the material and the height at which an explosion is observed for some predetermined fixed percentage of the drops is recorded as the critical impact height. Thus, the critical impact height is inversely proportional to the impact sensitivity. In the commonly employed Bruceton method [39], the explosion percentage is set to 50% and the critical impact height is symbolised by h_{50}. While experimentally determined h_{50} values are heavily employed for correlation studies, it is a well known fact that such results are associated with a high degree of uncertainty. As pointed out by Rice *et al.* [20], the drop hammer test does not have the resolution or reproducibility to be considered a research tool. This is much due to the subjectivity of the human observer, which may severely influence the results — where one scientist

may observe an explosion, another may not. Additionally, the measured values have proven to be quite sensitive to small changes in experimental setup and conditions [7, 40]. Apart from the high degree of uncertainty associated with the results, obvious drawbacks of the drop hammer test include the large amount of wasted material and the method's inability to predict the sensitivity of novel (not yet synthesised) energetic materials. Thus, predictive theoretical models for impact sensitivity are desired.

While the impact sensitivity depends on molecular properties related to the kinetics and thermodynamics of the decomposition reactions, solid state properties such as particle size, polymorphism, crystal defects, and crystal orientation also play important roles [19]. Defects are particularly important since they form so-called hot-spots under fast compression of the material. Although the initiation of an energetic material is a complex, multi-scale process [7, 14, 20, 41], one may roughly divide it into two main steps. The first step involves compression and deformation of the material, which leads to heating of the hot-spots. In the second step, the material inside and surrounding the hot-spots self-ignites and propagates into an explosion, provided that the hot-spot temperatures are sufficiently high [19, 42].

There is a desire within the field of energetic materials to produce compounds with combined high performance and low sensitivity. This is a great challenge as it turns out that the two concepts are inherently contradictory [18, 43, 44]. The task of producing novel energetic materials is further complicated by the ever more strict environmental, health, and safety standards to which novel energetic materials must comply. In order to avoid a highly inefficient trial and error process, predictive sensitivity models are needed. In the quest for understanding, many scientists [15, 17, 19–24, 38, 45–50] have turned to correlation studies. In these studies, one or several descriptors (or functions thereof) are calculated or measured for a series of molecules and plotted against some function of the critical impact height. Among popular descriptors are electrostatic surface potential [51–53], nitro group charge [24, 54–56], band gap [47, 50, 57, 58], bond dissociation energy (BDE) [17, 19–24], heat of detonation [19, 48, 59], oxygen balance [46, 60], and Wiberg bond index [15, 28, 61, 62]. While numerous correlations have been found, the obtained relationships are usually only valid for certain families of molecules, and outliers tend to occur [15, 19, 46]. As pointed out by Kamlet and Adolph [46], the study of outliers may be one of the most promising paths towards increased understanding of underlying phenomena. Inspired by this, the main focus of this thesis is the investigation of such outliers. While correlation studies are helpful in determining standard behaviour, they are unsuited for the determination of mechanistic details. In the search for more detailed information about the factors that govern sensitivity, computational studies into plausible thermal unimolecular decomposition pathways of ortho-nitrotoluenes [5, 9, 30, 63, 64], ortho-nitrophenols [28, 29, 60, 63], and various other compounds have been performed. Additional computational and experimental studies have undertaken the possibility of bimolecular reactions in the early stages of decomposition in condensed phase energetic materials [35, 65].

Nitroaromatic compounds comprise an important class of energetic materials [9, 31] and include several explosives of historical significance, such as 2,4,6-trinitrotoluene (TNT) and 2,4,6-trinitrophenol (picric acid, abbreviated to PA). The nitro (NO_2) group is an important explosophore which presence as a substituent on the aromatic ring has been shown to sensitise energetic materials while at the same time enhancing their detonation performance [5, 20, 37, 65, 66]. At temperatures above where the thermal stability of nitroaromatics are normally studied, three modes of initiation have been proposed: a) Homolytic cleavage of the weakest C–NO_2 bond; b) inter- or intra-molecular hydrogen transfer to the nitro group, which in some cases may result in loss of HONO (nitrous acid) or water; and c) NO_2–ONO isomerisation [67]. The relative dominance of these decomposition pathways are believed to vary with temperature [7]. The homolysis described in a) is a high energy event mainly observed at high temperatures [5, 7, 65]. It represents a common assumption for the initiation of nitro-based explosives, namely that of the trigger linkage hypothesis. This hypothesis states that the first step of the initiation is a bond cleavage, and that the decomposition is triggered by the homolytic fission of an X–NO_2 bond, where X is either C, N or O [19, 46] (C for nitroaromatics). The hydrogen transfer reactions described in b) may be arranged into different categories based on the origin of the transferred hydrogen atom.

On the basis of experimental and computational studies, intramolecular hydrogen transfer from the hydroxyl substituent to the neighbouring nitro group has been proposed as the dominant initiation step for ortho-nitrophenol and its derivatives at low to moderate temperatures [7, 28, 29, 60, 68]. The C–H α-attack pathway is thought to play a similar role in ortho-nitrotoluene, TNT, and their derivatives [5, 9, 32, 65]. While the former may result in the formation of HONO and a pentacycloketene derivative through what will be termed "the ketene-forming pathway" in later discussions, the latter pathway results in the formation of anthranil (2,1-benzisoxazole) derivatives and water. For nitro derivatives of phenols and methylbenzenes, the above-mentioned NO_2–ONO isomerisation pathway has on several occasions [5, 9, 30] been deemed unimportant compared to the C–NO_2 homolysis and C–H α-attack pathways. For instance, in a DFT study on TNT performed by Cohen *et al.* [5], it was concluded that while NO_2–ONO isomerisation is thermodynamically favoured over C–NO_2 homolysis at room temperature, and more exergonic than both C–NO_2 homolysis and C–H α-attack at high temperatures, it is kinetically unfavourable over the studied temperature range (298–3500 K). Consequently, it is only expected to contribute to TNT initiation in a minor fashion. The same conclusion was drawn by Chen *et al.* [30], who found the NO_2–ONO isomerisation to be less significant than other decomposition pathways for TNT through a separate DFT study.

In my previous work [69], the 3-methyl-2,4,6-trinitrophenol (mPA) molecule was studied with the objective of rationalising its anomalous impact sensitivity. The trigger linkage hypothesis was assumed, and the BDE of the weakest C–NO_2 bond was used as a sensitivity measure. Since Kamlet and Adolph [46] have suggested the unexpectedly low sensitivity of mPA to come about as a result of highly coplanar nitro groups in the crystal phase, the effect of forced nitro

group twisting on the C–NO_2 BDE was studied. While a correlation supporting the hypothesis was observed, the results indicated that the bending of the methyl group out of the ring plane was more significant than that of the nitro groups. Calculations performed for 3,5-dimethyl-2,4,6-trinitrophenol (dmPA), which Kamlet and Adolph found to be significantly more sensitive than expected, gave similar trends. However, there were many possible sources of error. Since the crystal structures of mPA and dmPA were not obtained and the number of data points was quite small, no firm conclusions were drawn.

The current work is also focused on substituted nitrophenols. Specifically, PA and its methylated derivatives mPA and dmPA are under study. While PA is a historically important explosive that has been the subject of many previous studies, mPA and dmPA have, to my knowledge, not been investigated in such detail. In 1979 Kamlet and Adolph [46] correlated critical impact height with oxygen balance and found the two latter compounds to be outliers. Despite having molecular structures that only differ from each other by one methyl substituent, mPA is astonishingly less sensitive than PA and dmPA. dmPA is the most sensitive compound of the three. As pointed out by Dlott [41], care must be taken before drawing mechanistic conclusions based on simple correlation studies due to the large degree of complexity of energetic material initiation. However, the extreme sensitivity variations of the seemingly similar compounds may indicate that there are significant chemical differences that are yet to be understood, making these systems interesting to study.

Over the last three decades, DFT has enjoyed a meteoric rise in computational chemistry [70], and is now an immensely popular tool applied to a wide range of calculations. Most quantum chemical program packages include some implementation of the theory, as well as an ever increasing number of approximate exchange-correlation functionals. In conjunction with the incredible technological advancements of (super)computers, this has opened up a whole new world of opportunities for computational chemists. In the context of energetic material sensitivity and studies of its correlation with molecular properties, DFT dominates the literature [15, 17, 19–24, 33, 47, 54, 60, 61, 71–77]. The same holds for detailed studies on the initiation mechanisms of energetic molecules [5, 29, 30, 33, 36, 69]. Therefore, DFT stands out as an obvious choice for the current work.

In this thesis, the energetics of three unimolecular decomposition pathways, namely the C–NO_2 homolysis, ketene-forming, and C–H α-attack pathways, are investigated for PA, mPA, and dmPA. The work is purely computational, and all results are obtained through DFT calculations at the M06-2X/def2-TZVP level of theory. The objective of the thesis is to identify the cause of the astonishingly large variation in the impact sensitivities of these three compounds. While the C–NO_2 homolysis and ketene-forming pathways are relevant for all three molecules, the C–H α-attack pathway is only possible for mPA and dmPA as it requires the presence of a methyl substituent.

2

THEORETICAL BACKGROUND

The aim of this chapter is to guide the reader through theory relevant for the upcoming discussions. Sections 2.1 through 2.7 are concerned with fundamental concepts of computational quantum chemistry as well as some approximate methods for solving the Schrödinger equation. Section 2.8 is a short discussion on basis sets, Section 2.9 discusses BDEs, Section 2.10 gives a brief introduction to chemical kinetics, and Section 2.11 discusses thermodynamic and kinetic stability. The chapter ends with Section 2.12, which introduces some important experimental techniques and discusses the challenge of tying together experimental and theoretical explosives research.

2.1 THE SCHRÖDINGER EQUATION

The non-relativistic time-independent electronic Schrödinger equation, within the Born-Oppenheimer approximation, can be expressed as

$$\hat{H}\psi(\vec{r_1}, \vec{r_2}, ...; \vec{R_1}, \vec{R_2}, ...) = E(\vec{R_1}, \vec{R_2}, ...)\psi(\vec{r_1}, \vec{r_2}, ...; \vec{R_1}, \vec{R_2}, ...), \tag{2.1}$$

where ψ is the time-independent electronic wavefunction, $\vec{r_1}, \vec{r_2}, ...$ and $\vec{R_1}, \vec{R_2}, ...$ are respectively the electronic and nuclear coordinates in real space, $E(\vec{R_1}, \vec{R_2}, ...)$ is the electronic energy, and $\hat{H}$ is the Hamiltonian operator. The Hamiltonian, here expressed in atomic units, takes the form

$$\hat{H} = -\frac{1}{2}\sum_{i}^{N_e}\nabla_i^2 - \sum_{i}^{N_e}\sum_{I}^{N_n}\frac{Z_I}{r_{Ii}} + \frac{1}{2}\sum_{i\neq j}^{N_e}\frac{1}{r_{ij}} + \sum_{I\neq J}^{N_n}\frac{Z_I Z_J}{r_{IJ}} \tag{2.2}$$

where N_e is the number of electrons in the system, N_n is the number of nuclei, Z_I is the charge of nucleus I, and r_{pq} is the distance between particle p and particle q. The summation variables i and I run over the electronic and nuclear coordinates, respectively. ∇_i^2 is the Laplacian operator given by $\left(\frac{\partial^2}{\partial {x_i}^2} + \frac{\partial^2}{\partial {y_i}^2} + \frac{\partial^2}{\partial {z_i}^2}\right)$, where x, y, z are the Cartesian coordinates. In Equation (2.2) the fourth and final term of the right hand side represents the nucleus-nucleus repulsion. Since this term only involves the charges and positions of the nuclei, it is readily calculated for a given molecular geometry. For this reason, electronic structure programs usually exclude it from the Hamiltonian and simply add it as a classical term at the end of the calculation [78].

Due to the complexity brought on by the electron-electron interaction term, Equation (2.1) cannot be solved analytically for systems containing more than one electron. Indeed, numerous approximations must be made when molecular systems are of interest. This fact has led to the development of many different approximate methods, and some of them will be covered in the following sections. Among these are Hartree-Fock (HF) theory — which is considered to be a corner stone of quantum chemistry — and the extremely popular density functional theory (DFT).

To close off this section, some remarks about the wavefunction itself are in order. The wavefunction is not just any mathematical function. On the contrary, it must satisfy a number of conditions in order to serve as a valid description of a quantum chemical system. For example, electrons are indistinguishable, meaning that the probability density $|\psi(\vec{r_1}, \vec{r_2}), ...|^2$ must be invariant under any permutation of the electrons. Additionally, since electrons obey the Pauli principle, two electrons with equal spin cannot occupy the same spatial state simultaneously. Consequently, the wavefunction of an electronic system must be antisymmetric, *i.e.* it must change sign upon the exchange of two electrons. The electron-electron interaction resulting from this antisymmetrisation is termed the exchange interaction or Pauli repulsion.

2.2 POTENTIAL ENERGY SURFACES AND GEOMETRY OPTIMISATIONS

The dependency of the electronic energy on the nuclear coordinates $\vec{R}_1, \vec{R}_2, ...$ as illustrated in Equation (2.1) points towards the important notion of a potential energy surface (PES). In the case of a diatomic molecule, the molecular geometry can be described by a single variable, namely the interatomic distance (bond length) R. The parametric dependency of the electronic energy on the nuclear coordinates as illustrated in Equation (2.1) may thus be written as $E(R)$. By computing $E(R)$ for different values of R and plotting these quantities in an energy vs. bond length diagram, one obtains the PES of the diatomic molecule. In this case, the PES is one dimensional. For molecules containing more than two atoms, additional bond lengths and angles increase the number of geometric degrees of freedom, making the PES multidimensional and difficult to visualise.

The geometries for which a molecule is stable corresponds to the minima of its PES, and are termed equilibrium geometries. At any local or global minimum of the PES, the derivative of the energy with respect to the nuclear coordinates equals zero. Since the gradient is the negative of the forces, the forces are also zero at these points, meaning that equilibrium geometries correspond to stationary points of the PES [79]. Geometry optimisations as performed by various quantum chemical software packages attempt to locate such stationary points by moving stepwise along the PES, starting from some initial guess of the geometry. At each step, the forces and energy are computed and the obtained values are used to determine the size and direction of the next step. Due to numerical inaccuracies, the forces are seldom found to be exactly zero, and cutoff values are thus defined in order to reach convergence. However, numerical inaccu-

racies could also lead the optimisation to converge to a structure that is not a true minimum of the PES. As a guard against this, optimisation algorithms usually include several convergence criteria which must all be satisfied in order for the optimisation to be deemed successful. Consequently, common convergence criteria include the maximum values and root mean square values of both the forces and the calculated step size.

While the stationary points described above are minima in all directions, the PES may also include stationary points that do not satisfy this property, namely maxima and saddle points. A k'th order saddle point has the property of being a maximum in k directions and a minimum in all remaining directions. First order saddle points are of large chemical significance, as they represent so-called transition states (TSs). A TS is a particular configuration along the reaction coordinate, and is defined as the state corresponding to the highest potential energy along the reaction coordinate. In other words, it connects two minima of the PES through a reaction path. The difference in energy between the TS and its corresponding reactants constitutes the activation energy, E_a, of the reaction. This is illustrated in Figure 2.1 which displays the potential energy profile of a hypothetical reaction path consisting of two steps. E_{RX} is the overall reaction energy, and the hypothetical reaction is seen to be exergonic. Note that the reactants, products, and intermediates all correspond to minima of the reaction path, whereas the TSs correspond to maxima. While modern quantum chemical optimisation tools typically offer saddle point optimisations, locating a TS can be a tedious and challenging task.

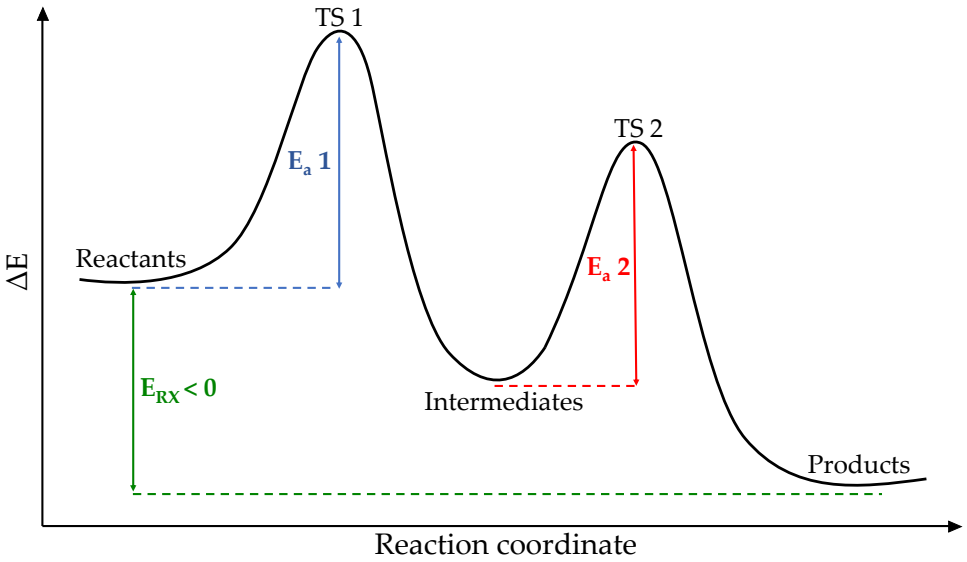

Figure 2.1: A potential energy curve representing a hypothetical, two-step, reaction path along a PES. E_a and E_{RX} are respectively the activation and reaction energy.

Any successful optimisation locates a stationary point, although not always the one that was intended. Fortunately, the nature of a stationary point located by a geometry optimisation can be determined by calculating the vibrational frequencies associated with the obtained molecular structure. An equilibrium

structure is characterised by having only real frequencies, while a transition state has one and only one imaginary frequency. These features result from the use of the harmonic approximation, which is explained in Section 2.3.

2.3 VIBRATIONAL FREQUENCIES AND HOW THEY ARE COMPUTED

Energy calculations and geometry optimisations as performed by quantum chemical program packages ignore the vibrations in molecular systems. In reality, as predicted by quantum theory, the nuclei in molecules are constantly in motion. In equilibrium states, the molecular vibrations are regular and predictable, and molecules can be identified by their characteristic spectra [79].

A nonlinear molecule consisting of N_{atom} atoms has $3N_{atom} - 6$ independent modes of vibration. For a linear molecule, the number is $3N_{atom} - 5$. These modes can be represented in a number of ways, but some descriptions are more convenient than others. The key to a good description of molecular vibrations is to identify the so-called normal modes of the molecule. In general, a normal mode is an independent, synchronous motion of atoms or groups of atoms that may be excited without leading to the excitation of any other normal mode and without involving translation or rotation of the molecule as a whole [80].

Each normal mode can be approximated to behave as an independent harmonic oscillator. To understand why this is the case, consider the following one-dimensional example: A general potential energy curve, $V(x)$, for a molecular vibration in one dimension can be expanded as a Taylor series, such that

$$V(x) = V(x_0) + V'(x_0)(x - x_0) + \frac{V''(x_0)(x - x_0)^2}{2!} + \frac{V'''(x_0)(x - x_0)^3}{3!} + \ldots, \quad (2.3)$$

where x_0 and x are, respectively, the equilibrium position for the vibration and the displacement of the oscillating mass away from this equilibrium. For small x, *i.e.* when $|x - x_0| \ll 1$, the terms of order 3 and higher in $(x - x_0)$ are negligible compared to the first and second order terms. Since x_0 signifies the equilibrium position for the vibration (*i.e.* a stationary point of the PES), $V'(x_0)$ is zero, and since the reference for the potential is arbitrary, $V(x_0) = 0$ is both a simple and valid choice. Furthermore, the coordinate system may be chosen such that $x_0 = 0$. Thus, the potential has been simplified to

$$V(x) \approx \frac{V''(0)}{2} x^2, \quad \text{for } x \text{ close to } 0, \quad (2.4)$$

which corresponds to the energy of a harmonic spring with force constant $C \equiv V''(0)$, $V(x) = Cx^2/2$. By taking the second derivative of the potential energy, one thus obtains the force constant C. From solving Newton's second law for the force given by $-\frac{dV}{dx}$, one finds that the frequency of the oscillation is proportional to the square root of the force constant. For the multidimensional PES, the

second derivative of the energy with respect to geometric parameters is stored in a matrix termed the Hessian. The main idea is, however, the same.

Computationally, the vibrational frequencies are found via the Hessian, which can be computed by finite difference for any ab initio wavefunction that has analytic gradients or by analytic methods for self-consistent field and DFT [81]. Within the harmonic approximation, this matrix may be diagonalised to yield the force constant of each normal mode from which each frequency is calculated. A vibration along a dimension of the PES for which the equilibrium geometry is a minimum corresponds to a positive force constant. A vibration along any dimension in which the equilibrium structure is a maximum corresponds to a negative force constant. Remembering that harmonic frequencies are proportional to the square root of their respective force constants, it is now clear why a transition state (first order saddle point) is characterised by having one imaginary frequency while a minimum has only real frequencies.

While the harmonic approximation simplifies the calculation of vibrational frequencies, there are cases in which this approach becomes too simple. The importance of anharmonic vibration, that is vibrational behaviour differing from that of a harmonic oscillator, increases with the degree of vibrational excitation of a molecule [78]. Thus, the quality of the harmonic approximation decreases with increasing temperate. For the calculations performed in this thesis, the harmonic approximation is believed to be a good one due to the low temperatures used (0 and 298.15 K).

2.4 HARTREE-FOCK THEORY

In 1928, two years after the Schrödinger equation was published, Hartree proposed a method for solving this equation for multi-electron systems [82], known as the Hartree method. In order to solve the appearing system of non-linear equations, he incorporated the so-called self-consistent field method, which was the first procedure of finding atomic orbitals numerically. Later on, Fock [83] and Slater [84] improved the Hartree method by including electron exchange effects, yielding the famous HF method.

In the HF framework, the antisymmetry of the electronic wavefunction is achieved through the use of a Slater determinant. The spinorbitals $\bar{\varphi}_i(\vec{x})$ from which it is built are defined as a product between a spatial function (molecular orbital) $\varphi_i(\vec{r})$ and a spin function $\sigma(s)$.

The molecular orbitals are expanded in a set of atomic orbitals,

$$\varphi_i(\vec{r}) = \sum_{\mu} c_{\mu i} \chi_{\mu}(\vec{r}) \tag{2.5}$$

where the atomic orbitals χ_μ are known functions in the sense that in practical calculations, they are selected by the user based on the problem at hand. The expansion coefficients $c_{\mu i}$ are determined according to the variational principle,

which states that for any approximate wavefunction ψ^{trial} the expectation value for its energy satisfies

$$\mathbf{inf}(\xi) \leq \frac{\langle \psi^{trial} | \hat{H} | \psi^{trial} \rangle}{\langle \psi^{trial} | \psi^{trial} \rangle} \leq \mathbf{sup}(\xi) \tag{2.6}$$

where ξ is the energy spectrum of the true wavefunction ψ, *i.e.* it is the set of energy eigenvalues satisfying Equation (2.1) for some molecular geometry. The denominator of Equation (2.6) is a normalisation factor, which equals unity in the case of a normalised trial function. An important result of the variational theorem is that for ground state calculations, the energy associated with a trial wavefunction is an upper bound of the true electronic energy.

Minimisation under the constraints that both the electronic wavefunction and the molecular orbitals should be normalised yields a set of implicit equations which must be solved iteratively. The solution to this set of equations is termed the Hartree-Fock wavefunction and is the Slater determinant associated with the lowest obtainable energy for a given choice of basis.

The development of HF theory was a great milestone of quantum chemistry. The theory does, however, lack the extreme level of accuracy that is needed for many chemical problems. For instance, the HF method is not suitable for quantitative treatment of the energetics even of simple chemical reactions [85]. To accurately describe most molecular properties, one must include the effects of electron correlation.

The goal of post-HF methods is to improve the HF wavefunction by accounting for electron correlation effects. Examples of such methods include Møller-Plesset perturbation theory, coupled cluster theory, and configuration interaction.

2.5 ELECTRON CORRELATION

The post-HF methods make up a considerable fraction of the quantum chemical ab initio methods that exist to date. These methods attempt to improve the Hartree-Fock wavefunction by accounting for various types of electron correlation. Electron correlation was defined by Löwdin in 1959 [86], somewhat arbitrarily, as $E_{corr} = E - E_{HF}$, where E_{corr} is the correlation energy, E is the true electronic energy, and E_{HF} is the electronic energy obtained by a HF calculation. In other words, any contribution to the electronic energy that is not captured by HF is electron correlation. Note that since the Slater determinant accounts for Pauli repulsion, Pauli repulsion is — by definition — not electron correlation. Thus, electron correlation as defined above refers to the correlated movement of electrons resulting from the Coulomb interaction only.

It is common to distinguish between dynamical and non-dynamical (static) correlation. Dynamical correlation is related to the correlated movement of electrons in real space, *i.e.* how the movement of one electron instantaneously

adjusts to the movement of other electrons to minimise repulsion. Dynamical correlation is thus present for all multi-electron systems. Non-dynamical correlation effects arise when the ground state of the electronic system is only well described by a linear combination of more than one (nearly) degenerate Slater determinants. In such situations, the single Slater determinant of HF is qualitatively wrong. Although the distinction is made between dynamical and non-dynamical correlation, it should be noted that there are few systems for which one can distinguish unambiguously between the two types [87].

2.6 DENSITY FUNCTIONAL THEORY

Scaling is a long standing challenge in the field of quantum chemistry, and the wish to combine great accuracy with low computational cost was probably the greatest motivation for the construction of DFT [85]. In this framework, the complicated many-electron wavefunction is replaced by the much simpler electron density $\rho(\vec{r})$. Although attempts to use the electron density as an alternative to the wavefunction dates all the way back to the works of Thomas and Fermi in 1927 [88, 89], DFT as it is known today was formulated in 1964 by Hohenberg and Kohn [70]. In fact, Hohenberg and Kohn were the first to successfully prove some of the chief assumptions of the Thomas-Fermi model, namely that the electron density determines the ground state properties of a molecule and that the ground state energy is correctly given by a variational theorem [78].

An important consequence of the Hohenberg-Kohn Existence Theorem is that the ground state energy of a molecule, E_0, may be expressed as a functional of the ground state electron density, ρ_0, such that

$$E_0[\rho_0(\vec{r})] = T[\rho_0(\vec{r})] + V_{e-e}[\rho_0(\vec{r})] + \int \rho_0(\vec{r}) v_{n-e}(\vec{r}) d\vec{r}, \tag{2.7}$$

where T is the kinetic energy of the electrons, V_{e-e} represents the electron-electron interaction and v_{n-e} is the potential brought on by the nuclear-electron attraction [70]. Note that in Equation (2.7), some terms are universal in the sense that their form is not system-dependent. Indeed, the terms representing the electronic kinetic energy and the electron-electron interaction take the same form for all molecular systems. In contrast, the nuclear-electron term qualitatively depends on the molecular geometry, the type of atoms involved (*i.e.* their nuclear charges), and the total number of electrons. By collecting the universally valid terms into a new quantity, one obtains the Hohenberg-Kohn functional, F_{HK}, as $F_{HK} = T[\rho_0(\vec{r})] + V_{e-e}[\rho_0(\vec{r})]$. That is, upon feeding the Hohenberg-Kohn functional with some arbitrary trial density $\rho^{trial}(\vec{r})$, it gives the expectation value $\langle \psi^{trial} | \hat{T} + \hat{V}_{e-e} | \psi^{trial} \rangle$ as output, where ψ^{trial} is the ground state wavefunction associated with the density $\rho^{trial}(\vec{r})$.

Unfortunately, it turns out that identifying the Hohenberg-Kohn functional is a whole lot more challenging than proving its existence. If one was able to identify F_{HK} exactly, one would effectively have solved the Schrödinger equation — not

approximately, but exactly — rendering all other electronic structure methods obsolete for ground states.

Even though the explicit forms of both the $V_{e-e}[\rho(\vec{r})]$ and $T[\rho(\vec{r})]$ functionals are unknown, one may extract the classic Coulomb contribution, $J[\rho(\vec{r})]$, from the former. Then,

$$F_{HK}[\rho(\vec{r})] = T[\rho(\vec{r})] + J[\rho(\vec{r})] + V_{ncl}[\rho(\vec{r})], \tag{2.8}$$

where V_{ncl} represents the non-classical electron-electron contribution. In Equation (2.8), only $J[\rho]$ is known. Following the successful approach formulated by Kohn and Sham in 1965 [90], this equation is further reformulated by introducing a fictions model system as a reference point for the calculation. The idea is to compute as much as possible of the true kinetic energy exactly, and approximate whatever remains. One then begins by calculating the kinetic energy of a non-interacting reference system having the same density as the real system. Denoting this non-interacting kinetic energy by T_s, one may rewrite the Hohenberg-Kohn functional as

$$F_{HK}[\rho(\vec{r})] = T_s[\rho(\vec{r})] + J[\rho(\vec{r})] + E_{XC}[\rho(\vec{r})], \tag{2.9}$$

where E_{XC} is the famous exchange-correlation functional. A quick comparison of Equations (2.8) and (2.9) reveals that E_{XC} contains the contributions to the kinetic energy not covered by T_s as well as the non-classical electron-electron interaction. In other words, the exchange-correlation functional is the only unknown term of Equation (2.9). Finding more accurate, and more universal, approximations to this functional are some of the main objectives in Kohn-Sham DFT.

The Kohn-Sham method consists of writing the density of the system $\rho(\vec{r})$ as the sum of the square moduli of a set of one-electron orthonormal orbitals [91],

$$\rho(\vec{r}) = \sum_{i=1}^{N} |\varphi_i(\vec{r})|^2, \tag{2.10}$$

and applying the variational method to determine the molecular orbitals. That is, the energy is minimised by varying the orbitals φ_i under the constraint that the integral of the density over the entire space should yield the total number of electrons, N. By this procedure, one obtains the Kohn-Sham equations, which are solved using a self-consistent approach to yield the Kohn-Sham (KS) orbitals, φ_i^{KS} [91]. Of course, for this procedure to make sense, an approximation for the exchange-correlation functional must be available. In this context, it should be noted that the quality of the density functional approach depends solely on the accuracy of this approximation [70]. In the following section, some important classes and specific examples of approximate exchange-correlation functionals are introduced.

2.7 EXCHANGE-CORRELATION FUNCTIONALS: CLASSES AND EXAMPLES

As mentioned previously, the key to success (or otherwise) when using DFT is the approximation to the exchange-correlation functional [91]. Therefore, a great deal of work is put into constructing approximate functionals with the ability to yield results of high accuracy.

Although no systematic approach for constructing new approximate exchange-correlation functionals exist [70], one may separate the approximations into classes based on their mathematical build-up. Functionals of the simplest form are so-called local density approximations (LDAs) based on the uniform electron gas model [91]. In this approach the electron density is assumed constant throughout space, and the approximate exchange-correlation functional, $\tilde{E}_{XC}$, takes the form

$$\tilde{E}_{XC}^{LDA}[\rho(\vec{r})] = \int f(\rho(\vec{r}))d\vec{r}, \tag{2.11}$$

where $f(\rho(\vec{r})) = \rho(\vec{r})\epsilon_{XC}(\rho(\vec{r}))$, and $\epsilon_{XC}(\rho(\vec{r}))$ is the exchange-correlation energy per electron as a function of the density of a uniform electron gas [91]. While such local approximations yield realistic results for certain systems, there are many situations in which the LDAs cannot provide sufficient accuracy. For instance, LDAs are known to overestimate binding energies [70].

One path to elaborate on the simple LDA approach is to suppose that the exchange-correlation functional should depend not only on the electron density but also on its gradient [78]. This is called the generalised-gradient approximation (GGA), and the functionals belonging to this class take the form

$$\tilde{E}_{XC}^{GGA}[\rho(\vec{r})] = \int g(\rho(\vec{r}), \nabla\rho(\vec{r})), \tag{2.12}$$

where g is a suitably chosen function. A well-known example of a GGA is the Perdew-Burke-Ernzerhof [92] (PBE) functional. One could elaborate further by including in the dependency of g also the second derivatives of the density, however in the meta-generalised gradient approximation (mGGA), a somewhat more complicated step is taken. That is, in the dependency of g the terms that represent the kinetic energy density is included, and as a result mGGAs are of the form

$$\tilde{E}_{XC}^{mGGA}[\rho(\vec{r})] = \int g(\rho(\vec{r}), \nabla\rho(\vec{r}), \nabla^2\rho(\vec{r}), \tau(\vec{r})), \tag{2.13}$$

where, in atomic units,

$$\tau(\vec{r}) = \frac{1}{2}\sum_i \nabla\varphi_i^{KS*}(\vec{r})\nabla\varphi_i^{KS}(\vec{r}), \tag{2.14}$$

where the sum runs over occupied orbitals.

Although more classes exist, the last that will be touched upon here is that of so-called hybrid functionals. A hybrid functional accounts for exchange effects by adding a fraction of HF exchange into the mix. Mathematically, the hybrid functionals are linear combinations of HF exchange, DFT exchange terms, and DFT correlation [78]. An example of such a hybrid functional is the extremely popular B3LYP [93, 94], which combines HF exchange with one LDA and two GGAs. Another example is the Minnesota functional M06-2X [95, 96], which is a hybrid meta functional including both HF exchange and mGGA terms. While B3LYP includes 20 % of the exact HF exchange, M06-2X includes 54 % (two times more than the M06 functional, hence the "2X").

2.8 BASIS SETS

In the context of theoretical and computational chemistry, a basis set is a set of functions which are combined in linear combinations to create molecular orbitals. For quantum chemical calculations, these basis functions are typically atomic orbitals, as shown in Section 2.4. It is worth noting that the name "basis set" itself can be misleading, as the basis sets used in calculations are not basis sets in the strict mathematical sense; in theory, one would need to include an infinite amount of basis functions in order to represent the molecular orbitals exactly, and this is not possible in practice. Thus, an error will always be present in actual calculations due to the use of an incomplete basis. This error is termed the basis set truncation error.

Among the basis sets most commonly used in ab initio calculations one finds Slater type orbitals (STOs) [84] and Gaussian type orbitals (GTOs) [97]. An atomic basis function is comprised of an angular part and a radial part, in which the angular component is universal [98] and consists of the spherical harmonics. While the radial part of STOs ensures correct behaviour close to the atomic nucleus, it makes the integrals that appear in the HF energy expression difficult to solve for multi-atom systems. In contrast, the radial part of GTOs significantly simplifies the integrals, but also brings several unphysicalities. Firstly, its exponential dependence on r^2, where r is the distance from the nucleus, leads to violation of the cusp condition. Secondly, the GTOs fall off too rapidly as r becomes large. In other words, a single GTO has problems with representing proper behaviour both close to, an at large distances from, the nucleus. Fortunately, it turns out that the behaviour of an STO may be obtained by adding several GTOs together (thus overcoming the problems GTOs have at the nucleus and at long-range). This makes GTOs the preferred type of basis functions for electronic structure calculations for multi-atom systems.

A minimal basis set contains just the number of functions needed to accommodate all the filled orbitals in each of the atoms comprising the molecular system. Such basis sets are well known to have several deficiencies [91]. A minimal basis set cannot, for example, describe non-spherical aspects of the distribution of electrons. The problems of minimal basis sets can be addressed if each (atomic)

orbital is represented by more than one function. In a so-called double zeta basis, the number of functions is doubled with respect to the minimal basis. Adding more functions lead to triple zeta basis sets, quadruple zeta basis sets, an so on. An alternative solution to the minimal basis problems is to double (or triple, quadruple etc.) the number of functions used to describe the valence electrons while only using a single function for the inner shells. Such basis sets are termed split valence double (or triple, quadruple etc.) zeta basis sets, and the rationale for the approach is that the core orbitals, unlike the valence orbitals, do not affect chemical properties very much and vary only slightly from one molecule to another [91].

It should be noted that there are situations in which simply increasing the number of basis functions does not yield a more accurate description of the molecular orbitals. For systems that have a significant amount of electron density away from the nuclear centres, *e.g.* anions, one may add diffuse functions to remedy this deficiency. Diffuse functions are shallow Gaussian basis functions which more accurately represent the behaviour at large distances from the nucleus. For highly anisotropic charge distributions, one might benefit from adding functions with higher angular momentum quantum numbers which better describe polarisation effects. Such functions are commonly referred to as polarisation functions.

Generally, increasing the size of the basis set improves the accuracy of the computations within the given theory. However, it also increases the computational cost. In a world of finite resources, the trade-off between accuracy and computational cost will always be important for practical purposes. The goal is therefore to choose a basis that is not too expensive while at the same time producing only a small basis set truncation error. That being said, the required level of accuracy varies with the nature of the hypothesis being tested. While a large basis set is needed for quantitative results of high accuracy, smaller basis sets may suffice for studies that are qualitative in nature. Lastly, there exists certain "lucky combinations" of theories and basis sets where error cancellation occurs. Thus it is not only important to consider theories and basis sets separately — thought should also be put into how they work with, or against, each other.

2.9 BOND DISSOCIATION ENERGIES

The bond dissociation energy (BDE) is a measure of chemical bond strength. It is defined as the enthalpy per mole required to break a given bond by homolysis [99]. For the chemical bond connecting the chemical species A and B in the neutral molecule AB, the BDE is given by the equation

$$\mathrm{BDE(A{-}B)} = E(\mathrm{A}\cdot) + E(\mathrm{B}\cdot) - E(\mathrm{A{-}B}), \tag{2.15}$$

where the dot notation is employed for the resulting free radicals, $\mathrm{A{-}B}$ denotes the bond, and $E(i)$ is the energy of species i where $i = \mathrm{A}\cdot, \mathrm{B}\cdot, \mathrm{A{-}B}$. Although the IUPAC definition refers to the energy change at absolute zero temperature,

it is not uncommon to compute the BDE at other temperatures. Note also that even though the BDE is formally defined as an enthalpy change, the Gibbs energy is often used whenever convenient. In this thesis, the latter is referred to as the "Gibbs BDE" to avoid confusion.

The BDE is commonly considered to be a central quantity when it comes to predicting impact sensitivities for energetic materials. Since X–NO_2 homolysis, where X is either a C, N or O atom, is assumed to be the initial step of decomposition for many nitro-based energetic materials at high temperatures, the strength of these so-called trigger bonds has been given much attention in the literature.

2.10 TRANSITION STATES AND CHEMICAL KINETICS

TSs are of great chemical interest, as they define the energy barrier which must be overcome in order for a reaction from reactants to products to occur. Indeed, the activation energy E_a of a chemical reaction may be defined as the energy difference between the TS and the reactants, such that

$$E_a = E(\text{TS}) - E(\text{Reactants}), \tag{2.16}$$

where $E(\text{TS})$ is the energy of the TS, and $E(\text{Reactants})$ is the energy of the reactants. When the activation energy is calculated for intermediate reaction steps, the reactants in Equation (2.16) simultaneously serve as intermediate species for the overall reaction sequence. These concepts are illustrated in Figure 2.1. Note that the terms activation energy, (energy) barrier, and barrier to reaction will be used interchangeably throughout this thesis.

The activation energy is tightly connected to the chemical kinetics of the reaction, and is thus an important parameter for determining how readily the reactants transform into the products. By comparing the activation energies of different reaction steps, one can under certain conditions identify a rate-determining step (RDS). By comparing computational activation energies for energetic material initiation with experimental ones, one may also be able to conclude whether a single mechanism dominates the initiation or if several mechanisms are in strong competition with each other.

The rate of a chemical reaction is often found to be proportional to the concentrations of the reactants raised to some power [80]. The proportionality constant of such a relation is called the rate constant. While this quantity, to a good approximation, is independent of the concentration of reactants, it is often dependent on the temperature. Indeed, the rate constant k_r of most reactions increase with temperature, and it is found experimentally for many reactions that a plot of ln k_r against the reciprocal of temperature $1/T$ gives a straight line [80]. Reactions exhibiting this behaviour follow the Arrhenius equation, given by

$$k_r = A \exp\left(-\frac{E_a}{RT}\right), \tag{2.17}$$

where A is the pre-exponential or frequency factor, R is the universal gas constant, and T is temperature. Since E_a is found from the slope of the plot of ln k_r against $1/T$, a high E_a signifies a strong temperature dependence of k_r. While the kinetics of some reactions are non-Arrhenius in the sense that a straight line is not obtained from the ln k_r vs. $1/T$ plot, the activation energy at any temperature can be generally defined as

$$E_a = RT^2 \left(\frac{\mathrm{d} \ln k_r}{\mathrm{d}T} \right). \tag{2.18}$$

The RDS of a chemical reaction sequence is in most cases given by the slowest reaction step of the sequence (*i.e.* the step with lowest rate). Not all reaction mechanisms have an RDS, but when one does occur, the overall rate of reaction is limited by this step [100]. The number of molecules or ions that participate in the RDS determine the molecularity of the overall reaction kinetics. A mechanism in which two reacting species combine in the TS of the RDS is called bimolecular, while one in which a single species makes up the TS is called unimolecular. In an elementary reaction, the power to which the concentration of a reactant is raised in the rate expression coincides with the stochiometric coefficient of the reactant in the corresponding chemical equation.

For a sequence of elementary chemical reactions, each having rate constants that obey the Arrhenius law, one may identify the RDS as the step with highest activation energy, given that the concentration of reactants are sufficiently high and that the frequency factors of the different steps are of comparable magnitudes. An additional prerequisite for identifying a step as the RDS is that no alternative, less energy-requiring reaction routes are available. That is, if a high-barrier reaction step can be sidestepped in the journey from reactants to products, it is not rate-determining [80].

In real life reactions, the situation is often far more complicated than the scenario described above. Firstly, not all reactions adhere to the Arrhenius law. Secondly, for multi-route (or composite) reactions, the competition between different routes typically increases with temperature, and the idea of an RDS may no longer serve any useful purpose. While defining an RDS may simplify many complex kinetic problems, misinterpretations can occur as a result, and one should therefore be careful about drawing conclusions based on such simplifications [101, 102]. In other words, it may not always be constructive to try and identify an RDS at all. However, the notion that a high activation energy gives a small rate constant is intuitive, and ought to be kept in mind.

So far, the frequency factor A in Equation (2.17) has for the most part been ignored. Although not as important as the relation between activation energy and rate for the current work, the frequency factor deserves a brief description. In collision theory, in which two gas molecules must collide in the correct orientation for a reaction to occur between them, the frequency factor describes how often two molecules collide in this manner. In transition state theory, the frequency factor is derived using the quantities and laws of thermodynamics. For

unimolecular reactions, the treatment and interpretation of the frequency factor depends on the theory employed. In Kassel's theory [103], A is a constant representing the frequency with which internal transfers carry energy into the critical oscillator. In the variety of formulations employed by Slater [104], A is a specially weighted average of the vibration frequencies in the molecules which always lies between the least and the greatest of the fundamental frequencies [105]. In any case, the frequency factor says something about how often the reactant molecules find themselves in a state in which they are susceptible to participate in the chemical reaction.

2.11 THERMODYNAMIC AND KINETIC STABILITY

Usually, both thermodynamic and kinetic quantities are important when the feasibility of a chemical reaction is to be assessed. In general, thermodynamics dictates which processes are possible under a given set of conditions, while the focus of kinetics is the rate at which reactions occur.

The reaction energy, E_{RX}, of the chemical reaction 'Reactants $\rightarrow$ Products' is given by

$$E_{RX} = \sum_{p \in prod.} E(p) - \sum_{r \in reac.} E(r), \tag{2.19}$$

where p runs over the product species and r runs over the reactant species. From thermodynamics it is known that from the internal energy $U(S, V, n)$, one may derive the enthalpy $H(S, P, n)$ and the Gibbs energy $G(T, P, n)$ using Legendre transformations. Here, S is entropy, V is volume, n is number of moles, P is pressure, and T is temperature. On integrated form, the relations between these quantities are

$$\begin{aligned} H &= U + PV \\ G &= H - TS. \end{aligned} \tag{2.20}$$

Furthermore, by combining the first and second laws of thermodynamics, the total differential of the internal energy can be written as

$$\mathrm{d}U = T\mathrm{d}S - P\mathrm{d}V, \tag{2.21}$$

which emphasises how the internal energy depends on the temperature through the entropy term. At absolute zero temperature, both the enthalpy and Gibbs energy reduces to the internal energy of the system. As the temperature increases, so does the internal energy U. In addition, the pressure-volume component, PV, and the product of temperature and entropy, TS, become increasingly significant for the enthalpy and Gibbs energy as the temperature rises.

Since the temperature and pressure are often the easiest variables to control in experiments, chemists usually employ the Gibbs energy for thermodynamic discussions on stability. Under constant temperature and pressure, the value of the reaction Gibbs energy, ΔG, determines whether or not the reaction can occur spontaneously. The more negative the ΔG, the more thermodynamically favourable the reaction.

For a system to be thermodynamically stable, no spontaneous reactions can be available. However, a system can be kinetically stable even though this requirement is not met. If the available spontaneous reaction routes have low enough rates (*i.e.* occur slowly enough), the system will remain in the thermodynamically unfavourable state for a long time, and is in this sense stable. A classic example of this is the conversion of diamond into graphite. While the ΔG of this reaction is negative, making graphite thermodynamically favoured over diamond, this reaction will not occur under ordinary conditions due to its extremely high activation energy.

For the reaction pathways studied in this thesis, the kinetic aspects are considered more important than the thermodynamic ones. This is the case firstly because the reaction schemes are thought to occur as a result of mechanical impact, such that a significant amount of energy is added to the system for these reactions to occur (no spontaneity needed). Secondly, each of the reaction schemes are thought to be followed by fast, highly exergonic reactions which eventually cause the materials to explode.

2.12 ON BRIDGING EXPERIMENTAL AND THEORETICAL EXPLOSIVES RESEARCH

While theoretical studies utilising DFT or molecular dynamics simulations are routinely performed for energetic materials, experimental knowledge still plays an essential role in the search for new and improved descriptions of sensitivity phenomena. Since there are still many unanswered questions regarding reaction mechanisms and factors that determine sensitivity, being able to compare theoretical findings with experimental ones is important.

This section aims to give the reader a brief introduction to common experimental methods, and to point out the most prevalent challenges of bridging experimental and theoretical explosives research. Special attention is given to polynitroaromatic compounds since PA, mPA, and dmPA all belong to this molecular family.

2.12.1 EXPERIMENTAL METHODS

As mentioned introductory, impact sensitivities are usually determined using drop hammer tests [19, 37, 38] (see Chapter 1 for details). Note that these tests are unable to reveal details about the thermal decomposition mechanisms.

Differential scanning calorimetry, differential thermal analysis, and manometry are methods based on slow heating over minutes or hours while the change of heat flow or pressure is closely monitored. The decomposition rates extracted from experiments of this kind usually correspond to the lower activation energy processes and tend to reflect the overall process rather than any particular step [7].

If a moderate heating rate is desired, one may resolve to so-called T-jump methods, in which heating times in the range of 20–500 μs to a chosen high temperature can be achieved [106, 107]. The results obtained by such experiments may serve as especially valuable input for discussions on impact sensitivity. In fact, Wenograd [106] found for a series of diverse explosives that the impact sensitivity roughly correlated with the temperature required to produce an explosion in 250 μs. He concluded that impact sensitivity is linked to thermally induced chemistry, supporting the earlier conclusions drawn by Robertson and Yoffe [108]. While the drop hammer impact sensitivity test cannot provide details about the thermal decomposition reactions, other techniques exist that can at least provide some details about these processes. An example is T-jump/FTIR spectroscopy [107], where FTIR abbreviates “Fourier Transform InfraRed". Not only can this method separate and detect some of the dominant reaction branches during rapid heating, but also determine the temperature dependence of some of these branches [7, 107, 109].

High heating rates can be achieved through a variety of methods. Such experiments typically simulate the conditions that exist under shock-wave initiation of energetic materials, and thus refer to shock sensitivity rather than impact sensitivity. However, the shock sensitivity of many polynitroaromatic compounds have been seen to follow similar trends as the impact sensitivity [37], meaning that experimental methods of this kind may still prove useful for discussions of the latter. For the study of unimolecular gas phase reactions, one may employ a laser pulse [110] or a shock wave created by a burst of gas pressure [111, 112] to heat molecules to a high temperature in times ≤ 1 μs. Through the use of shock-tube and laser pyrolysis, one can achieve temperatures in excess of 1070 K. Under such conditions, lower and higher activation energy processes can be expected to compete strongly [7].

A great deal of research has been done on the mass spectrometry of explosives [113, 114] due to some interesting parallels between the early stages of decomposition by explosive shock and the fragmentation under electron impact in the mass spectrometer [115–119]. In electron impact mass spectrometry, ions containing excess energy are formed before they decompose into a series of fragments. The resulting mass spectrum indicates the presence of the ions, but does not give any information about their routes of formation. However, by combining tandem mass spectroscopy (MS/MS) with collision induced dissociation (CID), one obtains a powerful tool for the study and determination of fragmentation processes and pathways of individual ions [113].

2.12.2 PREVALENT CHALLENGES

According to Brill and James [7], relatively unperturbed unimolecular decomposition kinetics can be determined only for molecules in the gas phase at low pressure. Since most explosives begin to react in the condensed phase, it is not always straightforward to make sense of such experimental results or relate them to behaviour observed in the bulk condensed phase. This calls for a great deal of attentiveness from theoretical scientists as they compare their findings with experimental ones.

It is important to be aware of the dependency of experimental results on the choice of experimental setup and procedure. That is, the results — and ultimately, the description of thermal decomposition of an explosive — depend on the amount and configuration of the sample, the rate and magnitude of energy loading, the diagnostics employed and the interpretative scheme [7]. A complex organic molecule in the bulk condensed phase may typically decompose through a large number of different reaction mechanisms, each having their own rate constant and sensitivity to temperature. Since the product distribution depends both on the temperature and the rate at which such a material is heated, so does the description of decomposition processes. This has led to many contradictory assertions over the years, and continue to complicate the discussion of sensitivity phenomena to this day [7]. Furthermore, not only the chemical properties of an energetic material affect the decomposition process, but physical properties such as thermal conductivity, hardness, void volume, and heat capacity contribute. Such physical details are believed to be important for decomposition triggered by mechanical stress [120], and can thus be significant for impact sensitivity. In other words, the thermal decomposition of an energetic material is an extremely complex process, and keeping track of all the experimental conditions can in itself be challenging.

Theoretical studies on decomposition kinetics may focus on individual gas phase molecules, but can also stretch to larger systems. Molecular dynamics simulations using periodic boundary conditions can be helpful for assessing the reaction kinetics for materials with known crystal structures.

2.12.3 COMMON ASSUMPTIONS

The complexity of energetic material decomposition cannot be overstated. The fact that so many questions remain unanswered more than 100 years after detonation phenomena was first observed, reflects both the inherent complexity of the chemical and physical processes involved, and how difficult it is to properly measure or simulate these processes. In order to generate results, one must often make assumptions about the chemistry that takes place.

Firstly, it is commonly assumed that the chemical reactions exhibit Arrhenius behaviour, *i.e.* that their rate constants obey Equation (2.17). Although several observations [121, 122] indicate that an aggregation of many time-dependent chemical and physical processes exists during the thermal decomposition of an

energetic material in the condensed phase, large temperature segments of the decomposition regime of some polynitroaromatics has been shown to obey the Arrhenius law [7].

Secondly, many nitroaromatic explosives are assumed to decompose through a series of unimolecular chemical reactions even in the condensed phase. In fact, this assumption is often employed for TNT, although there have been varying reports regarding its validity [5, 35].

Thirdly, even though many other decomposition pathways are investigated, the trigger linkage hypothesis is quite commonly assumed to hold for nitro-based explosives. This is especially the case for correlation studies which attempt to find relationships between impact sensitivity and various molecular descriptors. Several scientists [7, 25, 46] have argued for the need to distinguish between molecules that contain an α-CH bond and molecules that do not, when correlations between $X-NO_2$ BDE and impact sensitivity are to be investigated. Here, X is either a C, N, or O atom. However, some studies do not make this distinction [19, 20].

3

METHODOLOGY

In this chapter, the methodology of the current work is described. The chapter is organised into three parts, wherein the first describes the computational details, the second rationalises the choice of methods, and the third presents the reaction pathways that are currently under study.

3.1 COMPUTATIONAL DETAILS

All calculations are performed using the open-source high-performance computational chemistry software NWChem [4]. Resources are provided by the NTNU IDUN computing cluster [3] as well as UNINETT Sigma2 — the National Infrastructure for High Performance Computing and Data Storage in Norway. Molecular graphics are constructed by the use of UCSF Chimera [1], and energy plots are made using the MechaSVG software [2].

All calculations are performed using DFT with the Minnesota hybrid functional M06-2X [95, 96] and the triple zeta valence polarised basis set def2-TZVP [123, 124].

Geometry optimisations are performed for all molecules treated in the thesis (see the abbreviations list on page xiii as well as Figures 4.1, 4.3, and 4.7). Vibrational frequency calculations are employed to confirm each structure as either a minimum or saddle point on the PES, and to obtain the zero-point and thermal corrections to the molecular energies. The energy of each molecule at absolute zero temperature is obtained by adding the zero-point correction, scaled by a factor 0.9754 in accordance with the results of Kesharwani *et al.* [125], to the single-point energies obtained in the final step of each geometry optimisation. The Gibbs energies at temperature 298.15 K are obtained by adding to these single-point energies the enthalpy correction and subtracting the product of the computed entropy and the absolute temperature. No scaling factor is employed for the calculation of Gibbs energies.

Because it is usually more challenging to locate TSs than equilibrium structures, constrained geometry optimisations are performed prior to the saddle point optimisations. The output structure of each constrained optimisation is then provided as the input geometry for a saddle point optimisation. While all calculations are performed at the M06-2X/def2-TZVP level of theory, the standard grid and DFT convergence criteria are here found insufficient for confirming all optimised TS structures as true saddle points. That is, when the frequency calculations are run using the standard grid and DFT convergence criteria, more

than one imaginary frequency is found for several of the TS structures obtained by saddle point optimisations. In principle, this could simply mean that the optimisations have been unsuccessful in locating the saddle points. However, the frequency outputs show a considerable gap between the largest and second largest (in absolute value) frequencies, which points towards the possibility that the additional imaginary frequencies are unphysical and simply a result of numerical inaccuracies. By running frequency calculations using a significantly larger grid and tighter DFT convergence criteria this is confirmed to be the case, as these calculations successfully return one and only one imaginary frequency for these TSs. For each TS structure, the zero-point correction, enthalpy correction and total entropy is fetched from the calculation in which one and only one imaginary frequency was obtained.

Activation energies are calculated according to Equation (2.16), while reaction energies are found via Equation (2.19).

The optimised geometries of the molecules studied in this thesis as well as some example input files can be found in the supplementary information starting on page 66. Using this information, one should be able to reproduce all results presented in Chapter 4.

3.2 CHOICE OF THEORY AND BASIS

As described in Section 3.1, all calculations are performed using DFT with the Minnesota hybrid functional M06-2X [95, 96] and the polarised triple zeta valence basis set def2-TZVP [123, 124]. In this section, the choice of theory and basis is explained and discussed, with emphasis on previous work and the trade-off between accuracy and computational cost.

For the choice of functional, the popular B3LYP [93, 94, 126] is first considered. While this functional has served chemists well for a long time, it certainly has its limitations. For instance, B3LYP has been shown to underestimate reaction barrier heights [127, 128] and BDEs [129, 130]. Overcoming these limitations was an important goal of Truhlar and coworkers when they constructed the M06 suite of functionals [95, 96, 131]. Following their introduction in the early 2000s, these functionals have gained popularity in the field, and the M06-2X functional has indeed been shown to outperform B3LYP in energy calculations and in the computation of $C-NO_2$ BDEs for a wide range of organic molecules [74, 77, 132, 133]. For geometry optimisations, M06-2X and B3LYP seem to yield results of similar accuracy [61, 134, 135]. With the additional knowledge that M06-2X is commonly employed in studies on energetic materials [15, 24, 36, 56, 72], applying it for the current work seems appropriate.

Next, a basis set must be chosen. The triple zeta valence polarised basis set def2-TZVP is one of the redefined Karlsruhe basis sets developed by Ahlrichs *et al.* [123, 124]. In a 2020 basis set study in which the performance of the Dunning, Jensen, and Karlsruhe bases were compared for a variety of molecules, Kirschner *et al.* [136] highlighted the def2-TZVP basis set as a very suitable

choice to balance speed and accuracy. Additionally, the computational investigations by St. John *et al.* [77] from the same year showed that the functional/basis combination M06-2X/def2-TZVP has an excellent trade-off between empirical accuracy and computational efficiency. In fact, out of the seven that were tested, this combination was found to have the best trade-off for BDE calculations on a database containing organic closed-shell compounds consisting only of C, H, N, O atoms. Adding to this the fact that several studies on energetic materials have combined a hybrid functional and a Karlsruhe triple zeta basis set due to the appreciable accuracy they provide [15, 38, 61], def2-TZVP stands out as a good choice for the current work.

3.3 REACTION PATHWAYS

The three reaction pathways under study are sketched in Figure 3.1. Table 3.1 serves as a supplement to this figure, and explains the positioning of the substituents in PA, mPA, and dmPA. Details about the procedures followed in the study of these pathways are provided in Chapter 4.

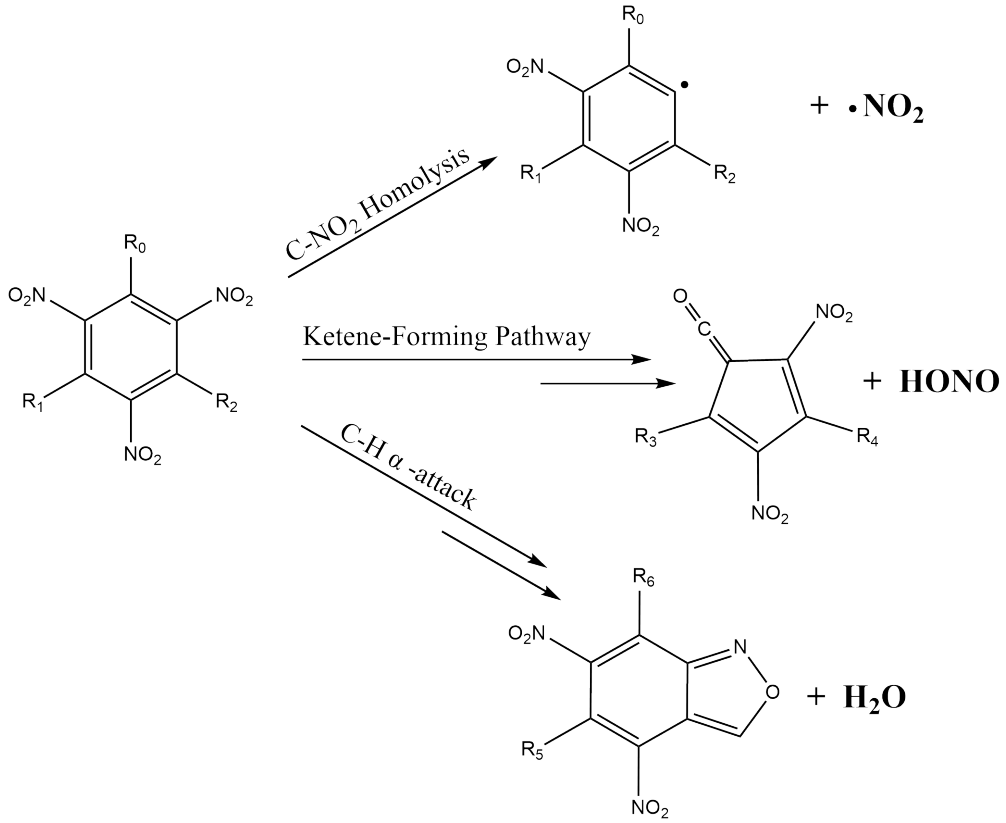

Figure 3.1: Schematic overview of the three reaction pathways studied for PA, mPA, and dmPA in this thesis. The double arrows indicate that the reaction proceeds along a multistep pathway. See Table 3.1 for details on the R groups for each molecule.

Note that while the C−NO_2 homolysis and C−H α-attack pathways are mentioned with high frequency in the literature, the ketene-forming pathway does not seem to have an agreed-upon name in the field. Note also that the abbrevi-

Table 3.1: Substituents for the three nitroaromatic compounds studied here. For the structures, see Figure 3.1.

Molecule	(R_0, R_1, R_2, R_3, R_4, R_5, R_6)
PA	(OH, H, H, H, H, –, –)
mPA	(OH, H, CH_3, H, CH_3, H, OH)
dmPA	(CH_3, OH, CH_3, CH_3, CH_3, OH, CH_3)

ations used for the molecules in this thesis are not completely in line with what is used in the literature. That is, PA is a common abbrevation for picric acid, but mPA and dmPA are usually referred to by abbreviations more closely resembling their IUPAC names. Although both using IUPAC and following common naming conventions in the field are in general good practices, a choice is here made to prioritise the reader. Since the upcoming chapters are mainly focused on comparing the three molecules, an attempt has been made to construct short abbreviations that clearly convey where the molecules are similar as well as where they differ. Thus, the PA abbreviation is used as a base, while the letters m and dm are added to signify the extra methyl group(s). Hence, PA = picric acid, mPA = methyl picric acid, and dmPA = dimethyl picric acid.

4

RESULTS AND DISCUSSION

In this chapter, the computational results will be presented and discussed. The three proposed reaction pathways displayed in Figure 3.1 will be treated separately in Sections 4.1, 4.2, and 4.3. A discussion on their relative significance and temperature dependencies follows in Section 4.4, before the chapter is rounded off with a discussion on alternative mechanisms that may contribute to the experimentally observed sensitivity differences in Section 4.5.

Before the different pathways are considered, a clarification regarding the molecular structure of mPA is in order. With respect to its hydroxyl substituent, one finds a methyl group at one of the meta positions and a hydrogen atom at the other. Combined with the directionality of hydroxyl, this opens the possibility for two distinct minima connected by rotation about the C–O bond. Indeed, two such minima were located by geometry optimisations and confirmed as such by frequency calculations returning no imaginary frequencies. The conformer in which the phenolic hydrogen points away from the methyl substituent was found to be the most stable of the two, by a difference in molecular energies of 19 kJ mol^{-1}. This structure was chosen for further investigation, and appears in Figures 4.1, 4.2, 4.3, and 4.7 under the abbreviation mPA.

4.1 C-NO_2 HOMOLYSIS PATHWAY

Based on the importance of X–NO_2 homolysis in the decomposition of nitroaliphatics, nitramines (R_2NNO_2), and nitrate esters ($RONO_2$), where X is respectively a C, N, or O atom, C–NO_2 homolysis is a logical reaction for the initiation of nitroaromatics [7, 14]. The C–NO_2 bond is usually the weakest bond in nitroaromatic molecules. C–NO_2 homolysis has experimentally been shown to occur in the decomposition of ortho-nitrotoluene [110–112], and it represents a common assumption for studies on substituted nitroaromatics [15, 19, 20].

Since impact sensitivity is a measure of the mechanical energy that must be provided to an energetic material to make it explode, it is considered closely connected to the activation energies of the initiation reactions. However, the C–NO_2 homolysis pathway is usually studied by calculating the C–NO_2 BDE, *i.e.* the reaction energy of the bond-breaking process, in contrast to other mechanisms for which the activation energy is the central quantity. There are several reasons why the BDE has become a common quantity for studies on energetic material sensitivity. Firstly, the BDE has on many occasions been seen to correlate with impact sensitivity [17, 19, 20, 23]. Secondly, the activation energy of the homolytic bond breaking process can be challenging to calculate since

the corresponding TS can be especially difficult — or even impossible — to locate. This was highlighted by Nikolaeva *et al.* [137] who studied C–NO_2 homolysis in nitrobenzene at the B3LYP/6-31G(d,p) level of theory. In this work, no pronounced maximum in the electronic energy was found for the reaction path along the PES corresponding to homolytic cleavage of the C–NO_2 bond. Instead, the electronic energy was found to increase monotonically from reactants to products. Thirdly, it has been proposed that the BDE is proportional to the activation energy for compounds where the resonance stabilisation and the structure of the TS are relatively similar [19]. Worth mentioning in this context are the results of Khrapkovskii *et al.* [73], who reported a significant correlation between the measured value of activation energy for C–NO_2 homolysis in a variety of substituted nitroaromatics and the values of BDEs calculated at the B3LYP/6-31G(d,p) level of theory. The coefficient of determination, R^2, was found to be 0.72. Adding to this that several previous papers [5, 9, 30] have compared the C–NO_2 BDE with activation energies of other reaction mechanisms to identify the most favourable initiation process, it seems appropriate to do the same in this thesis.

Figure 4.1 displays the optimised geometries and nomenclature of the structures treated in the study of the C–NO_2 homolysis pathway.

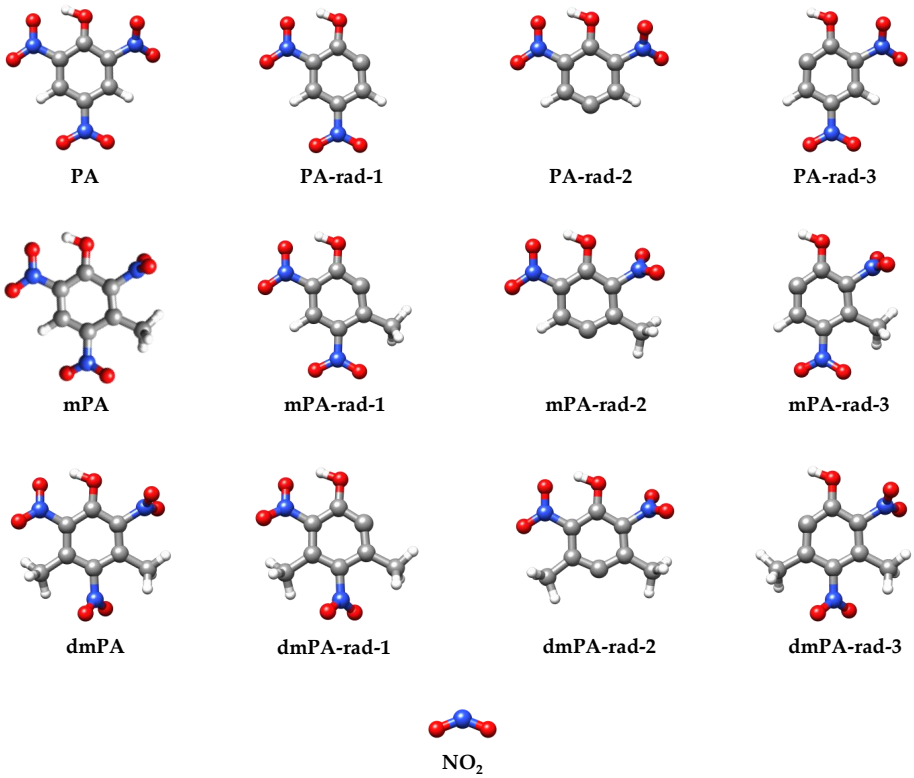

Figure 4.1: Optimised structures of the different stationary points (minima) investigated in the study of the C–NO_2 homolysis pathway. "Rad" is short for radical.

Figure 4.2 shows the optimised molecular structures of PA, mPA, and dmPA, complete with the calculated BDEs of their C–NO_2 bonds. For each structure, the C–NO_2 bond with the lowest BDE is identified as the trigger bond in the gas phase. Table 4.1 displays the trigger bond BDE and critical impact height, h_{50}, of each compound. The impact sensitivity data has been fetched from Reference [46].

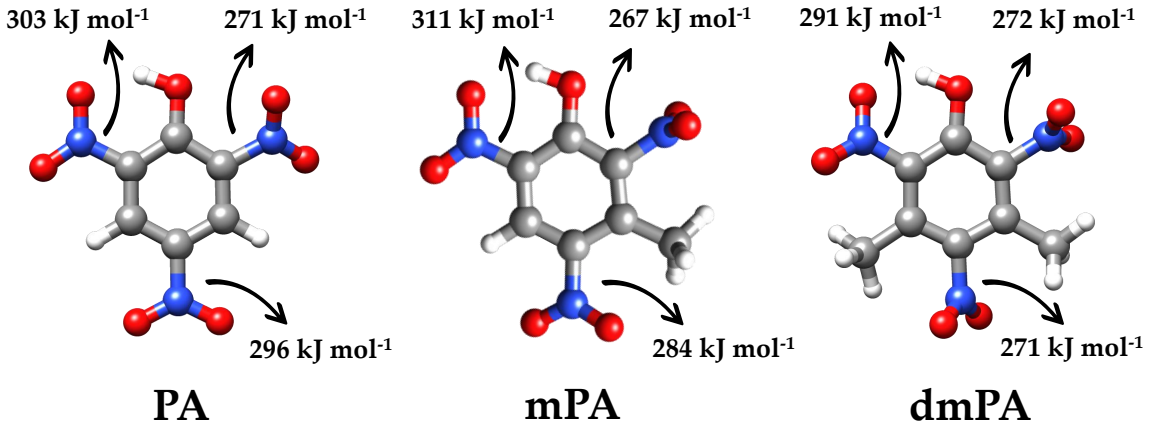

Figure 4.2: Optimised molecular structures of PA, mPA, and dmPA, complete with the calculated BDEs of their C–NO_2 bonds.

As may be observed in Table 4.1, the trigger bond BDEs are all found to lie within the range 267 - 271 kJ mol^{-1}. This is in good agreement with the results of Shoaf *et al.* [15], who found the trigger bond BDEs of PA and mPA to be 270.0 and 263.6 kJ mol^{-1}, respectively, at the M06-2X/TZVP level of theory. Rice *et al.* [20] and Wang *et al.* [60] found the trigger bond BDE of PA to be somewhat lower (251.5 and 252.4 kJ mol^{-1}, respectively) using B3LYP in conjunction with the somewhat smaller basis set 6-31G* [138, 139]. However, B3LYP is known to underestimate BDE values [19] and to be less accurate than M06-2X for C–NO_2 BDEs [74], so this is not a cause of concern.

Table 4.1: The calculated trigger bond BDEs of PA, mPA, and dmPA, and their critical impact heights, h_{50}s, as reported by Reference [46].

Molecule	BDE [kJ mol^{-1}]	h_{50} [cm]
PA	271	87
mPA	267	191
dmPA	271	77

Upon further examination of Table 4.1, one may note that there is only a small variation in the calculated BDEs. The lowest and highest value differ by only 4 kJ mol^{-1}, and the trigger bond BDEs of PA and dmPA are equal. Based on various benchmark studies [77, 95], 4 kJ mol^{-1} is believed to lie within the uncertainty area of the method. In other words, no significant variation in the BDEs is observed.

The absence of a correlation between trigger bond BDE and impact sensitivity may be indicative of several phenomena. Firstly, it is possible that some, or all, of the molecules decompose through a different reaction scheme. While it is common to assume that nitroaromatics decompose via C–NO_2 homolysis at high temperature and other mechanisms at low to moderate temperature, the anomalous impact sensitivities of mPA and dmPA may suggest that the common assumptions do not hold for these molecules. Secondly, the effects of solid state properties like crystal structure and the density and nature of defects may be determining for impact sensitivity in these compounds. This is discussed in more detail in Section 4.5, while the next sections discuss the computational results for the ketene-forming and C–H α-attack pathways.

4.2 KETENE-FORMING PATHWAY

While it is common to assume that C–NO_2 homolysis initiates nitroaromatic decomposition, the experimental evidence for this mechanism is not as compelling for nitroaromatics as for other molecular families. Although NO_2 (g) has been reported from decomposition of nitrobenzene at temperature T = 548 K [140] and from pyrolysed 1,3-dinitrobenzene [119], 1,4-dinitrobenzene [119], and 1,3,5-trinitrobenzene [141] by mass spectroscopy, NO_2 (g) is rarely observed from decomposition of substituted nitrobenzene compounds in the bulk state [7]. In a MS/MS-CID study by Yinon [113], early loss of NO_2 was detected for TNT, but not for mPA. These observations suggest that substituted nitroaromatic compounds may have alternative decomposition channels with lower activation energies than those of C–NO_2 homolysis.

The presence of a hydroxyl substituent on a neighbouring site to a nitro group opens for the possibility of intramolecular hydrogen transfer from the former to the latter. Such a tautomerisation, resulting in a quinoid or aci-structure, has been proposed as a possible reaction step in the early stages of decomposition of nitrophenols.

In a 2016 DFT study, Vereecken *et al.* [36] performed a comprehensive mapping of the ground and first excited state PESs of ortho-nitrophenol. Results for the ground state PES pointed towards the existence of several unimolecular mechanisms ending in the formation of cyclopentaketene and HONO. Ketenes are known to be extremely reactive, and are in this sense not unlikely intermediates in a series of reactions leading up to an explosion.

One of the mechanisms found by Vereecken *et al.* [36] is a one-step process occurring via a single TS, whereas the remaining mechanisms are multistep and include all from one to three different aci-structures. The multistep processes are all initiated by a tautomerisation in which ortho-nitrophenol transforms to an aci-structure. Vereecken *et al.* [36] found this reaction step to be associated with a relatively low activation energy, making it an unlikely candidate for the RDS of the multistep processes for PA, mPA, and dmPA. However, it is still an interesting step to study due to its frequent occurrence in the literature [28, 32, 60] and for the sake of comparing the different pathways. Hence, this reaction

step is treated in the current work. In addition, the steps found to be associated with high activation energies in ortho-nitrophenol, *i.e.* the steps in which cyclopentaketene and HONO are formed from either ortho-nitrophenol or an aci-structure, are investigated, with one exception: Using the notation of Reference [36], the step corresponding to the transformation of aci-NP-4 to cycloketene and HONO for ortho-nitrophenol is not studied for PA, mPA, or dmPA. This step is omitted from the current work because Vereecken *et al.* [36] found its activation energy to be significantly (about 30 kJ mol^{-1}) lower than those found for the steps in which aci-NP-2 and aci-NP-3 transform to cycloketene and HONO. Thus, the mechanism including three different aci-structures is not treated in this thesis. In addition, the step in which one aci-structure transforms into the other is not considered, since its activation energy is assumed insignificant to the overall rate based on the results of Vereecken *et al.* [36].

For the ketene-forming pathway, both reaction and activation energies are of interest. In order to calculate these quantities, geometry optimisations of both minima and TSs are required. The supplementary information provided by Vereecken *et al.* [36] to their 2016 DFT study on ortho-nitrophenol has been tremendously helpful in this context. In fact, all presently used input geometries have been created by manually adding extra nitro (and, for mPA and dmPA, methyl) groups to the optimised structures reported by Vereecken *et al.* In the constrained optimisations employed in the search for TSs, all atom positions are kept fixed except those corresponding to the manually added substituents.

Figure 4.3 displays the optimised geometries and nomenclature of the structures investigated in the study of the ketene-forming pathway. The TSs are characterised by molecule names including the TS abbreviation in Figure 4.3. Inspection of each imaginary mode confirmed each TS to connect the desired reactant and product states.

Figures 4.4, 4.5, and 4.6 display energy plots of the ketene-forming pathway for PA, mPA, and dmPA, respectively. Both the one- and multistep processes found on the PES of ortho-nitrophenol by Vereecken *et al.* [36] are identified for all three molecules. For each molecule, the largest activation energy is found for the one-step process in which HONO and Y-ket (Y $\in$ {PA, mPA, dmPA}) are formed via a single TS. The barriers to the steps in which an aci-tautomer reacts to form HONO and Y-ket are, for Y $\in$ {PA, mPA}, found to be about 90 kJ mol^{-1} lower than those associated with the one-step process. For Y = dmPA the difference is about 80 kJ mol^{-1}.

Under the assumptions that unimolecular processes are determining for impact sensitivity and that PA, mPA, and dmPA all decompose through the same mechanism, one would expect the most sensitive compound (dmPA) to be associated with the lowest activation energies and the least sensitive compound (mPA) with the highest. The energy plots shown in Figures 4.4 and 4.5 reveal that for corresponding reaction steps of PA and mPA, the associated activation energies are essentially equal. For dmPA, however, the activation energies are found to be somewhat lower, as may be observed in the energy plot shown in Figure 4.6. That is, for the tautomerisation in which dmPA reacts to aci-dmPA-2, the

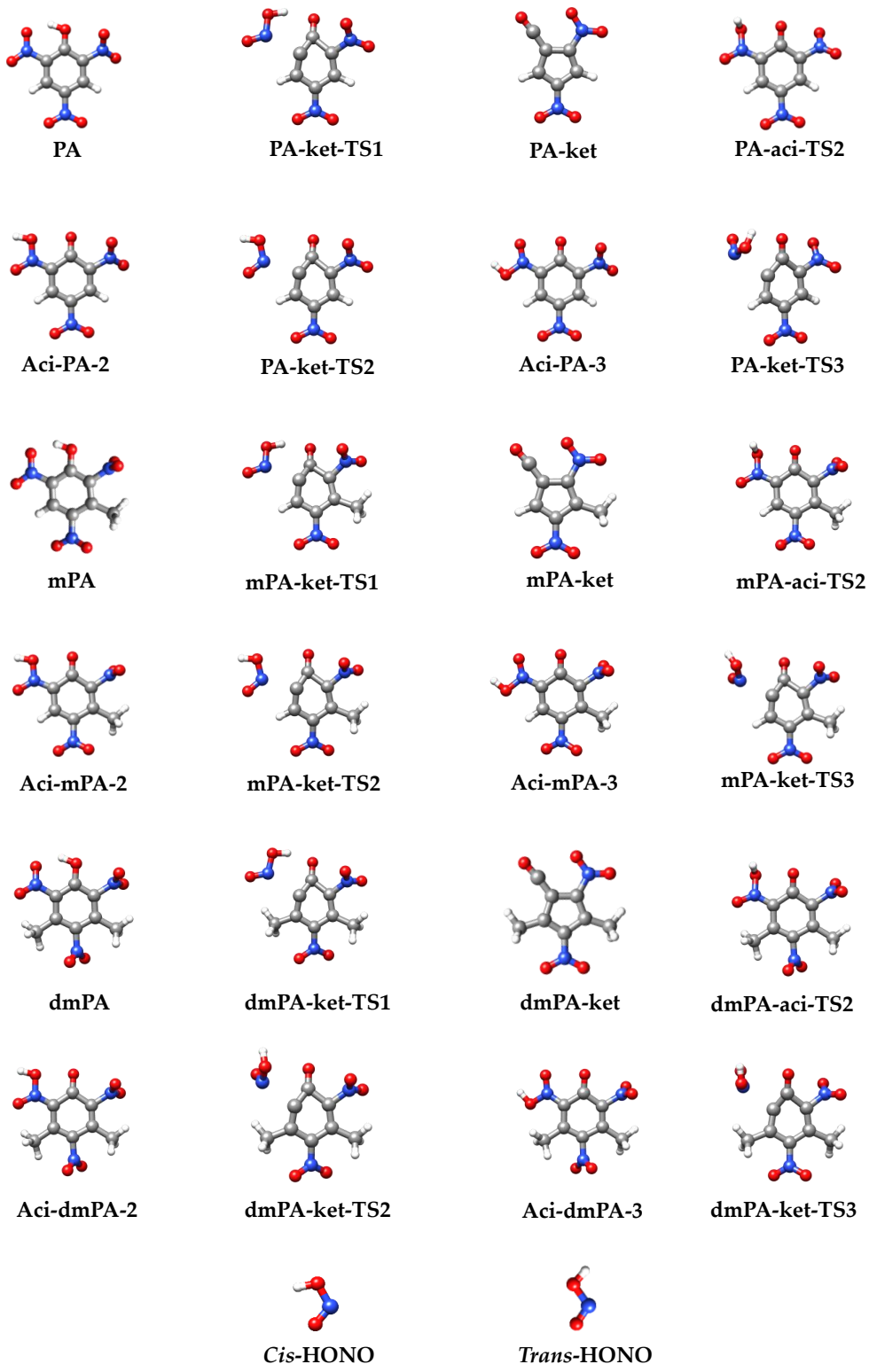

Figure 4.3: Optimised structures of the different stationary points (minima and TSs) investigated in the study of the ketene-forming pathway.

differences are so small (8 kJ mol^{-1} with respect to PA and 5 kJ mol^{-1} with respect to mPA) that they might be within the uncertainty range of the method. A larger difference in activation energies is found for the reaction steps in which

the aci-Z compounds (aci-PA-Z, aci-mPA-Z, and aci-dmPA-Z), with Z ∈ {2, 3}, reacts to form HONO and cyclopentaketene derivatives (PA-ket, mPA-ket, and dmPA-ket, respectively). Here, the calculated barriers to reaction is found to be about 30 kJ mol^{-1} lower for dmPA than for the other molecules.

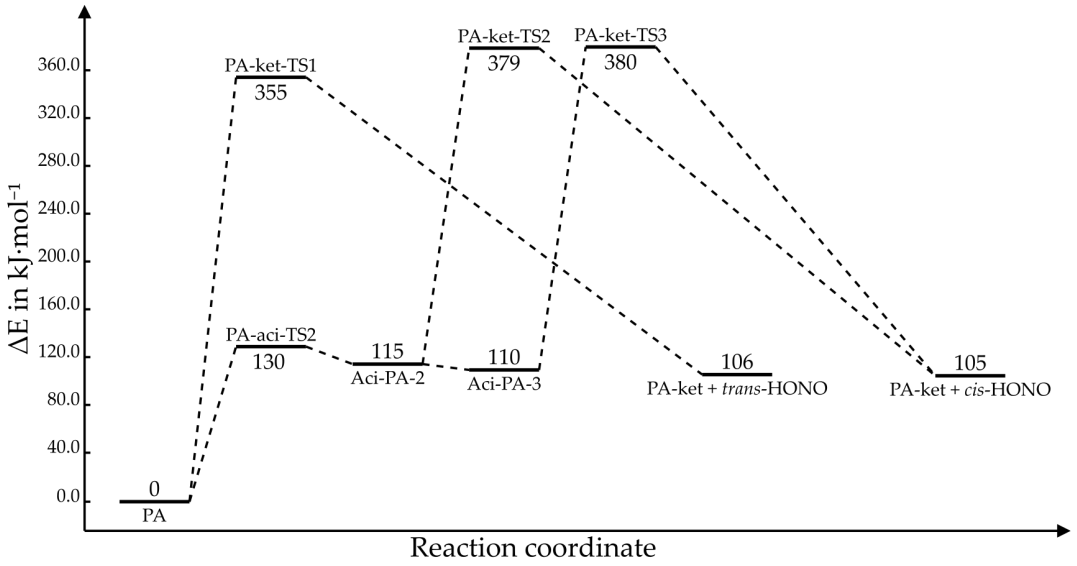

Figure 4.4: Energy plot for the ketene-forming pathway of PA. See nomenclature in Figure 4.3 and in the list of abbreviations on page xiii. A barrier to the reaction Aci-PA-2 → Aci-PA-3 is assumed, but is not calculated since it is thought to be insignificant to the total rate of reaction.

Clearly, if one considers the high-barrier steps of the energy plots in Figures 4.4, 4.5, and 4.6 simultaneously, the relative activation energies between molecules do not reflect the large variation in the species' critical impact heights. The fact that PA and mPA are found to be associated with virtually equal activation energies while displaying drastically different sensitivity behaviour may indicate that one of them, both of them, or in fact all three molecules decompose via another mechanism. For instance, it is possible that mPA and dmPA decompose via C–H α-attack — a mechanism unavailable for PA due to its lack of methyl substituents. This reaction pathway is considered in detail in Section 4.3.

While the results raise questions about whether or not these molecules decompose through this mechanism, it is still interesting to have a closer look at the tautomerisation reaction that initiate the multistep versions of the ketene-forming pathway. This reaction step has been studied for a variety of compounds containing adjacent nitro and hydroxyl groups, and correlations between impact sensitivity and activation energy have been observed [28, 60]. Due to the possibility that the first step is followed by bimolecular reactions in condensed phase explosives, studying the first step may in itself be fruitful. The activation energy obtained for each molecule is, for this reaction step, 130 kJ mol^{-1} for PA, 127 kJ mol^{-1} for mPA, and 122 kJ mol^{-1} for dmPA. A comparison of these values with the BDEs of Table 4.1 shows that the tautomerisation requires only about half the energy that is needed to homolytically cleave the C–NO_2 trigger bonds. This coincides with previous findings described by Oxley [67] among

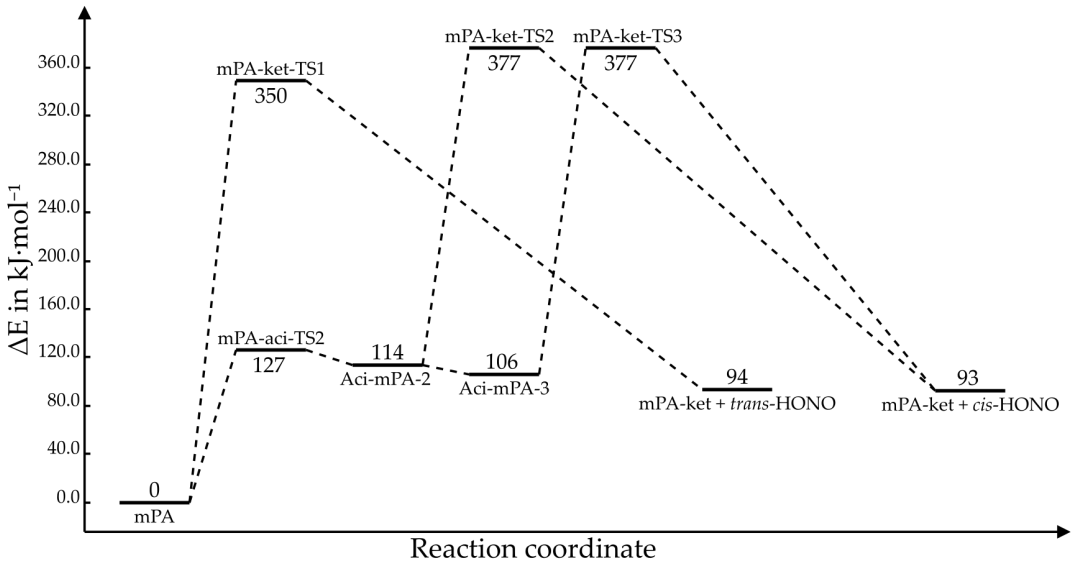

Figure 4.5: Energy plot for the ketene-forming pathway of mPA. See nomenclature in Figure 4.3 and in the list of abbreviations on page xiii. A barrier to the reaction Aci-mPA-2 → Aci-mPA-3 is assumed, but is not calculated since it is thought to be insignificant to the total rate of reaction.

others. However, the differences in activation energies between molecules are clearly insignificant and do not reflect the drastically different sensitivities that are observed experimentally.

Several studies have highlighted the first tautomerisation step as central to the decomposition of energetic materials with neighbouring nitro and hydroxyl substituents. By reaction force analyses, Murray *et al.* [29] found the aci-tautomerisation of PA to be feasible. However, they concluded that the PA $\rightleftharpoons$ aci-PA equilibrium that is formed favors the nitro form. While low activation energies are usually linked to high sensitivity, Xiong *et al.* [63] investigated the first tautomerisation step from another angle. Using DFT, they studied the idea of a reversible, intramolecular hydrogen transfer reaction in the early stages of energetic material decomposition as a possible source of *low* impact sensitivity. The idea is, in the words of the authors themselves, that "the reversibility of hydrogen transfer buffering against external stimuli to facilitate low sensitivity is implemented through two mutually reversible reactions with energy storage and release" [63]. In order for such a tautomerisation reaction to be termed reversible, Xiong *et al.* required the barrier to the hydrogen transfer to be lower than the barrier to $X-NO_2$ homolysis (where X is either C, N or O), and the barrier of the reverse hydrogen transfer to be lower than 30 kcal mol^{-1} ($\approx$ 126 kJ mol^{-1}) at ambient temperature. According to their results, the aci-tautomerisation of PA may be defined as reversible by this definition. However, they also defined PA as an insensitive explosive, and even claimed it to be less sensitive than TNT. The data presented by Storm *et al.* [37] and Wilson *et al.* [142] contradict this by agreeing that PA is definitely more impact sensitive than TNT. Under the common classification of PA as a sensitive explosive, the

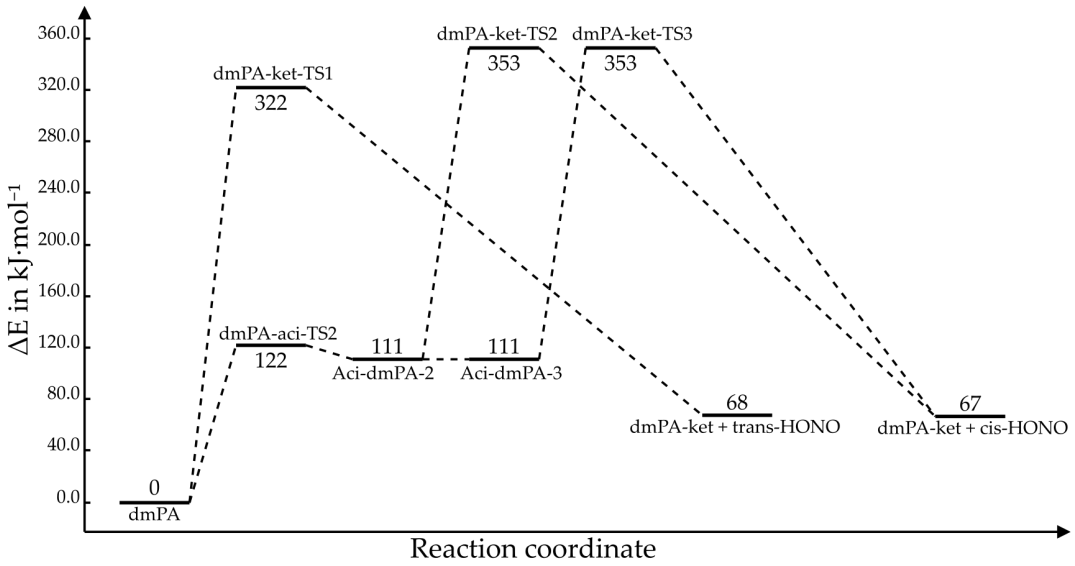

Figure 4.6: Energy plot for the ketene-forming pathway of dmPA. See nomenclature in Figure 4.3 and in the list of abbreviations on page xiii. A barrier to the reaction Aci-dmPA-2 $\rightarrow$ Aci-dmPA-3 is assumed, but is not calculated since it is thought to be insignificant to the total rate of reaction.

desensitising effect of the so-called reversible reaction does not seem to apply, or at least not to be dominant, in condensed phase PA.

As may be observed in the energy plots in Figures 4.4, 4.5, and 4.6, the barriers to the reverse reaction of the initial tautomerisation are low in all cases. Explicitly, it is 15 kJ mol^{-1} for PA, 13 kJ mol^{-1} for mPA, and only 11 kJ mol^{-1} for dmPA. The reverse reactions are clearly kinetically favoured over the reaction steps in which HONO and ketene derivatives are formed. As previously discussed, the initial tautomerisation requires significantly less energy than C$-$NO$_2$ homolysis. The barriers have also been calculated for temperature T = 298.15 K (see Section 4.4 for a more detailed discussion of the results), and they are still well below the limit of 126 kJ mol^{-1}. These results imply that PA, mPA, and dmPA all qualify for the reversible intramolecular hydrogen-transfer term as defined by Xiong *et al.* [63]. Considering the anomalously low sensitivity of mPA compared to those of PA and dmPA, one may raise questions about the validity of the claim that reversible intramolecular hydrogen transfer promotes low sensitivity. The computational results of this thesis can, of course, neither confirm nor deny that such an effect exists. However, it may be concluded that such an effect does not lead to low sensitivity in PA or dmPA.

4.3 C-H α-ATTACK PATHWAY

Similarly to how the ketene-forming pathway is thought important for the decomposition of ortho-nitrophenols, the C$-$H α-attack pathway is believed to play an important role in the decomposition of ortho-nitrotoluenes. There exists a number of clear indications that an α-CH bond ortho to the nitro substituent on an aromatic ring activates the thermal decomposition processes of

such compounds [7, 143–145]. The formation of anthranil has been observed for gas phase ortho-nitrotoluene by laser-assisted homogeneous pyrolysis [110] and in shock tube pyrolysis [111, 112]. Computational investigations on the feasibility of this pathway for TNT [5, 30] have indicated that it dominates the early phase of decomposition at temperatures below 1250–1500 K for this compound. To the knowledge of the present author, mPA and dmPA have not yet been subjects of such studies.

In a 2007 DFT study, Cohen *et al.* [5] investigated the thermal unimolecular decomposition of TNT. They studied three different reaction mechanisms: C–NO_2 homolysis, C–H α-attack, and NO_2–ONO rearrangement. The results showed that for TNT, the C–H α-attack pathway consists of four reaction steps, in which the first is a tautomerisation reaction, the second is a rotation about a C–N bond, the third is a ring closure, and the fourth and final step is the elimination of water. While the activation energies associated with the initial tautomerisation and the elimination of water were found to be similar in size, the ring closure reaction required less than half as much energy. The activation energy for the bond rotation (second reaction step) was not calculated, but is assumed to be small relative to the others based on previous studies [36, 146, 147]. In a DFT study on substituted ortho-nitrotoluenes, Fayet *et al.* [9] found that internal hydrogen transfer can occur as an alternative to the bond rotation in the second step. The activation energy of this process was, however, also found to be about half the size of those associated with the tautomerisation of the first step and H_2O elimination of the last step. Fayet *et al.* [9] also identified an additional reaction step in the mechanism. This step occurs after the initial tautomerisation but prior to the bond rotation/H-transfer, and is a rotation about the N–OH bond which activation energy was found to be insignificant (5 kJ mol^{-1}). The molecular structures of mPA and dmPA only differ from that of TNT by one and two hydroxyl substituents, respectively, and it is assumed that the second and third reaction steps identified by Cohen *et al.* [5] plus the additional step found by Fayet *et al.* [9] are unimportant for the overall rate of reaction for these molecules. For the current work, a choice was therefore made to only investigate the initial tautomerisation and the final H_2O elimination steps.

Figure 4.7 shows the optimised geometries and nomenclature of the structures treated in the study of the C–H α-attack pathway. The TSs are characterised by molecule names including the TS abbreviation in Figure 4.7. Inspection of each imaginary mode confirmed that each TS connects the desired reactant and product states.

In contrast to a hydroxyl substituent with two neighboring nitro groups, which due to its directionality may only donate its hydrogen in one direction, a methyl substituent with two neighbouring nitro groups can donate a hydrogen atom in any of the two directions. Consequently, the C–H α-attack pathway may occur in two distinct ways in mPA, and four distinct ways in dmPA.

For mPA, the present computational results show that none of the two distinct ways in which the C–H α-attack pathway may occur is kinetically favoured over the other. One of them is however slightly more thermodynamically favou-

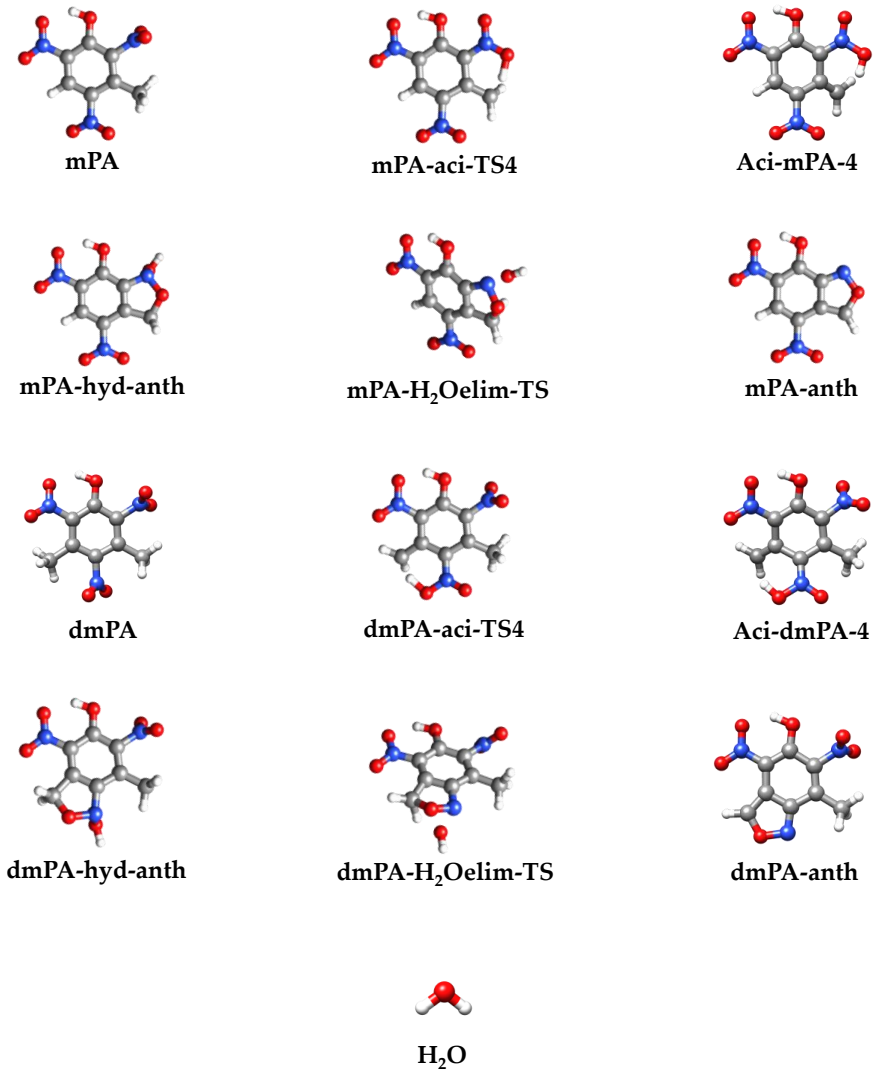

Figure 4.7: Optimised structures of the different stationary points (minima and TSs) investigated in the study of the C–H α-attack pathway.

rable, and is therefore chosen for further discussions. The molecules involved in this process are displayed in Figure 4.7. For the four distinct processes that may occur in dmPA, the lowest and highest activation energies found for the initial tautomerisation step vary with 12 kJ mol^{-1} while those found for the H_2O elimination vary with 9 kJ mol^{-1}. Conveniently, the most kinetically favourable process is also thermodynamically favoured. It is therefore chosen for further discussions, and the molecules involved are displayed in Figure 4.7.

Figures 4.8 and 4.9 show energy plots of the reaction steps of interest in the C–H α-attack pathway for mPA and dmPA, respectively. The blue-framed text boxes have been included to illustrate the intermediate steps (hydrogen transfer and ring closure reactions) that are not considered in the current work. In other

words, aci-mPA-4 does not directly connect to mPA-hyd-anth, and neither does aci-dmPA-4 to dmPA-hyd-anth. Similarly to what Cohen *et al.* [5] found for TNT at the uB3LYP/cc-pVDZ level of theory, the H_2O elimination step is found have the largest activation energy of the investigated reaction steps, both for mPA and dmPA. This also coincides with findings of Khrapkovskii *et al.* [64], who concluded based on DFT calculations that for trinitrotoluenes with an α-CH bond, the RDS of thermal decomposition is not the initial tautomerisation but rather a later reaction step.

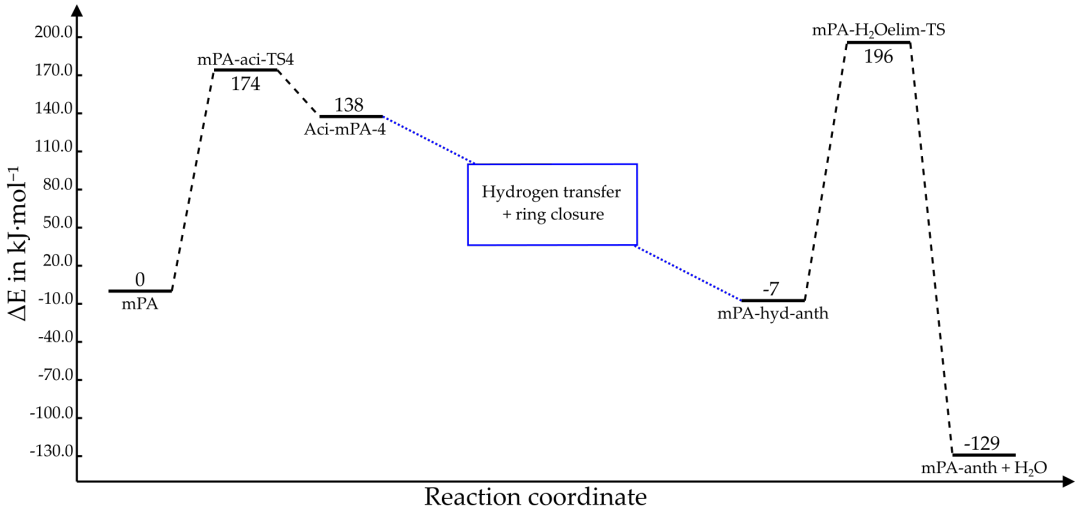

Figure 4.8: Energy plot for the C–H α-attack pathway of mPA. See nomenclature in Figure 4.7 and in the list of abbreviations on page xiii.

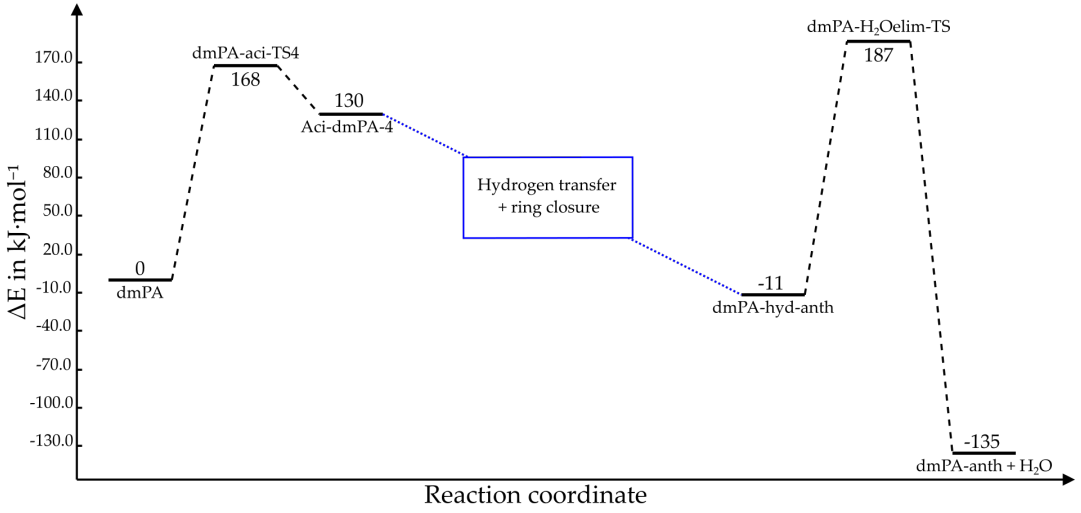

Figure 4.9: Energy plot for the C–H α-attack pathway of dmPA. See nomenclature in Figure 4.7 and in the list of abbreviations on page xiii.

By comparing the energy plots in Figures 4.8 and 4.9, one may note that the barrier to the tautomerisation of the first step is found to be 6 kJ mol^{-1} higher in mPA than in dmPA. For the H_2O elimination of the final step, the difference in barriers is found to be 5 kJ mol^{-1}. Upon assuming that the H_2O elimination step is the RDS in the decomposition of these materials, one would certainly expect

mPA to possess the highest activation energy of the two, due to being drastically less impact sensitive than dmPA. A difference of only 6 kJ mol^{-1} is, however, too small a difference to explain the drastically different sensitivity behaviour of mPA and dmPA. In fact, based on the results of previous benchmark studies [77, 95] it might even lie within the uncertainty range of the computational method.

4.4 DOMINANT REACTION PATHWAYS AND TEMPERATURE DEPENDENCE

The above sections discuss the computational results for the three different pathways separately. In this section, computational results taken at temperature 298.15 K are presented and the computational approach explained. The section is then divided into two parts, where the first discusses the relative dominance of the reaction pathways at 0 and 298.15 K, and the second focuses on the temperature dependencies of the pathways (*i.e.* how the energetics *change* as the temperature is increased from 0 to 298.15 K).

Optimally, this section would provide computational results for a number of temperatures chosen from an interval including the temperatures at which PA, mPA, and dmPA have been observed to explode (*i.e.* temperatures far higher than 298.15 K). For this thesis, however, a choice was made to not perform calculations at such high temperatures, but rather compare results taken at 0 and 298.15 K. There are several reasons for this. Firstly, the limited time frame of a master's thesis makes it challenging to give these calculations the attention they require. Secondly, the accuracy of the harmonic approximation significantly decreases with increasing temperature. Therefore, thermodynamic calculations based on static DFT at temperatures $\sim$1000 K are associated with a large degree of uncertainty. Thirdly, for reactions in which the products comprise a larger number of molecules than do the reactants, the products are to a significant extent stabilised by the entropic contribution at high temperatures. It is unclear how well (or otherwise) this represents the events taking place in the reacting explosives. Not only are PA, mPA, and dmPA believed to be in a condensed state when they start reacting, but the complex conditions in and around the hot-spots in which the reactions begin may even result in a poorly defined state of matter. Thus, as the temperature increases, the approximations made in computing the entropy (harmonic approximation, gas phase) successively becomes more crude. To summarise, gas phase calculations at high temperatures are associated with an uncertainty so large that they are not believed to add a significant amount of insight compared to results taken at temperature 298.15 K. Considering simultaneously the time frame of a master's thesis, the usefulness of these calculations does not seem to justify their cost. Therefore, results taken at temperature 298.15 K, rather than higher temperatures, are discussed in the following. Note, however, that the aim is then not to draw detailed conclusions about temperature dependence, but rather to show general tendencies.

Figures 4.10, 4.11, and 4.12 display energy plots combining all studied reaction pathways at temperatures 0 K and 298.15 K, for PA, mPA, and dmPA, respectively.

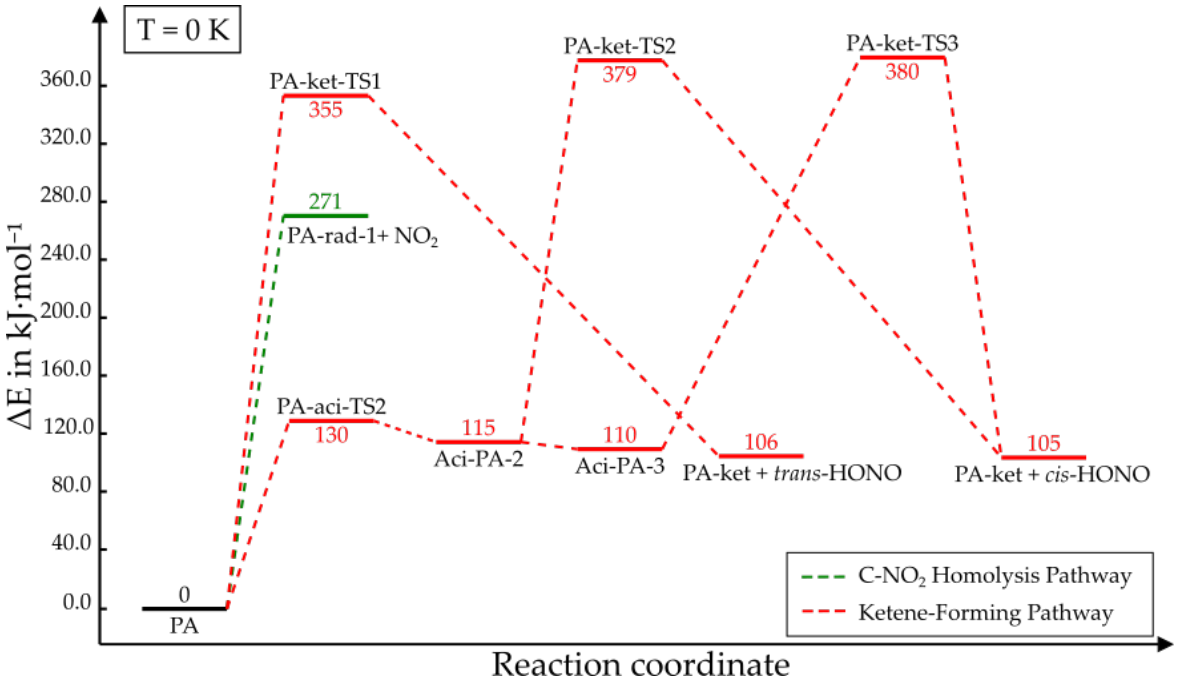

(a)

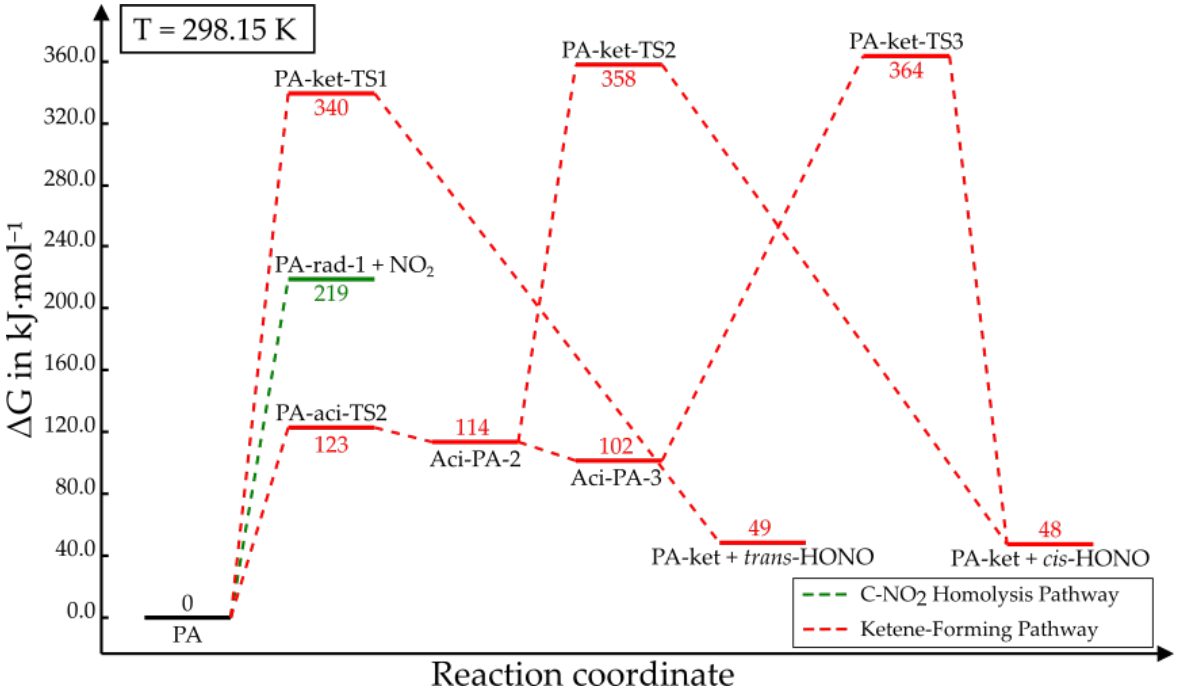

(b)

Figure 4.10: (a): Energy plot of all reaction pathways investigated for PA, at temperature T = 0 K. (b): Energy plot of all reaction pathways investigated for PA, at temperature T = 298.15 K.

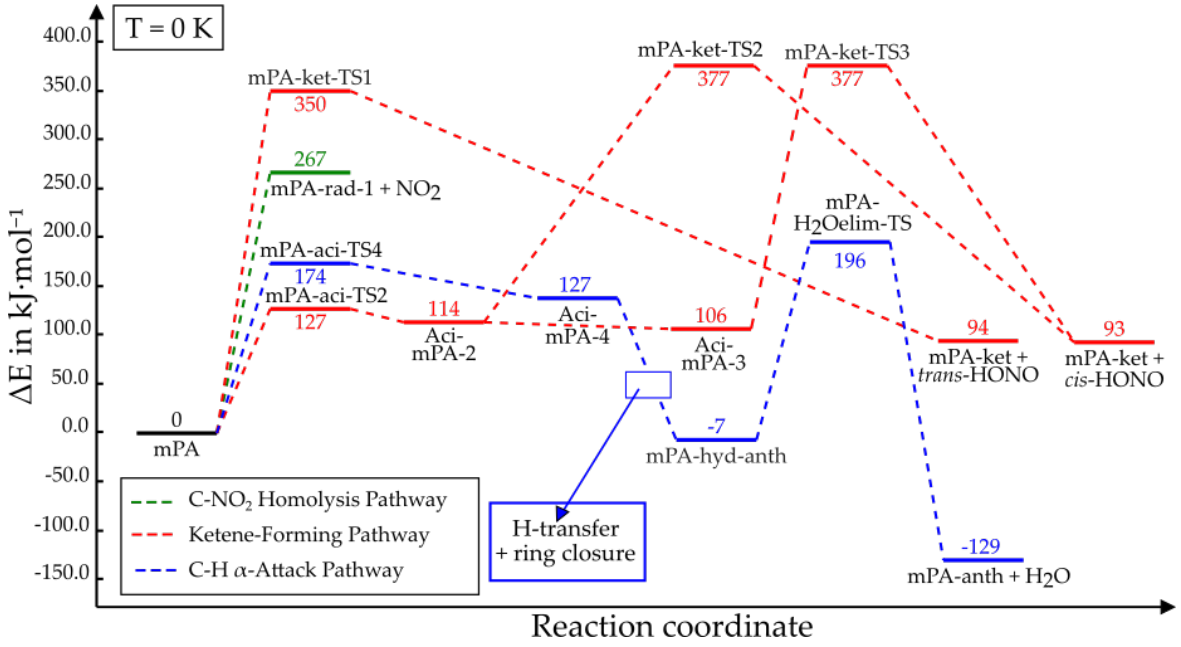

(a)

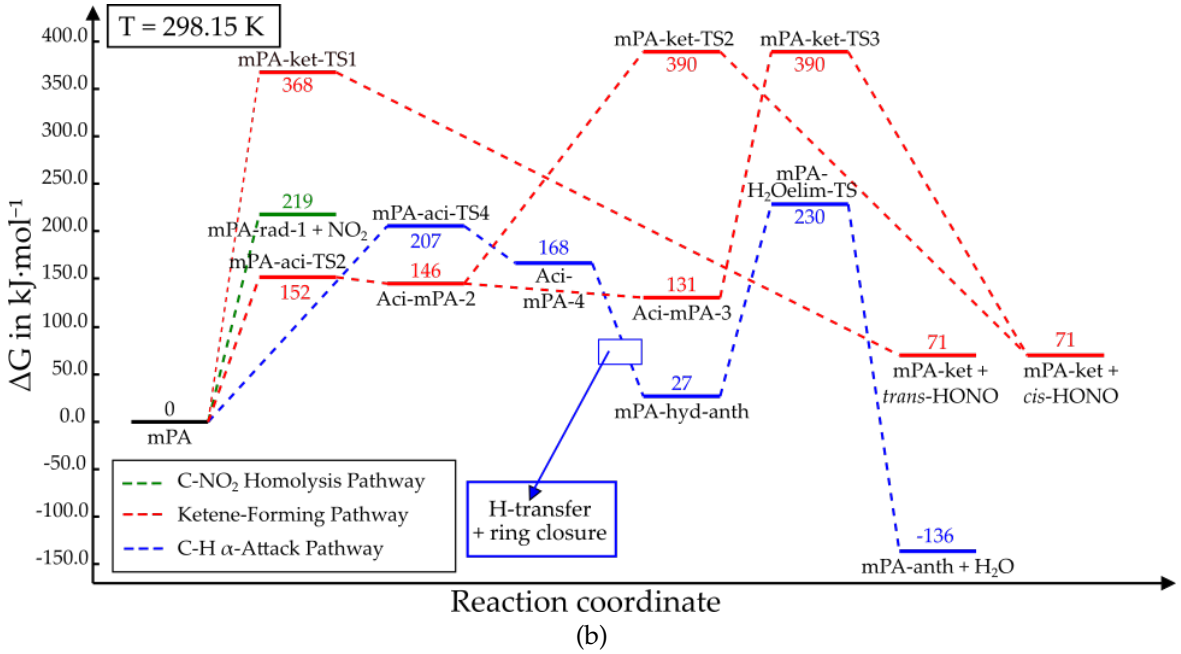

(b)

Figure 4.11: (a): Energy plot of all reaction pathways investigated for mPA, at temperature T = 0 K. (b): Energy plot of all reaction pathways investigated for mPA, at temperature T = 298.15 K.

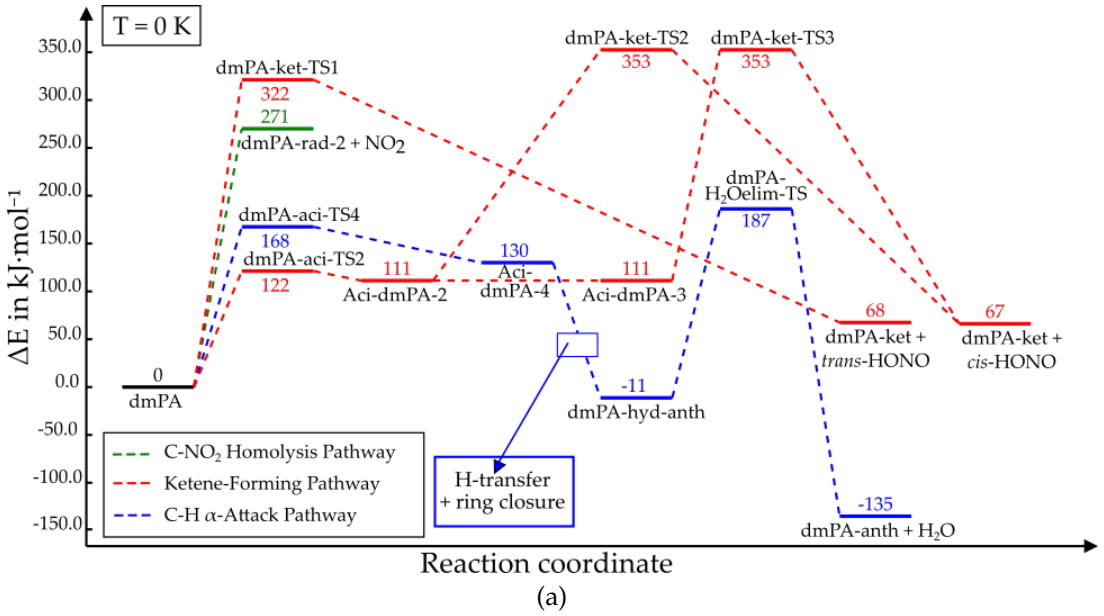

(a)

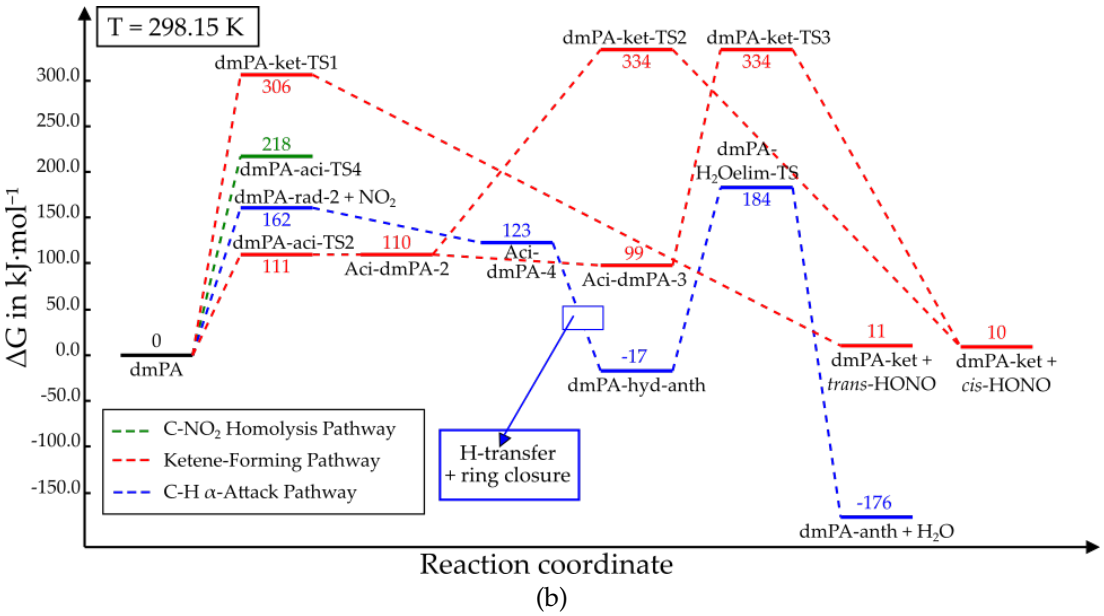

(b)

Figure 4.12: (a): Energy plot of all reaction pathways investigated for dmPA, at temperature T = 0 K. (b): Energy plot of all reaction pathways investigated for PA, at temperature T = 298.15 K.

4.4.1 RELATIVE IMPORTANCE OF REACTION PATHWAYS

By comparing results for corresponding reaction pathways for PA, mPA, and dmPA in Figures 4.10b, 4.11b, and 4.12b, one may observe that the trigger bond BDEs are essentially equal (218-219 kJ mol^{-1}) for all three compounds at temperature 298.15 K. For the C–H α-attack pathway, the activation energies found for mPA and dmPA still only differ with maximum 6 kJ mol^{-1}. Thus, as was found for absolute zero temperature, the results for these two pathways still do not reflect the large sensitivity differences observed in experiments. Lastly, for the ketene-forming pathway, the activation energies of both the one-step process and the initial tautomerisation step of the multistep processes show a trend that is somewhat consistent with the trend in the species' impact sensitivities. Based on this, it may be tempting to assume that the ketene-forming pathway dominates the early stage of decomposition of these compounds and causes the anomalous sensitivity behaviour. However, the following discussion will show that by assessing the energy changes of each pathway with the increase in temperature from 0 to 298.15 K, it seems unlikely that the ketene-forming pathway is kinetically favoured at high temperatures.

At both of the studied temperatures, the tautomerisation step initiating the multistep versions of the ketene-forming pathway has the lowest activation energy out of all reaction steps, for all three molecules. Thus, if one only considers the first step of each mechanism, that of the (multistep) ketene-forming pathway is kinetically favoured over those of the other pathways at these temperatures. However, since both the ketene-forming and C–H α-attack pathways are multistep processes, and the ketene-forming pathway additionally has parallel reactions, it is more complicated to determine which pathway dominates for each molecule. On the one hand, the high-barrier steps of the ketene-forming pathway are found to have higher activation energies than does the assumed rate-determining step of the C–H α attack pathway. On the other hand, the products of the former pathway can be formed through all from one to four reaction steps, through four somewhat parallel reaction branches. The latter pathway may occur in two distinct ways in mPA and four distinct ways in dmPA, however all of these distinct processes are comprised of the same number of steps which are all crucial for the formation of products. Since impact initiation has been claimed to result in competitive contributions of different reaction pathways for several polynitroaromatics [7], one ought to be extra careful about drawing conclusions based on gas phase calculations at low temperatures.

4.4.2 TEMPERATURE DEPENDENCE

For all molecules, the most eye-catching difference between the energy plots for absolute zero temperature and those for temperature T = 298.15 K is the lowering of the trigger bond BDE. Figure 4.10 shows that for PA, the activation Gibbs energies of the ketene-forming pathway are lowered by 7-20 kJ mol^{-1} while the trigger bond Gibbs BDE is lowered by 52 kJ mol^{-1}. Figure 4.11 shows that for mPA, the trigger bond Gibbs BDE is lowered by 48 kJ mol^{-1}. For the ketene-forming pathway, the activation Gibbs energies of the steps in which aci-

mPA-2 and aci-mPA-3 transform to mPA-ket and *cis*-HONO are lowered by 19 and 12 kJ mol^{-1}, respectively. Interestingly, the activation Gibbs energies of the one-step process and the tautomerisation of mPA into mPA-aci-2 are found to increase with the increase in temperature. For the former, the difference is 18 kJ mol^{-1}, while it is 25 kJ mol^{-1} for the latter. This behaviour separates mPA from the other two molecules for which all the activation Gibbs energies of the ketene-forming pathway decrease with increasing temperature. For the C–H α-attack pathway, the H_2O elimination step is found to have the highest activation Gibbs energy of this reaction sequence at both the studied temperatures. In fact, the Gibbs energies of mPA-hyd-anth and mPA-H_2Oelim-TS increase by an identical amount, such that the activation energy is the same for temperatures 0 and 298.15 K. However, the first step of this pathway is seen to increase with 33 kJ mol^{-1} with the change in temperature, which might indicate that this step becomes rate-determining for the C–H α-attack pathway at higher temperatures.

According to the results of Cohen *et al.* [5], the activation Gibbs energy of the assumed RDS of the C–H α-attack pathway (*i.e.* the H_2O elimination step) of TNT depends only slightly on temperature, while the C–NO_2 homolysis pathway becomes increasingly exergonic as the temperature rises and the entropic contribution becomes more important. At the same time, they found the reaction barriers of the C–H α-attack pathway to increase significantly with temperature, making C–NO_2 homolysis kinetically favoured. Thus, the temperature dependency of the C–H α-attack pathway seems to be similar for mPA and TNT.

As may be observed in Figure 4.12, the trigger bond Gibbs BDE for dmPA is found to be lowered by 48 kJ mol^{-1} as the temperature is increased from 0 to 298.15 K. Additionally, the activation energies of the ketene-forming and C–H α-attack pathways are found to decrease with all from 3 to 18 kJ mol^{-1}.

To summarise, the trigger bond Gibbs BDE is lowered to a significantly larger extent than the activation energies of the other reaction pathways, for all molecules. Thus, the C–NO_2 homolysis pathway seems to depend most strongly on temperature. Additionally, this pathway consists of only one step, in contrast to the other mechanisms (except the one-step process of the ketene-forming pathway) for which multiple steps must occur in order for the products to be formed. These results may indicate that the C–NO_2 homolysis pathway becomes kinetically favoured for all molecules as the temperature is elevated further. Such a trend would coincide with the findings of several previous computational studies on TNT [5, 30] and ortho-nitrotoluene [148], which suggest C–NO_2 homolysis to dominate the decomposition of these molecules for temperatures above $\sim$1100–1500 K.

Based on experimental studies, Brill and James [7] concluded that the initial decomposition step of PA involves the tautomer aci-PA-2 in the temperature range 418.15–623.15 K. Thus, there are indications that the ketene-forming pathway, or at least a part of it, is important for PA decomposition. However, the fact that the reaction is important in some temperature interval does not necessarily mean that it is relevant for impact sensitivity. That is, if it is an event that only

occurs to a notable extent at temperatures that are too low to initiate the self-sustained exothermic reactions that eventually leads to an explosion, it cannot be determining for the impact sensitivity. It may, however, be important for the general thermal stability of the material, which dictates how and for how long the material should be stored. That being said, the importance of the ketene-forming pathway for the impact initiation of PA cannot be ruled out based on computational results taken at only two (low) temperatures.

An additional interesting finding is how the temperature dependency of the ketene-forming and C–H α-attack pathways seem to be different for mPA than for the other molecules. The fact that the Gibbs energy of both the one-step process and aci-tautomerisation step of the ketene-forming pathway are found to increase with temperature suggests that this pathway becomes less kinetically favoured as the temperature rises. For the C–H α-attack pathway, the tautomerisation in which mPA transforms to aci-mPA-4 is found to have an activation Gibbs energy only 12 kJ mol^{-1} lower than the trigger bond Gibbs BDE at temperature T = 298.15 K. Thus, by increasing the temperature from 0 K to only 298.15 K, the difference in activation energy of these processes has decreased from 93 to 12 kJ mol^{-1}. Based on this tendency, one can only assume that a further increase in temperature up to $\sim$1000 K will both make the tautomerisation mPA $\longrightarrow$ mPA-aci-4 rate-determining for the C–H α-attack pathway and ensure that this pathway becomes the least kinetically favourable of them all. In total, these results suggest that the C–NO_2 homolysis pathway becomes more strongly kinetically favoured at a lower temperature than it does for PA and dmPA, and that the competition between the different mechanisms at elevated temperatures is stronger for the latter two compounds.

An important question that now needs to be addressed is whether the seemingly different temperature dependency of the ketene-forming and C–H α-attack pathways of mPA compared to that of the corresponding pathways of the other molecules can actually be linked to mPAs anomalously low impact sensitivity. This is the only qualitative difference found between mPA and the two other species from the present results. If the C–H α-attack pathway is crucial, this could possibly contribute towards an explanation. Intermolecular interactions are perhaps a more likely cause, as will be discussed in the following.

4.5 POSSIBLE MECHANISMS GIVING RISE TO SENSITIVITY DIFFERENCES

In the previous sections, the calculated energetics of the three unimolecular reaction pathways have been discussed in relation to the drastically varying impact sensitivities of PA, mPA, and dmPA. Few significant differences are found in the energetics of the different molecules, and the results are thus unable to explain the unexpected sensitivity behaviour that is observed experimentally. There is a possibility that the condensed phases of PA, mPA, and dmPA favour different initiation reactions than those studied in this thesis. However, it is important to note that there exists alternative mechanisms that may give rise to the experimentally observed sensitivity behaviour.

Firstly, the gas phase calculations performed in this thesis may not be representative for the unimolecular processes when they occur in the condensed phases of PA, mPA, and dmPA. If the geometry of each individual molecule in the crystal phase of any of these compounds is severely distorted from the optimised gas phase molecular geometry, this might mean that the kinetic and thermodynamic stability of the condensed phase molecules significantly differs from that of the gas phase molecules. In fact, my previous work [69] revealed that the $C-NO_2$ trigger bond BDE of mPA at absolute zero temperature is quite sensitive to the angles with which the methyl and nitro substituents twist out of the ring plane. On a somewhat related note, the steric repulsions that arise between neighbouring methyl and nitro groups on an aromatic ring has been studied by Trotter [149]. Through infrared spectroscopy experiments, he found that the twisting of nitro groups that results from such repulsions leads to lessened resonance stabilisation. On a related note, Aina *et al.* [150] found through computational investigations that the variations in NO_2 conformations that occur in crystal structures cause significant changes to the molecular charge distribution. These changes were in turn shown to affect previously proposed empirical correlations between impact sensitivity and molecular electrostatic properties. These results all illustrate that care should be taken before drawing conclusions based solely on gas phase calculations.

Secondly, how molecules are packed in the condensed phase affects the feasibility of both intra- and intermolecular hydrogen transfer. Whether the individual molecules of PA, mPA, and dmPA are approximately planar in their crystal structures or if their substituents are significantly twisted out of the molecular plane especially affects the former, while the way that the molecules are ordered with respect to their neighbour molecules in the crystal phase is crucial for the latter. If bimolecular reactions are favoured over unimolecular ones for one, two, or even all of the studied compounds, then it is no wonder that the results of this thesis alone cannot explain the observed sensitivity differences.

Spectroscopic evidence exists [151] that the nitro groups of dmPA twist significantly out of the ring plane in isoöctane (2,2,4-trimethylpentane) solution. While the crystal structure of this compound is not known to the present author, it is possible that the same holds for the crystal phase. Furman *et al.* [35] showed how bimolecular reactions can lower the activation energy for decomposition of condensed phase TNT and thus play an important role in the decomposition of this compound. There is a possibility that similar studies of PA, mPA and dmPA would yield similar results. However, without the crystal structures of mPA and dmPA, and before actually running the simulations, these will remain speculations. An important objective of future work is therefore to experimentally determine the crystal structures of mPA and dmPA (that of PA is already known). When this has been achieved, one may utilise DFT and molecular dynamics simulations to investigate the feasibility of bimolecular reaction schemes and compare them to the unimolecular ones.

There are even more reasons why the crystal structures are interesting now that gas phase calculations have been found unable to describe the sensitivities of these compounds. One feature of the crystal structure important for impact

sensitivity is crystal defects. As mentioned introductory, crystal defects form hot-spots during the fast compression and deformation of the material. Thus, a crystal with few defects is more stable and likely less sensitive than a crystal with a high density of defects. Another feature of the crystal structure believed linked to sensitivity is face-to-face π-stacking. Due to the ready sliding of this stacking to efficiently buffer against external stimuli, it is believed to promote low impact sensitivity [44, 63, 152–154]. Additionally, other solid state properties such as particle size, crystal orientation, and polymorphism are believed to affect the sensitivity of an energetic material. If neither the activation energies found for unimolecular reactions nor those obtained for bimolecular reactions for the crystal geometries can explain the observed sensitivity differences of PA, mPA, and dmPA, it is likely that such solid state effects are in fact more determining for the sensitivities of these compounds than are the stabilities of each individual molecules in the crystals. Based on experimental results, Oxley *et al.* [65] suggested this as an explanation for the extremely low sensitivity of 1,3,5-triamino-2,4,6-trinitrobenzene (TATB). Specifically, they suggested that in the condensed phase, intermolecular attractive forces may be more important than the intrinsic molecular structure, and that the thermal stability of TATB may be more a function of its lattice stability than an intrinsic property of the isolated molecule [65].

5

CONCLUSIONS AND FUTURE WORK

5.1 CONCLUSIONS

The energetics of the C–NO_2 homolysis, ketene-forming, and C–H α-attack pathways for decomposition have been investigated for PA, mPA, and dmPA at the M06-2X/def2-TZVP level of theory. The overall aim of this thesis has been to rationalise the large differences in impact sensitivity between the three compounds through gas phase calculations. Geometry optimisations of equilibrium structures and TSs have been performed for a large number of molecules, and the optimised geometries are displayed in Figures 4.1, 4.3, and 4.7. Frequency calculations have been employed to confirm each structure as either an equilibrium structure or TS and to get zero-point corrections to the energies, thermal enthalpy corrections, and calculated total entropy. The latter two quantities were calculated for temperature 298.15 K, and were used to calculate the Gibbs energy of all structures at this temperature. For the study of the C–NO_2 homolysis pathway, the BDE of each C–NO_2 bond of PA, mPA, and dmPA has been calculated. For each molecule, the bond found to have the lowest BDE was defined as the trigger bond in the gas phase. For the remaining two pathways, the relative energies of all molecules involved (see Figures 4.3 and 4.7) have been calculated and displayed in energy plots. From the plots, the activation and reaction energy of each reaction step can be explicitly calculated.

Upon assuming that PA, mPA, and dmPA decompose via the same reaction pathway, one would expect either the calculated trigger bond BDEs of the C–NO_2 homolysis pathway or the calculated activation energies of the ketene-forming pathway to correlate with the impact sensitivities of the three compounds. At absolute zero temperature, this was found not to be the case. At temperature 298.15 K, the activation energies of both the one-step process and the initial tautomerisation of the multistep versions of the ketene-forming pathway were found to correlate with impact sensitivity. However, considering how the energetics of the different pathways change with increasing temperature, it seems unlikely that the ketene-forming pathway dominates at elevated temperatures. If one were to assume that mPA and dmPA decompose via the C–H α-attack pathway while PA follows one of the other reaction schemes, the results could still not explain the strongly varying sensitivities.

Investigated in relation to the ketene-forming pathway was the idea of reversible hydrogen transfer from the hydroxyl substituent to a neighbouring nitro group, which by Xiong *et al.* [63] has been proposed to promote low impact sensitivity in ortho-nitrophenol derivatives. According to the computational results of

this thesis PA, mPA and dmPA all qualify for having their aci-tautomerisations (of the ketene-forming pathway) described as reversible by the definition of Xiong *et al.* Given the drastic variation in their impact sensitivities, it seems unlikely that such an effect plays a significant role for these compounds. While the present results can neither confirm nor deny the existence of such an effect, one may conclude that it is least not a dominating one for PA or dmPA, which are both regarded as sensitive compounds.

The temperature dependence of the reaction pathways was assessed by calculating the trigger bond Gibbs BDEs for the $C-NO_2$ homolysis pathway and the activation and reaction Gibbs energies for the other two pathways at temperature 298.15 K, and comparing the results to those found at absolute zero temperature. Since PA, mPA, and dmPA have been seen to explode at significantly higher temperatures, and since only two different temperatures are considered, no detailed conclusions can be drawn about temperature dependence based on these calculations. However, one can get an idea about the general tendencies.

By comparing the results for temperatures 0 and 298.15 K, the $C-NO_2$ homolysis pathway seems to be the pathway depending most strongly on temperature for all three compounds. As the temperature is increased, the trigger bond Gibbs BDEs are lowered significantly more than the activation Gibbs energies of the other pathways. Combined with the fact that this pathway only consists of one step, while most of the others are multistep, this might indicate that the $C-NO_2$ homolysis pathway is kinetically favoured at elevated temperatures.

There are several possible explanations why the results do not reflect the drastically varying sensitivities of PA, mPA, and dmPA. Firstly, the gas phase calculations performed in this thesis may not be representative for the studied pathways when they occur in the condensed phases of the materials. Thus, it is possible that the pathways studied here are related to impact sensitivity even though no significant trends are revealed by the gas phase calculations. Secondly, how the molecules are packed in the condensed phases, *i.e.* the crystal structure of each compound, may affect the decomposition processes in a number of ways. While twisting of functional groups out of the ring plane may affect both the $C-NO_2$ bond strength and the feasibility of intramolecular hydrogen transfer, the orientation and geometry of each molecule with respect to its neighbouring molecules affects the feasibility of bimolecular reactions. Furthermore, solid state properties like particle size, crystal orientation, and polymorphism are believed to affect the sensitivity of an energetic material. Lastly, whether or not the stacking of the molecules allow for sliding as a buffer against external stimuli may also be important.

The exact cause of the drastically varying impact sensitivities of PA, mPA, and dmPA has not been identified in this thesis. However, the present results indicate that the cause of this unexpected sensitivity behaviour likely must be found in bimolecular reactions, crystal effects, or both.

5.2 FUTURE WORK

The results of this thesis have shown that the calculated gas phase reaction and activation energies of the three studied thermal unimolecular decomposition pathways, at temperatures 0 and 298.15 K, cannot explain the observed differences in impact sensitivity for PA, mPA, and dmPA. Thus, future work ought to focus on the condensed phases.

Firstly, the crystal structures should be identified experimentally. How the molecules are packed in the condensed phase is believed to affect both the $C-NO_2$ bond strengths and the feasibility of unimolecular and bimolecular reactions. Additionally, the way in which the compounds crystallise can also give information about how likely defects are to form.

Secondly, I suggest the dynamics of initiation of the three compounds to be studied through molecular dynamics simulations. After the crystal structures have been determined, one may simulate the initiation of the condensed phases of PA, mPA, and dmPA at different temperatures.

Thirdly, it would be interesting to redo the calculations of this thesis, only with molecular geometries equal to those found in the condensed phases. This would not only be useful for further assessing the plausibility of the unimolecular pathways in the condensed phase, but could also point towards a weak point of many previously obtained correlations between impact sensitivity and molecular descriptors. Considering the work of Aina *et al.* [150] which showed that nitro group twisting leads to changes in charge distributions, which again leads to changes in previously obtained relationships, it seems likely that the same would be found for correlations based on *e.g.* the $C-NO_2$ BDE. If this was found to be the case, the need for a focus shift from purely molecular parameters to a combination of molecular and crystal parameters, would appear even clearer.

REFERENCES

[1] E. F. Pettersen, T. D. Goddard, C. C. Huang, G. S. Couch, D. M. Greenblatt, E. C. Meng, and T. E. Ferrin. "UCSF Chimera – A Visualization System for Exploratory Research and Analysis". *J Comput Chem.* 25.13 (2004), 1605–1612. DOI: 10.1002/jcc.20084.

[2] R. A. Angnes. *MechaSVG, GitHub repository*. 2020. DOI: 10.5281/zenodo.4065333.

[3] M. Själander, M. Jahre, G. Tufte, and N. Reissmann. *EPIC: An Energy-Efficient, High-Performance GPGPU Computing Research Infrastructure*. 2019. arXiv: 1912.05848 [cs.DC].

[4] E. Aprà, E. J. Bylaska, W. A. de Jong, N. Govind, K. Kowalski, T. P. Straatsma, M. Valiev, H. J. J. van Dam, Y. Alexeev, J. Anchell, V. Anisimov, F. W. Aquino, R. Atta-Fynn, J. Autschbach, N. P. Bauman, J. C. Becca, D. E. Bernholdt, K. Bhaskaran-Nair, S. Bogatko, P. Borowski, J. Boschen, J. Brabec, A. Bruner, E. Cauët, Y. Chen, G. N. Chuev, C. J. Cramer, J. Daily, M. J. O. Deegan, T. H. Dunning, M. Dupuis, K. G. Dyall, G. I. Fann, S. A. Fischer, A. Fonari, H. Früchtl, L. Gagliardi, J. Garza, N. Gawande, S. Ghosh, K. Glaesemann, A. W. Götz, J. Hammond, V. Helms, E. D. Hermes, K. Hirao, S. Hirata, M. Jacquelin, L. Jensen, B. G. Johnson, H. Jónsson, R. A. Kendall, M. Klemm, R. Kobayashi, V. Konkov, S. Krishnamoorthy, M. Krishnan, Z. Lin, R. D. Lins, R. J. Littlefield, A. J. Logsdail, K. Lopata, W. Ma, A. V. Marenich, J. Martin del Campo, D. Mejia-Rodriguez, J. E. Moore, J. M. Mullin, T. Nakajima, D. R. Nascimento, J. A. Nichols, P. J. Nichols, J. Nieplocha, A. Otero-de-la Roza, B. Palmer, A. Panyala, T. Pirojsirikul, B. Peng, R. Peverati, J. Pittner, L. Pollack, R. M. Richard, P. Sadayappan, G. C. Schatz, W. A. Shelton, D. W. Silverstein, D. M. A. Smith, T. A. Soares, D. Song, M. Swart, H. L. Taylor, G. S. Thomas, V. Tipparaju, D. G. Truhlar, K. Tsemekhman, T. Van Voorhis, Á. Vázquez-Mayagoitia, P. Verma, O. Villa, A. Vishnu, K. D. Vogiatzis, D. Wang, J. H. Weare, M. J. Williamson, T. L. Windus, K. Woliński, A. T. Wong, Q. Wu, C. Yang, Q. Yu, M. Zacharias, Z. Zhang, Y. Zhao, and R. J. Harrison. "NWChem: Past, present, and future". *J. Chem. Phys.* 152.18 (2020), 184102. DOI: 10.1063/5.0004997.

[5] R. Cohen, Y. Zeiri, E. Wurzberg, and R. Kosloff. "Mechanism of Thermal Unimolecular Decomposition of TNT (2,4,6-Trinitrotoluene): a DFT Study". *J. Phys. Chem. A* 111.43 (2007), 11074–11083. DOI: 10.1021/jp072121s.

[6] D. H. Liebenberg, A. W. Armstrong, and J. J. Gilman. "Preface". In: *Materials Research Society Symposium Proceedings volume 296: Structure and Properties of Energetic Materials*. Materials Research Society, 1992, p. ix.

[7] T. B. Brill and K. J. James. "Kinetics and Mechanisms of Thermal Decomposition of Nitroaromatic Explosives". *Chem. Rev.* 93.8 (1993), 2667–2692. DOI: 10.1021/cr00024a005.

[8] Y. Peng, X. Xiu, G. Zhu, and Y. Yang. "Predicting the Initial Thermal Decomposition Path of Nitrobenzene Caused by Mode Vibration at Moderate-Low Temperatures: Temperature-Dependent Anti-Stokes Raman Spectra Experiments and First-Principals Calculations". *J. Phys. Chem. A* 122 (2018), 8336–8343. DOI: 10.1021/acs.jpca.8b06458.

[9] G. Fayet, L. Joubert, P. Rotureau, and C. Adamo. "A Theoretical Study of the Decomposition Mechanisms in Substituted o-Nitrotoluenes". *J. Phys. Chem. A* 113 (2009), 13621–13627. DOI: 10.1021/jp905979w.

[10] M. Berthelot and P. Vieille. "Sur la Vitesse de Pragation des Phénomènes Explosifs dans les Gaz". *C. R. Acad. Sci.* 93 (1881).

[11] E. Mallard and H. le Chatelier. "Sur les Vitesses de Propagation de L'inflamation dans les Mélanges Gazeux Explosifs". *C. R. Acad. Sci.* 93 (1881).

[12] D. L. Chapman. "VI. On the Rate of Explosion in Gases". *Philos. Mag.* 47.284 (1899), 90–104. DOI: 10.1080/14786449908621243.

[13] E. Jouguet. "On the Propagation of Chemical Reactions in Gases". *J. Math. Pures Appl.* 2 (1905).

[14] R. V. Tsyshevsky, O. Sharia, and M. M. Kuklja. "Molecular Theory of Detonation Initiation: Insight from First Principles Modeling of the Decomposition Mechanisms of Organic Nitro Energetic Materials". *Molecules* 21.2 (2016). DOI: 10.3390/molecules21020236.

[15] A. L. Shoaf and C. A. Bayse. "Trigger Bond Analysis of Nitroaromatic Energetic Materials Using Wiberg Bond Indices". *J. Comput. Chem.* 39.19 (2018), 1236–1248. DOI: 10.1002/jcc.25186.

[16] Bernstein Group. *Decomposition Mechanisms for Energetic Materials*. Colorado State University. 2016. URL: https://sites.chem.colostate.edu/bernsteinlab/energetic.htm.

[17] X.-S. Song, X.-L. Cheng, and X.-D. Yang. "Relationship between the Bond Dissociation Energies and Impact Sensitivities of Some Nitro-Explosives". *Propellants Explos. Pyrotech.* 31.4 (2006), 306–310. DOI: 10.1002/prep.200600042.

[18] P. Politzer and J. S. Murray. "Chapter One – Detonation Performance and Sensitivity: a Quest for Balance". *Advances in Quantum Chemistry* 69 (2014), 1–30.

[19] T. L. Jensen, J. Moxnes, D. Christensen, and E. Unneberg. "Models for Predicting Impact Sensitivity of Energetic Materials Based on the Trigger Linkage Hypothesis and Arrhenius Kinetics". *J. Mol. Model.* 26.4 (2020). DOI: 10.1007/s00894-019-4269-z.

[20] B. M. Rice, S. Sahu, and F. J. Owens. "Density Functional Calculations of Bond Dissociation Energies for NO_2 Scission in Some Nitroaromatic Molecules". *J MOL STRUC-THEOCHEM* 583 (2002), 69–72. DOI: 10.1016/S0166-1280(01)00782-5.

[21] Z. Mei, F. Zhao, S. Xu, and X. Ju. "A Simple Relationship of Bond Dissociation Energy and Average Charge Separation to Impact Sensitivity for Nitro Explosives". *J. Serb. Chem. Soc.* 84.1 (2019), 27–40. DOI: 10.2298/JSC180404059M.

[22] J. Li. "Relationships for the Impact Sensitivities of Energetic C-Nitro Compounds Based on Bond Dissociation Energies". *J. Phys. Chem.* 114.6 (2010), 2198–2202. DOI: 10.1021/jp909404f.

[23] X.-H. Li, D.-F. Han, and X.-Z. Zhang. "Investigation of Correlation between Impact Sensitivities and Bond Dissociation Energies in Benzenoid Nitro Compounds". *J. Struct. Chem.* 54.3 (2013), 499–504. DOI: 10.1134/S0022476613030049.

[24] S.-j. Chang, H.-l. Bai, F.-d. Ren, X.-c. Luo, and J.-J. Xu. "Theoretical Prediction of the Impact Sensitivities of Energetic C-Nitro Compounds". *J. Mol. Model.* 28.6 (2020), 301–307. DOI: 10.1007/s00894-020-04481-7.

[25] S. Zeman and M. Jungová. "Sensitivity and Performance of Energetic Materials". *Propellants Explos. Pyrotech.* 41.3 (2016), 426–451. DOI: 10.1002/prep.201500351.

[26] N. R. Badders, C. Wei, A. A. Aldeeb, W. J. Rogers, and M. S. Mannan. "Predicting the Impact Sensitivities of Polynitro Compounds Using Quantum Chemical Descriptors". *J. Energ. Mater.* 24.1 (2006), 17–33. DOI: 10.1080/07370650500374326.

[27] S. Zeman and M. Krupka. "New Aspects of Impact Reactivity of Polynitro Compounds, Part III. Impact Sensitivity as a Function of the Imtermolecular Interactions". *Propellants Explos. Pyrotech.* 28.6 (2003), 301–307. DOI: 10.1002/prep.200300018.

[28] J. Fan, Z. Gu, H. Xiao, and H. Dong. "Theoretical Study on Pyrolysis and Sensitivity of Energetic Compounds. Part 4. Nitro Derivatives of Phenols". *J. Phys. Org. Chem* 11.3 (1998), 177–184. DOI: 10.1002/(SICI)1099-1395(199803)11:3<177::AID-POC990>3.0.CO;2-9.

[29] J. S. Murray, P. Lane, M. Göbel, T. M. Klapötke, and P. Politzer. "Reaction Force Analyses of Nitro-Aci Tautomerizations of Trinitromethane, the Elusive Trinitromethanol, Picric Acid and 2,4-dinitro-1 H-imidazole". *Theor Chem Acc* 124.5 (2009), 355–363. DOI: 10.1007/s00214-009-0620-2.

[30] X.-F. Chen, J.-F. Liu, Z.-H. Meng, and K.-L. Han. "Thermal Unimolecular Decomposition Mechanism of 2,4,6-trinitrotoluene: a First-Principles DFT Study". *Theor. Chem. Acc.* 127 (2010), 327–344. DOI: 10.1007/s00214-009-0720-z.

[31] P. C. Chen, W. Lo, and S. C. Tzeng. "Molecular Structures of Mononitrophenols and their Thermal Decomposition Tautomers". *J MOL STRUC-THEOCHEM* 428 (1998), 257–266. DOI: 10.1016/S0166-1280(97)00289-3.

[32] J. S. Murray, P. Lane, P. Politzer, P. R. Bolduc, and R. L. McKenney Jr. "A Computational Analysis of Some Possible Hydrogen Transfer and Intramolecular Ring Formation Reactions of o-Nitrotoluene and o-Nitroaniline". *J MOL STRUC-THEOCHEM* 209 (1990), 349–359. DOI: 10.1016/0166-1280(90)80087-5.

[33] Q. Yan, W. Zhu, A. Pang, X. Chi, X. Du, and H. Xiao. "Theoretical Studies on the Unimolecular Decomposition of Nitroglycerin". *J Mol Model* 19.4 (2013), 1617–1626. DOI: 10.1007/s00894-012-1724-5.

[34] P. C. Chen and C. W. Wu. "The Molecular Structures of Nitrotoluenes and their Thermal Decomposition Tautomers". *J MOL STRUC-THEOCHEM* 357.1 (1995), 87–95. DOI: 10.1016/0166-1280(95)04286-F.

[35] D. Furman, R. Kosloff, F. Dubnikova, S. V. Zybin, W. A. Goddard III, N. Rom, and Y. Zeiri. "Decomposition of Condensed Phase Energetic Materials: Interplay between Uni- and Bimolecular Mechanisms". *J. Am. Chem. Soc.* 136.11 (2014), 4192–4200. DOI: 10.1021/ja410020f.

[36] L. Vereecken, H. K. Chakravarty, B. Bohn, and J. Lelieveld. "Theoretical Study on the Formation of H- and O-Atoms, HONO, OH, NO, and NO_2 from the Lowest Lying Singlet and Triplet States in Ortho-Nitrophenol Photolysis". *Int. J. Chem. Kinet.* 48.12 (2016), 785–795. DOI: 10.1002/kin.21033.

[37] C. B. Storm, J. R. Stine, and J. F. Kramer. "Sensitivity Relationships in Energetic Materials". In: *Chemistry and Physics of Energetic Materials*. Ed. by S. N. Bulusu. Vol. 309. Dordrecht, The Netherlands: Kluwer Academic Publishers, 1990.

[38] D. Mathieu. "Toward a Physically Based Quantitative Modeling of Impact Sensitivities". *J. Phys. Chem. A* 117.10 (2013), 2253–2259. DOI: 10.1021/jp311677s.

[39] J. W. Dixon and A. M. Mood. "A Method for Obtaining and Analyzing Sensitivity Data". *J Am Stat Assoc* 43.241 (1948), 109–126. DOI: 10.1080/01621459.1948.10483254.

[40] R. K. Wharton and J. A. Harding. "A Study of Some Factors That Affect the Impact Sensitiveness of Liquids Determined Using the BAM Fallhammer Apparatus". *J. Hazard. Mater.* 37.2 (1994), 265–276. DOI: 10.1016/0304-3894(94)00004-2.

[41] D. D. Dlott. "Chapter 6 - Fast Molecular Processes in Energetic Materials". In: *Energetic Materials*. Ed. by P. Politzer and J. S. Murray. Vol. 13. Theoretical and Computational Chemistry. Elsevier, 2003, pp. 125–191. DOI: 10.1016/S1380-7323(03)80027-4.

[42] W. Zhu and H. Xiao. "Ab Initio Study of Energetic Solids: Cupric Azide, Mercuric Azide, and Lead Azide". *J. Phys. Chem. B* 110.37 (2006), 18196–18203. DOI: 10.1021/jp0643810.

[43] H.-H. Licht. "Performance and Sensitivity of Explosives". *Propellants Explos. Pyrotech.* 25.3 (2000), 126–132. DOI: 10.1002/1521-4087(200006)25:3<126::AID-PREP126>3.0.CO;2-8.

[44] F. Jiao, Y. Xiong, H. Li, and C. Zhang. "Alleviating the Energy & Safety Contradiction to Construct New Low Sensitivity and Highly Energetic Materials through Crystal Engineering". *CrystEngComm* 20.13 (2018), 1757–1768. DOI: 10.1039/C7CE01993A.

[45] M. H. Keshavarz. "A New General Correlation for Predicting Impact Sensitivity of Energetic Compounds". *Propellants Explos. Pyrotech.* 38.6 (2013), 754–760. DOI: 10.1002/prep.201200128.

[46] M.J. Kamlet and H. G. Adolph. "The Relationship of Impact Sensitivity with Structure of Organic High Explosives. II. Polynitroaromatic Explosives". *Propellants Explos. Pyrotech.* 4.2 (1979), 30–34. DOI: 10.1002/prep.19790040204.

[47] H. Zhang, F. Cheung, F. Zhao, and X.-L. Cheng. "Band Gaps and the Possible Effect on Impact Sensitivity for Some Nitro Aromatic Explosive Materials". *Int. J. Quantum Chem.* 109 (2009), 1547–1552. DOI: 10.1002/qua.21990.

[48] J. Edwards, C. Eybl, and B. Johnson. "Correlation between Sensitivity and Approximated Heats of Detonation of Several Nitroamines Using Quantum Mechanical Methods". *Int. J. Quantum Chem.* 100 (2004), 713–719. DOI: 10.1002/qua.20235.

[49] A. A. Denisaev, B. L. Korsunskii, V. I. Pepekin, and Y. N. Matyushin. "Impact Sensitivity of Liquid Explosives". *Combust. Explos. Shock Waves* 46.1 (2010), 74–80. DOI: 10.1007/s10573-010-0013-9.

[50] W. Zhu and H. Xiao. "First-Principles Study of Electronic, Absorption, and Thermodynamic Properties of Crystalline Styphnic Acid and its Metal Salts". *J. Phys. Chem. B* 113.30 (2009), 10315–10321. DOI: 10.1021/jp903982w.

[51] J. S. Murray, P. Lane, and P. Politzer. "Relationships between Impact Sensitivities and Molecular Surface Electrostatic Potentials of Nitroaromatic and Nitroheterocyclic Molecules". *Mol. Phys.* 85.1 (1995), 1–8. DOI: 10.1080/00268979500100891.

[52] J. S. Murray, M. C. Concha, and P. Politzer. "Links between Surface Electrostatic Potentials of Energetic Molecules, Impact Sensitivities and C–NO_2/N–NO_2 Bond Dissociation Energies". *Mol. Phys.* 107.1 (2009), 89–97. DOI: 10.1080/00268970902744375.

[53] B. M. Rice and J. J. Hare. "A Quantum Mechanical Investigation of the Relation between Impact Sensitivity and the Charge Distribution in Energetic Molecules". *J. Phys. Chem. A* 106.9 (2002), 1770–1783. DOI: 10.1021/jp012602q.

[54] C. Zhang, Y. Shu, Y. Huang, X. Zhao, and H. Dong. "Investigation of Correlation between Impact Sensitivities and Nitro Group Charges in Nitro Compounds". *J. Phys. Chem. B* 109.18 (2005), 8978–8982. DOI: 10.1021/jp0512309.

[55] C. Zhang. "Review of the Establishment of Nitro Group Charge Method and its Applications". *J. Hazard. Mater.* 161.1 (2009), 21–28. DOI: 10.1016/j.jhazmat.2008.04.001.

[56] R. S. S. Oliveira and I. Borges Jr. "Correlation between Molecular Charge Properties and Impact Sensitivity of Explosives: Nitrobenzene Derivatives". *Propellants Explos. Pyrotech.* 46.2 (2021), 309–321. DOI: 10.1002/prep.202000233.

[57] W. Zhu, X. Zhang, T. Wei, and H. Xiao. "First-Principles Study of Crystalline Mono-amino-2,4,6-trinitrobenzene, 1,3-diamino-2,4,6-trinitrobenzene, and 1,3,5-triamino-2,4,6-trinitrobenzene". *J MOL STRUC-THEOCHEM* 900 (2009), 84–89. DOI: 10.1016/j.theochem.2008.12.031.

[58] W. Zhu and H. Xiao. "First-Principles Band Gap Criterion for Impact Sensitivity of Energetic Crystals: a Review". *Struct Chem* 21.3 (2010), 657–665. DOI: 10.1007/s11224-010-9596-8.

[59] P. Politzer and J. S. Murray. "Impact Sensitivity and the Maximum Heat of Detonation". *J. Mol. Model* 21.10 (2015), 262. DOI: 10.1007/s00894-015-2793-z.

[60] G. Wang, G. Xuedong, Y. Liu, and H. Xiao. "A Theoretical Investigation on the Structures, Densities, Detonation Properties, and Pyrolysis Mechanism of the Nitro Derivatives of Phenols". *Int. J. Quantum Chem.* 110.9 (2010), 1691–1701. DOI: 10.1002/qua.

[61] L. K. Harper, A. L. Shoaf, and A. B. Craig. "Predicting Trigger Bonds in Explosive Materials through Wiberg Bond Index Analysis". *ChemPhysChem* 16.18 (2015), 3886–3892. DOI: 10.1002/cphc.201500773.

[62] M. H. Keshavarz. "Simple Relationship for Predicting Impact Sensitivity of Nitroaromatics, Nitramines, and Nitroaliphatics". *Propellants Explos. Pyrotech.* 35 (2010), 175–181. DOI: 10.1002/prep.200800078.

[63] Y. Xiong, Y. Ma, H. Xudong, X. Xianggui, and C. Zhang. "Reversible Intramolecular Hydrogen Transfer: a Completely New Mechanism for Low Impact Sensitivity of Energetic Materials". *Phys. Chem. Chem. Phys.* 21 (2019), 2397–2409. DOI: 10.1039/c8cp06350h.

[64] G. M. Khrapkovskii, E. V. Nikolaeva, D. L. Egorov, D. V. Chachkov, and A. G. Shamov. "Energy Barriers to Gas-Phase Unimolecular Decomposition of Trinitrotoluenes". *Russ. J. Org. Chem* 53.7 (2017), 999–1011. DOI: 10.1134/S1070428017070077.

[65] J. C. Oxley, J. L. Smith, H. Ye, R. L. McKenney, and P. R. Bolduc. "Thermal Stability Studies on a Homologous Series of Nitroarenes". *J. Phys. Chem.* 99 (1995), 9593–9602. DOI: 10.1021/j100023a043.

[66] J. Xu, J. Wu, H. Li, and J. Zhang. "Molecular Design of a New Family of Bridged Bis(multinitro-triazole) with Outstanding Oxygen Balance as High-Density Energy Compounds". *Int. J. Quantum Chem.* 120.1 (2020), e26056. DOI: 10.1002/qua.26056.

[67] J. C. Oxley. "A Survey of the Thermal Stability of Energetic Materials". In: *Energetic Materials Part 1. Decomposition, Crystal and Molecular Properties*. Ed. by P. Politzer and J. S. Murray. Vol. 12. Theoretical And Computational Chemistry. Amsterdam, The Netherlands: Elsevier B. V., 2003. Chap. 1.

[68] P. Politzer, J. M. Seminario, and P. R. Bolduc. "A Proposed Interpretation of the Destabilizing Effect of Hydroxyl Groups on Nitroaromatic Molecules". *Chem. Phys. Lett* 158.5 (1989), 463–469. DOI: 10.1016/0009-2614(89)87371-3.

[69] K. Wiik. *An Investigation of 3-methyl-2,4,6-trinitrophenol and its Impact Sensitivity Using Computational Quantum Chemistry*. Specialisation Project, The Norwegian University of Science and Technology (NTNU). 2020.

[70] W. Koch and M. C. Holthausen. *A Chemist's Guide to Density Functional Theory*. Weinheim, Germany: Wiley-VCH Verlag GmbH, 2001. ISBN: 3-527-60004-3.

[71] C. J. M. Pruitt and D. J. Goebbert. "The C – N Dissociation Energies of Nitrobenzene and Nitrotoluene Radical Anions and Neutrals". *Chem. Phys. Lett.* 580 (2013), 21–27. DOI: 10.1016/j.cplett.2013.06.050.

[72] F. C. Hill, L. K. Sviatenko, L. Gorb, S. I. Okovytyy, G. S. Blaustein, and J. Leszczynski. "DFT M06-2X Investigation of Alkaline Hydrolysis of Nitroaromatic Compounds". *Chemosphere* 88 (2012), 635–643. DOI: 10.1016/j.chemosphere.2012.03.048.

[73] G. M. Khrapkovskii, D. D. Sharipov, A. G. Shamov, D. L. Egorov, D. V. Chachkov, B. N. Van, and R. V. Tsyshevsky. "Theoretical Study of Substituents Effect on C – NO_2 Bond Strength in Mono Substituted Nitrobenzenes". *COMPUT THEOR CHEM* 1017 (2013), 7–13. DOI: 10.1016/j.comptc.2013.04.013.

[74] C. Qi, Q.-H. Lin, Y.-Y. Li, S.-P. Pang, and R.-B. Zhang. "C – N Bond Dissociation Energies: an Assessment of Contemporary DFT Methodologies". *J MOL STRUC-THEOCHEM* 961.1 (2010), 97–100. DOI: 10.1016/j.theochem.2010.09.005.

[75] J. Shao, X. Cheng, and X. Yang. "Density Functional Calculations of Bond Dissociation Energies for Removal of the Nitrogen Dioxide Moiety in Some Nitroaromatic Molecules". *J MOL STRUC-THEOCHEM* 755 (2005), 127–130. DOI: 10.1016/j.theochem.2005.08.008.

[76] J. Shao, X. Cheng, and X. Yang. "The C – NO_2 Bond Dissociation Energies of Some Nitroaromatic Compounds: DFT Study". *Struct Chem* 17 (2006), 547–550. DOI: 10.1007/s11224-006-9106-1.

[77] P. C. St. John, Y. Guan, Y. Kim, S. Kim, and R. S. Paton. "Prediction of Organic Homolytic Bond Dissociation Enthalpies at Near Chemical Accuracy with Sub-Second Computational Cost". *Nat Commun* 11.1 (2020), 2328–2339. DOI: 10.1038/s41467-020-16201-z.

[78] P. Atkins and R. Friedman. *Molecular Quantum Mechanics*. 5th ed. Oxford University Press, 2011. ISBN: 978-0-19-954142-3.

[79] J.B Foresman and Æ. Frisch. *Exploring Chemistry with Electronic Structure Methods*. Gaussian Inc., 1996. ISBN: 0-9636769-3-8.

[80] P. Atkins, J. de Paula, and J. Keeler. *Atkins' Physical Chemistry*. 11th ed. Oxford University Press, 2018. ISBN: 978-0-19-876986-6.

[81] B. G. Johnson and M. J. Fisch. "An Implementation of Analytic Second Derivatives of the Gradient-Corrected Density Functional Energy". *J. Chem. Phys.* 100.10 (1994), 7429–7442. DOI: 10.1063/1.466887.

[82] D. R. Hartree. "The Wave Mechanics of an Atom with a Non-Coulomb Central Field". *Math. Proc. Camb. Philos. Soc.* 24.1 (1928), 89–110; 111–132. DOI: 10.1017/S0305004100011920.

[83] V. Fock. "Näherungsmethode zur Lösung des Quantenmechanischen Mehrkörperproblems". *Z. Phys.* 61 (1930), 126–148. DOI: 10.1007/BF01340294.

[84] J. C. Slater. "Note on Hartree's Method". *Phys. Rev.* 35 (1930), 210–211. DOI: 10.1103/PhysRev.35.210.2.

[85] T. Tsuneda. *Density Functional Theory in Quantum Chemistry*. Springer, 2014.

[86] P.-O. Löwdin. "Correlation Problem in Many-Electron Quantum Mechanics I. Review of Different Approaches and Discussion of Some Current Ideas". *Adv. Chem. Phys* 2.207 (1959). DOI: 10.1002/9780470143483.ch7.

[87] C. L. Benavides-Riveros, N. N. Lathiotakis, and M. A. L. Marques. "Towards a Formal Definition of Static and Dynamic Electron Correlations". *Phys. Chem. Chem. Phys.* 19.20 (2017). DOI: 10.1039/C7CP01137G.

[88] L. H. Thomas. "The Calculation of Atomic Fields". In: *Mathematical Proceedings of the Cambridge Philosophical Society*. Vol. 23. Cambridge University Press, 1927.

[89] E. Fermi. "Eine statistische Methode zur Bestimmung einiger Eigenschaften des Atoms und ihre Anwendung auf die Theorie des periodischen Systems der Elemente". *Zeitschrift für Physik* 48.1-2 (1928), 73–79.

[90] W. Kohn and L.J. Sham. "Self-Consistent Equations Including Exchange and Correlations Effects". *Phys. Rev.* 140 (1965), A1133–A1138. DOI: 10.1103/PhysRev.140.A1133.

[91] A.R. Leach. *Molecular Modelling: Principles and Applications*. Pearson Education, 2001.

[92] J. P. Perdew, K. Burke, and M. Ernzerhof. "Generalized Gradient Approximation Made Simple". *Phys. Rev. Lett.* 77.18 (1996), 3865–3868. DOI: 10.1103/PhysRevLett.77.3865.

[93] C. Lee, W. Yang, and R. Parr. "Development of the Colle-Salvetti Correlation-Energy Formula into a Functional of the Electron Density". *Phys. Rev. B* 37.2 (1988), 785–789. DOI: 10.1103/PhysRevB.37.785.

[94] A.D. Becke. "Density-Functional Thermochemistry. III. The Role of Exact Exchange". *J. Chem. Phys.* 98.7 (1993), 5648–5652. DOI: 10.1063/1.464913.

[95] Y. Zhao and D. G. Truhlar. "The M06 Suite of Density Functionals for Main Group Thermochemistry, Thermochemical Kinetics, Noncovalent Interactions, Excited States, and Transition Elements: Two New Functionals and Systematic Testing of Four M06 Functionals and Twelve Other Functionals". *Theor. Chem. Acc.* 120 (2008), 215–241. DOI: 10.1007/s00214-007-0310-x.

[96] Y. Zhao and D. G. Truhlar. "Density Functionals with Broad Applicability in Chemistry". *Acc. Chem. Res.* 41.2 (2008), 157–167. DOI: 10.1021/ar700111a.

[97] S. F. Boys. "Electronic Wave Functions — I. A General Method of Calculation for the Stationary States of any Molecular System". *Proc. R. Soc. Lond. A* 200 (1950), 542–554. DOI: 10.1098/rspa.1950.0036.

[98] T. Helgaker, P. Jørgensen, and J. Olsen. *Molecular Electronic-Structure Theory*. John Wiley and Sons Ltd., 2000.

[99] IUPAC. *Compendium of Chemical Terminology*. 2nd ed. Compiled by A. D. McNaught and A. Wilkinson. Online version (2019-) created by S. J. Chalk. Blackwell Scientific Publications, 1997.

[100] D. A. McQuarrie and J. D. Simon. *Physical Chemistry: a Molecular Approach*. USA: University Science Books, 1997.

[101] K. J. Laidler. "Rate-Controlling Step: a Necessary or Useful Concept?" *J. Chem. Educ.* 65 (1988), 250–254. DOI: 10.1021/ed065p250.

[102] D. Y. Murzin. "Requiem for the Rate-Determining Step in Complex Heterogeneous Catalytic Reactions?" *Reactions* 1.1 (2020), 37–46. DOI: 10.3390/reactions1010004.

[103] L. S. Kassel. "Studies in Homogeneous Gas Reactions 1". *J. Phys. Chem* 32 (1928), 225–242. DOI: 10.1021/j150284a007.

[104] N. B. Slater. *Theory of Unimolecular Reactions*. Ithaca, New York: Cornell University Press, 1959.

[105] B. G. Gowenlock. "Arrhenius Factors (Frequency Factors) in Unimolecular Reactions". *Q. Rev. Chem. Soc.* 14.2 (1960), 133–145. DOI: 10.1039/QR9601400133.

[106] J. Wenograd. "The Behaviour of Explosives at Very High Temperatures". *Trans. Faraday Soc.* 57 (1961), 1612–1620.

[107] T. B. Brill, P. J. Brush, K. J. James, J. E. Shepherd, and K. J. Pfeiffer. "T-Jump/FT-IR Spectroscopy: a New Entry into the Rapid, Isothermal Pyrolysis Chemistry of Solids and Liquids". *Appl. Spectrosc.* 46.6 (1992), 900–911.

[108] A. J. B. Robertson and A. Yoffe. "Gases Liberated from Explosions Initiated by Impact". *Nature* 161 (1948), 806–807. DOI: 10.1038/161806a0.

[109] T. B. Brill, P. J. Brush, P. Gray, S. A. Kinloch, J. E. Field, and P. Gray. "Condensed Phase Chemistry of Explosives and Propellants at High Temperature: HMX, RDX and BAMO". *Philos. Trans. of the R. Soc. (Lond.) A* 339.1654 (1992), 377–385. DOI: 10.1098/rsta.1992.0043.

[110] A. C. Gonzales, C. W. Larson, D. F. McMillen, and D. M. Golden. "Mechanism of Decomposition of Nitroaromatics. Laser-Powered Homogeneous Pyrolysis of Substituted Nitrobenzenes". *J. Phys. Chem.* 89 (1985), 4809–4814. DOI: 10.1021/j100268a030.

[111] W. Tsang, W. Robaugh, and W. G. Mallard. "Single-Pulse Shock-Tube Studies on C–NO_2 Bond Cleavage during the Decomposition of Some Nitro Aromatic Compounds". *J. Phys. Chem.* 90 (1986), 5968–5973. DOI: 10.1021/j100280a101.

[112] Y. Z. He, J. P. Cui, W. G. Mallard, and W. Tsang. "Homogeneous Gas-Phase Formation and Destruction of Anthranil from o-Nitrotoluene Decomposition". *J. Am. Chem. Soc.* 110 (1988), 3759 –3762. DOI: 10.1021/ja00220a006.

[113] J. Yinon. "MS/MS of Energetic Compounds: Collision Induced Dissociation (CID) Studies of Fragmentation Processes in Energetic Molecules". In: *Chemistry and Physics of Energetic Materials*. Ed. by S. N. Bulusu, pp. 695–714.

[114] J. Yinon. "Mass Spectrometry of Explosives: Nitro Compounds, Nitrate Esters, and Nitramines". *Mass Spectr. Reviews* 1 (1982), 257–302. DOI: 10.1002/mas.1280010304.

[115] S. Meyerson, I. Puskas, and E. K. Fields. "Organic Ions in the Gas Phase. XVIII. Mass Spectra of Nitroarenes". *J. Am. Chem. Soc.* 88.21 (1996), 4974–4980. DOI: 10.1021/ja00973a036.

[116] E. K. Fields and S. Meyerson. "Reactions of Aromatic Compounds at High Temperatures". *Acc. Chem. Res.* 2.9 (1969), 273–278. DOI: 10.1021/ar50021a003.

[117] J. Stals. "Chemistry of Aliphatic Unconjugated Nitramines. Part 7.— Interrelations between the Thermal, Photochemical and Mass Spectral Fragmentation of RDX". *Trans. Faraday Soc.* 67 (1971), 1768–1775. DOI: 10.1039/TF9716701768.

[118] S. Bulusu, T. Axenrod, and G. W. A. Milne. "Electron-Impact Fragmentation of Some Secondary Aliphatic Nitramines. Migration of the Nitro Group in Heterocyclic Nitramines". *Org. Mass Spectrom.* 3.1 (1970), 13–21. DOI: 10.1002/oms.1210030103.

[119] E. K. Fields and S. Meyerson. "Mass Spectral and Thermal Reactions of Dinitrobenzenes". *J. Org. Chem.* 37.24 (1972), 3861–3866. DOI: 10.1021/jo00797a021.

[120] "Hot Spot Ignition Mechanisms for Explosives". *Acc. Chem. Res.* 25 (1992), 489–496. DOI: 10.1021/ar00023a002.

[121] A. J. B. Robertson. "The Decomposition, Boiling and Explosion of Trinitrotoluene at High Temperatures". *Trans. Faraday Soc.* 48 (1948), 977–983. DOI: 10.1039/TF9484400977.

[122] E. Catalano and P. C. Crawford. "An Enthalpic Study of the Thermal Decomposition of Unconfined Triaminotrinitrobenzene". *Thermochim. Acta* 61.1 (1983), 23–36. DOI: 10.1016/0040-6031(83)80301-3.

[123] F. Weigend and R. Ahlrichs. "Balanced Basis Sets of Split Valence, Triple Zeta Valence and Quadruple Zeta Valence Quality for H to Rn: Design and Assessment of Accuracy". *Phys. Chem. Chem. Phys.* 7.18 (2005), 3297–3305. DOI: 10.1039/B508541A.

[124] F. Weigend. "Accurate Coulomb-Fitting Basis Sets for H to Rn". *Phys. Chem. Chem. Phys.* 8.9 (2006), 1057–1065. DOI: 10.1039/B515623H.

[125] M. K. Kesharwani, B. Brauer, and J. M. L. Martin. "Frequency and Zero-Point Vibrational Energy Scale Factors for Double-Hybrid Density Functionals (and Other Selected Methods): Can Anharmonic Force Fields Be Avoided?" *J. Phys. Chem. A* 119 (2015), 1701–1714. DOI: 10.1021/jp508422u.

[126] A.D. Becke. "Perspective: Fifty Years of Density-Functional Theory in Chemical Physics". *J. Chem. Phys.* 140.18 (2014), 5648–5652. DOI: 10.1063/1.4869598.

[127] Y. Zhao, N. González-García, and D. G. Truhlar. "Benchmark Database of Barrier Heights for Heavy Atom Transfer, Nucleophilic Substitution, Association, and Unimolecular Reactions and its Use to Test Theoretical Methods". *J. Phys. Chem. A* 109.9 (2005), 2012–2018. DOI: 10.1021/jp045141s.

[128] Y. Zhao and D. G. Truhlar. "Design of Density Functionals That Are Broadly Accurate for Thermochemistry, Thermochemical Kinetics, and Nonbonded Interactions". *J. Phys. Chem. A* 109.25 (2005), 5656–5667. DOI: 10.1021/jp050536c.

[129] C. E. Check and T. M. Gilbert. "Progressive Systematic Underestimation of Reaction Energies by the B3LYP Model as the Number of C-C Bonds Increases: Why Organic Chemists Should Use Multiple DFT Models for Calculations Involving Polycarbon Hydrocarbons". *J. Org. Chem.* 70 (2005), 9828–9834. DOI: 10.1021/jo051545k.

[130] E. I. Izgorodina, M. L. Coote, and L. Radom. "Trends in R–X Bond Dissociation Energies (R = Me, Et, i-Pr, t-BU; X = H, CH_3, OCH_3, OH, F): a Surprising Shortcoming of Density Functional Theory". *J. Phys. Chem. A.* 109.33 (2005), 7558–7566. DOI: 10.1021/jp052021r.

[131] The Truhlar Group. *Density Functionals from the Truhlar Group*. 2020. URL: https://comp.chem.umn.edu/info/DFT.htm.

[132] Y. Zhao and D. Truhlar. "How Well Can New-Generation Density Functionals Describe the Energetics of Bond-Dissociation Reactions Producing Radicals?" *J. Phys. Chem. A* 112.6 (2008). DOI: 10.1021/jp7109127.

[133] B. Narayanan, P. C. Redfern, R. S. Assary, and L. A. Curtiss. "Accurate Quantum Mechanical Energies for 133000 Organic Molecules". *Chem. Sci.* 10 (2019), 7449–7455. DOI: 10.1039/C9SC02834J.

[134] M. Mancinelli, R. Franzini, A. Renzetti, E. Marotta, C. Villani, and A. Mazzanti. "Determination of the Absolute Configuration of Conformationally Flexible Molecules by Simulation of Chiro-Optical Spectra: a Case Study". *RSC. Adv.* 9 (2019), 18165–18175. DOI: 10.1039/C9RA03526E.

[135] R. Wałęsa and M. A. Broda. "The Influence of Solvent on Conformational Properties of Peptides with Aib Residue — a DFT study". *J. Mol. Model* 23.12 (2017). DOI: 10.1007/s00894-017-3508-4.

[136] K. N. Kirschner, D. Reith, and W. Heiden. "The Performance of Dunning, Jensen, and Karlsruhe Basis Sets on Computing Relative Energies and Geometries". *Soft Mater* 18 (2020), 200–214. DOI: 10.1080/1539445X.2020.1714656.

[137] "Transition State Structure of the Reaction of Homolytic Dissociation of the C–N Bond and Competition between Different Mechanisms of the Primary Act of Gas-Phase Monomolecular Decomposition of Nitrobenzene". *Russ. Chem. Bull., Int. Ed.* 68 (8 2019), 1510–1519. DOI: 10.1007/s11172-019-2585-1.

[138] W. J. Hehre, R. Ditchfield, and J. A. Pople. "Self-Consistent Molecular Orbital Methods. XII. Further Extensions of Gaussian-Type Basis Sets for Use in Molecular Orbital Studies of Organic Molecules". *J. Chem. Phys.* 56 (1972), 2257–2261. DOI: 10.1063/1.1677527.

[139] P. C. Hariharan and J. A. Pople. "The Influence of Polarization Functions on Molecular Orbital Hydrogenation Energies". *Theor. Chim. Acta* 28 (1973), 213–222. DOI: 10.1007/bf00533485.

[140] E. McCarthy and K. O'Brien. "Pyrolysis of Nitrobenzene". *J. Org. Chem.* 45.11 (1980), 2086–2088. DOI: 10.1021/jo01299a010.

[141] S. Meyerson, R. W. Vander Haar, and E. K. Fields. "Organic Ions in the Gas Phase. XXVI. Decomposition of 1,3,5-Trinitrobenzene under Electron Impact". *J. Org. Chem.* 37.25 (1972), 4114–4119.

[142] W. S. Wilson, D. E. Bliss, S. L. Christian, and D. J. Knight. "Explosive Properties of Polynitroaromatics" (1990).

[143] S. Zeman. "Kinetic Data from Low-Temperature Thermolysis in the Study of the Microscopic Initiation Mechanism of the Detonation of Organic Polynitro Compounds". *Thermochim. Acta* 49.2 (1981), 219–246. DOI: 10.1016/0040-6031(81)80176-1.

[144] J. C. Dacons, H. G. Adolph, and M. J. Kamlet. "Novel Observations Concerning the Thermal Decomposition of 2,4,6-Trinitrotoluene". *J. Phys. Chem.* 74.16 (1970), 3035–3040. DOI: 10.1021/j100710a002.

[145] R. N. Rogers. "Combined Pyrolysis and Thin Layer Chromatography — a Method for the Study of Decomposition Mechanisms". *Anal. Chem.* 39.7 (1967), 730–733. DOI: 10.1021/ac60251a036.

[146] P. C. Chen and S. C. Chen. "Theoretical Study of the Internal Rotational Barriers in Nitrobenzene, 2-Nitrotoluene, 2-Nitrophenol, and 2-Nitroaniline". *Int. J. Quantum Chem.* 83.6 (2001), 332–337. DOI: 10.1002/qua.1069.

[147] P. C. Chen and S. C. Chen. "Theoretical Study of the Internal Rotational Barriers in Nitrotoluenes, Nitrophenols, and Nitroanilines". *Computers & Chemistry* 26.2 (2002), 171–178. DOI: 10.1016/S0097-8485(01)00105-X.

[148] S. C. Chen, S. C. Xu, E. Diau, and M. C. Lin. "A Computational Study on the Kinetics and Mechanism for the Unimolecular Decomposition of o-Nitrotoluene". *J. Phys. Chem. A* 110.33 (2006), 10130–10134. DOI: 10.1021/jp0623591.

[149] J. Trotter. "Steric Inhibition of Resonance: V. Nitromesitylene". *Can. J. Chem.* 37.9 (1959), 1487–1490. DOI: 10.1139/v59-218.

[150] A. A. Aina, A. J. Misquitta, M. J. S. Phipps, and S. L. Price. "Charge Distributions of Nitro Groups Within Organic Explosive Crystals: Effects on Sensitivity and Modeling". *ACS Omega* 4 (2019), 8614–8625. DOI: 10.1021/acsomega.9b00648.

[151] C. E. Moore and R. Peck. "Effects of Steric Hindrance on Ultraviolet Absorption Spectra and Ionization Constants Through Mono- and Di-Alkyl Substitution In 2,4,6-trinitrophenol". *J. Org. Chem.* 20 (1955), 673–679. DOI: 10.1021/jo01123a020.

[152] C. Zhang, X. Wang, and H. Huang. "Pi-Stacked Interactions in Explosive Crystals: Buffers against External Mechanical Stimuli". *J. Am. Chem. Soc.* 130.26 (2008), 8359–8365. DOI: 10.1021/ja800712e.

[153] Y. Ma, A. Zhang, C. Zhang, D. Jiang, Y. Zhu, and C. Zhang. "Crystal Packing of Low-Sensitivity and High-Energy Explosives". *Cryst. Growth Des.* 14.9 (2014), 4703–4713. DOI: 10.1021/cg501048v.

[154] B. Tian, Y. Xiong, L. Chen, and C. Zhang. "Relationship between the Crystal Packing and Impact Sensitivity of Energetic Materials". *CrystEngComm* 20.6 (2018), 837–848. DOI: 10.1039/C7CE01914A.

SUPPLEMENTARY INFORMATION FOR THE MASTER'S THESIS:

UNIMOLECULAR DECOMPOSITION REACTIONS OF PICRIC ACID AND ITS METHYLATED DERIVATIVES – A DFT STUDY

By Kristine Wiik[a]

Supervised by Ida-Marie Høyvik[a], Ole Swang[b], and Erik Unneberg[c]

---

a: The Department of Chemistry, NTNU. 7034 Trondheim, Norway.
b: SINTEF Industry. 0314 Oslo, Norway.
c: The Norwegian Defence Research Establishment. 2007 Kjeller, Norway.

All calculations have been performed using NWChem [1]. The author acknowledges the computing resources provided by the IDUN/EPIC computing cluster [2] as well as those provided by UNINETT Sigma2 – the National Infrastructure for High Performance Computing and Data Storage in Norway.

CONTENTS

Example input files

Input for geometry optimisation of equilibrium structure (*cis*-HONO) followed by a frequency calculation for the optimised structure:

```
start GeomOpt
title cis-HONO_GeomOpt

geometry start units angstrom
O         -4.40056       -0.04878        0.05760
N         -3.09907        0.05132        0.00000
H         -4.72389       -0.52312        0.83950
O         -2.50663       -1.27428        0.14229
end

charge 0

set geometry start

basis
 * library def2-tzvp
end

driver
 print low
 maxiter 150  #Had to be raised to 250-300 for some optimisations to converge
 xyz          #To construct an xyz-file for the geometry of each optimisation step
end


dft
 xc m06-2x
 maxiter 110 #Had to be raised to 250-300 for some optimisations to converge
end

task dft optimize

task dft freq
```

Input for constrained geometry optimisation of transition state (PA-aci-TS2):

```
start ConsGeomOpt
title PA-aci-TS2_ConsGeomOpt

geometry start units angstrom noautoz             # noautoz must be provided for
C         -2.55408       -0.15319        0.08618  # the 'constraints' block to work
C         -1.86933       -1.42362       -0.00183
C         -0.52780       -1.47276       -0.05138
C          0.23697       -0.25529       -0.00080
C         -0.42926        1.07777       -0.04955
C         -1.88872        1.01281        0.08274
H         -3.63448       -0.15395        0.15075
N         -2.44735       -2.33609       -0.00768
H          0.01284       -2.40626       -0.09185
N         -2.39323        1.96751        0.12772
O          0.14572        2.12984       -0.25151
H          2.69462        1.05847       -0.45297
N          1.56097       -0.37994        0.02010
O          2.27830        0.74462        0.36338
O          2.20524       -1.39752       -0.14423
O         -1.87002        2.80146        0.12311
O         -3.37602        2.00324        0.17330
O         -1.81854       -3.13649       -0.07371
O         -3.07923       -2.33317       -0.80838
end

charge 0

set geometry start

basis
 * library def2-tzvp
end

driver
 print low
 maxiter 150
 xyz
end

constraints one
 fix atom 1 2 3 4 5 6 7 9 11 12 13 14 15    # Fixing atom positions corresponding
end                                         # to the optimised structure reported
                                            # by Cohen et al. [3]. I.e. only opti-
set constraints one                         # the manually added functional groups

dft
 xc m06-2x
 maxiter 110
end

task dft optimize
```

Input for saddle point optimisation of transition state (PA-aci-TS2) followed by a frequency calculation for the optimised structure:

```
start SaddleGeomOpt
title PA-aci-TS2_SaddleGeomOpt

geometry start units angstrom                    # Output from previous constrained
 C    0.66354605     1.45865877     0.16594478   # geometry optimisation
 C   -0.78196039     1.43557950     0.14146643
 C   -1.44368458     0.26926290     0.06147039
 C   -0.71232738    -0.96874962     0.01557580
 C    0.77411662    -0.98370788    -0.10082192
 C    1.39245551     0.33521725     0.07191328
 H    1.16178317     2.41511333     0.25753339
 N    1.51722859     2.69747473     0.23471167
 H   -2.52195760     0.21776737     0.06668542
 N    2.85315418     0.43282325     0.16240589
 O    1.43453978    -1.96463569    -0.38342237
 H   -0.69527656    -3.72825551    -0.58049727
 N   -1.42984284    -2.08861653     0.01109152
 O   -0.74602402    -3.25708491     0.26429528
 O   -2.63584328    -2.18735849    -0.10453799
 O    3.41031346    -0.40033973     0.82816234
 O    3.37344552     1.36481627    -0.40704368
 O   -2.72290116     2.64059719     0.20311354
 O   -0.85698937     3.70497096     0.33667673
end

set geometry start

basis
 * library def2-tzvp
end

driver
 print low
 maxiter 150     # Had to be raised to 250-300 for some optimisations to converge
 inhess 2        # Telling NWChem that the initial Hessian in the saddle point
end              # optimisation should be fetched from the first frequency
                 # calculation


dft
 xc m06-2x
 maxiter 110     # Had to be raised to 250-300 for some optimisations to converge
end

task dft freq

task dft saddle

task dft freq
```

Input for frequency calculation for transition state (PA-aci-TS2) with stricter DFT convergence criteria and enlargened grid. (To be used for those transition states which do not converge using the standard convergence criteria and grid):

```
start Freq_Tight-DFT
title PA-aci-TS2_Freq_Tight-DFT

geometry start units angstrom
 C  1.20770090     0.87090695     0.01515070
 C -0.06072119     1.53394893     0.00077544
 C -1.23013465     0.86779793    -0.01162115
 C -1.20437509    -0.55490522    -0.01962353
 C  0.05983867    -1.32720654    -0.17712242
 C  1.25028844    -0.46805468    -0.01459580
 H  2.11861256     1.45296252     0.05525025
 N -0.07787871     3.00171925     0.04692204
 H -2.17274377     1.39629894     0.01770003
 N  2.56257589    -1.12374048     0.06997431
 O  0.11503151    -2.48408552    -0.51292742
 H -2.53448802    -3.00702590    -0.46772638
 N -2.39177864    -1.18165376     0.01902308
 O -2.35485450    -2.50928519     0.34740523
 O -3.47629647    -0.68057337    -0.11032853
 O  2.61252245    -2.14676430     0.70309197
 O  3.49252244    -0.56769333    -0.46838237
 O -1.15492345     3.54839516     0.03108939
 O  0.99477916     3.55736664     0.09631404
end

set geometry start

basis
 * library def2-tzvp
end

dft
 xc m06-2x
 maxiter 200                     # Had to be raised to 300 for some optimisations
 convergence energy 1e-8         # to converge
 convergence density 1e-6
 convergence gradient 1e-4
 tolerances acccoul 16
 grid huge
 grid lebedev N 100 17 O 100 17 C 100 17 H 100 17
end

freq
 animate
end

task dft freq
```

Optimised molecular geometries

All optimised geometries are given in the XYZ file format in unit Å, and have been optimised at the M06-2X/def2-TZVP level of theory.

PA

```
19
Stoichiometry = C6H3N3O7
 O  0.02647055    -2.57468690    -0.08386357
 O  3.49557995    -0.40331294     0.00501222
 O -3.37178190    -0.77051152    -0.59593846
 O  2.56744264    -2.32924895    -0.10327736
 O -2.51146833    -2.29252947     0.66038734
 O  0.95393175     3.59111568     0.06156740
 O -1.19537590     3.51524572     0.04587018
 N  2.52507166    -1.10549728    -0.03691604
 N -2.46051455    -1.27740155     0.01588896
 N -0.10133218     3.00440628     0.04476792
 C  1.20661751    -0.47372591    -0.00924049
 C -1.17833684    -0.55185262    -0.00348749
 C  0.03627665    -1.26467172    -0.02125898
 C -0.05104614     1.53523034     0.02122127
 C  1.17208792     0.90885875     0.01990008
 C -1.23676615     0.81962766    -0.00354541
 H  2.08980071     1.47896972     0.03359205
 H -2.19202324     1.32544097    -0.02085071
 H  0.95830427    -2.88259106    -0.11777106
```

mPA

```
22
Stoichiometry = C7H5N3O7
 O -1.05324049    -2.43320069     0.04148677
 O -3.21779051    -0.16942477     1.01137399
 O -3.13791189    -0.56260509    -1.10595929
 O  2.54560759     2.60013155    -0.42058338
 O  0.80130011     3.51217471     0.43799842
 O  3.04994879    -2.06843384     0.06254329
 O  1.34660699    -3.36897680     0.07102392
 N -2.64169712    -0.30334193    -0.03929288
 N  1.41118308     2.56723498    -0.00676238
 N  1.86560063    -2.25786687     0.05240628
 C -0.67727145     1.17805096    -0.03473422
 C -1.17922774    -0.10793710    -0.01847458
 C  0.72674338     1.26447975    -0.02268221
 C -0.41646809    -1.27849912     0.01326418
 C  0.97528030    -1.10550481     0.01612397
 C  1.53983876     0.15638908    -0.01246445
 C -1.61025655     2.35193216    -0.09228506
 H  2.61427746     0.26622094    -0.02021061
 H -2.60127615     2.04376055    -0.41555138
 H -1.68695720     2.81130043     0.89267094
 H -1.23330033     3.11248350    -0.77047790
 H -0.38389654    -3.14862712     0.06053599
```

dmPA

```
25
```

Stoichiometry = C8H7N3O7

O	0.61621885	-2.66408937	0.04422077
O	-0.42785942	3.41069406	0.84217701
O	-1.39736030	3.06806330	-1.04762878
O	-2.06005275	-2.63746471	1.14430435
O	3.56109242	0.01962054	0.48449922
O	-2.66012663	-2.17043160	-0.87156343
O	3.02842752	-1.89385410	-0.30699474
N	-0.75309394	2.71358749	-0.08895255
N	-1.97644804	-2.02118938	0.11290704
N	2.74878559	-0.75672988	0.06007918
C	1.01478262	1.01389721	-0.06004656
C	-1.36562422	0.35502111	0.00683767
C	-0.33931175	1.29979993	-0.04657004
C	-0.95913886	-0.95892402	0.05212454
C	1.34972177	-0.34975058	-0.00458991
C	0.37521822	-1.36381509	0.02946455
C	2.02789509	2.11811627	-0.20576493
C	-2.81484861	0.74470971	0.02412076
H	2.47747765	2.35411039	0.75779806
H	2.82971536	1.81976885	-0.87673383
H	1.56062961	3.01713219	-0.59861426
H	-3.43176459	-0.05062355	0.43511467
H	-2.96334527	1.64662304	0.61722116
H	-3.14972729	0.95363078	-0.99243653
H	1.56917517	-2.80322014	-0.12560528

PA-rad-1

16

Stoichiometry = C6H3N2O5

O	-1.85229825	-2.38908093	-0.00798288
O	2.24113071	-1.86967375	0.02141727
O	0.58816081	-3.23072871	-0.01425412
O	1.58505345	2.83807735	0.00035084
O	-0.40216026	3.65705093	-0.00194646
N	1.06369702	-2.10050226	0.00229063
N	0.38133802	2.73614649	-0.00081438
C	0.12881375	-0.97797495	-0.00120670
C	-2.03336777	-0.05055955	-0.00603462
C	-1.26296098	-1.20616032	-0.00532086
C	-0.18372955	1.37926132	-0.00116871
C	0.66765415	0.30304189	0.00080037
C	-1.57477828	1.22301798	-0.00384251
H	1.73816085	0.44356165	0.00350914
H	-2.22163108	2.09028767	-0.00419806
H	-1.15266118	-3.07262757	-0.01249696

PA-rad-2

16

Stoichiometry = C6H3N2O5

O	-1.73487036	0.06598779	-0.13615217
O	0.30546948	-3.48250321	0.03056532
O	0.21685169	3.39540676	-0.57632959
O	-1.57961159	-2.48647318	-0.14843041
O	-1.38205771	2.59900919	0.62304438
N	-0.35802621	-2.48341400	-0.03655905
N	-0.34758627	2.50198160	0.01516688
C	0.32173356	-1.19236064	0.01595122
C	0.33029849	1.19464866	0.02086395
C	-0.42103842	0.00599858	-0.02351729
C	2.34755576	-0.00723154	0.12027962

```
 C  1.71438805    -1.21084687     0.09701169
 C  1.71160038     1.20689703     0.07134485
 H  2.23067632    -2.16055825     0.12965616
 H  2.23193571     2.15601283     0.07195506
 H -2.07275209    -0.85233146    -0.18320896
```

PA-rad-3

```
16
Stoichiometry = C6H3N2O5
 O  1.79882318    -2.41935982    -0.11508166
 O -2.16532594    -1.93423620    -0.43397866
 O -0.66909900    -3.15775719     0.50967183
 O  0.35782625     3.65223742     0.02155291
 O -1.61721203     2.80642077     0.07919228
 N -1.06137415    -2.12887589     0.01984052
 N -0.41353725     2.72081726     0.03784766
 C  2.01779780    -0.04006823    -0.06123451
 C -0.12414343    -0.99313297    -0.01083053
 C  1.26257410    -1.19853514    -0.05262899
 C  0.16822169     1.37085813     0.00467703
 C  1.55486942     1.23605117    -0.02977242
 C -0.67167382     0.27812680     0.00452769
 H  2.19380388     2.10883879    -0.03337016
 H -1.74434686     0.40318008     0.01630925
 H  2.75823130    -2.34369334    -0.18998706
```

mPA-rad-1

```
19
Stoichiometry = C7H5N2O5
 O -1.98748209    -2.32811905    -0.06199827
 O  2.18384682     2.29753047    -0.14303276
 O  0.42039660     3.46235060     0.22099533
 O  2.14277566    -2.36914798     0.07808874
 O  0.32141522    -3.49488897     0.01153554
 N  0.99277137     2.41362987     0.02534100
 N  0.94499004    -2.43806936     0.03325731
 C -1.23634412     1.23940640    -0.04582089
 C -1.82887154     0.01286106    -0.06416842
 C  0.17694584     1.18944952    -0.00223263
 C -1.23854791    -1.23805670    -0.04123603
 C  0.16981913    -1.20429196     0.00257394
 C  0.86258691    -0.00339792     0.01666384
 C -2.09441793     2.47226048    -0.09008623
 H  1.94157140    -0.00827282     0.04292642
 H -3.13400231     2.17684245    -0.21126393
 H -1.98152998     3.04934723     0.82556921
 H -1.79934929     3.12129282    -0.91252485
 H -1.38793482    -3.10084127    -0.04291605
```

mPA-rad-2

```
19
Stoichiometry = C7H5N2O5
 O -1.89128904    -0.35564134     0.08972210
 O -0.80246133     2.89421206     0.98646615
 O -1.63025821     2.29939528    -0.91012143
 O  0.58380627    -3.63938323    -0.05952268
 O -1.41725034    -2.88511995     0.05390193
 N -0.89398666     2.15709391     0.03222708
 N -0.20155526    -2.73045266    -0.01049419
 C  1.37962398     1.22988122    -0.03692015
 C  0.01397904     0.99700846     0.00528999
```

```
 C  2.15165000     0.08592863    -0.09073460
 C -0.57061699    -0.27543463     0.01506603
 C  0.31012783    -1.36919890    -0.02714320
 C  1.69472911    -1.19202220    -0.08745916
 C  1.97263479     2.60775032    -0.02861995
 H  2.34010308    -2.05934158    -0.12597660
 H  1.43062409     3.27281307    -0.70195473
 H  1.90780931     3.03240094     0.97388081
 H  3.01623435     2.56378683    -0.33143685
 H -2.13403768    -1.30309360     0.10063971
```

mPA-rad-3

```
19
Stoichiometry = C7H5N2O5
 O  1.87842695    -2.46244283     0.12202727
 O -1.38957242    -2.49172086     0.97308742
 O -0.85424240    -2.79644369    -1.09060014
 O  0.57324909     3.59123682    -0.36279336
 O -1.32238257     2.92307940     0.38822524
 N -0.80638215    -2.20275382    -0.04276770
 N -0.19144980     2.72896991     0.00517942
 C -0.56838373     0.25539972    -0.03422614
 C  0.04004590    -0.99365443    -0.00003452
 C  0.30803559     1.34524683     0.00887969
 C  1.41440237    -1.20547135     0.07556187
 C  2.18223883    -0.06500592     0.10537033
 C  1.69276007     1.20164731     0.06557697
 C -2.06440856     0.35661339    -0.15123414
 H  2.32224296     2.08081675     0.08056131
 H -2.48915618    -0.58439404    -0.49206601
 H -2.50171245     0.60934673     0.81343405
 H -2.34517210     1.14120097    -0.84823786
 H  2.84091471    -2.45955541     0.17904048
```

dmPA-rad-1

```
22
Stoichiometry = C8H7N2O5
 O -2.12059694    -2.35825003     0.06436924
 O  1.54091845     2.64938288     0.80111118
 O  0.35849459     3.23667555    -0.89567925
 O  1.87032638    -2.51322393     0.42036276
 O  0.14943521    -3.48171968    -0.40144477
 N  0.69503493     2.45142024    -0.03905622
 N  0.74665223    -2.48471622    -0.00660903
 C  0.74987952    -0.00469233    -0.08459841
 C -1.40190338     1.19472572     0.11507487
 C -0.00255982     1.15465383    -0.00684432
 C -1.99592534    -0.02632060     0.13881911
 C  0.02979898    -1.21464452    -0.03287871
 C -1.37812002    -1.25713867     0.04576236
 C  2.23873553     0.05932762    -0.30743212
 C -2.19271133     2.46736873     0.22072905
 H  2.77458592    -0.04957695     0.63449476
 H  2.56632621    -0.74021853    -0.96683612
 H  2.51663794     1.01201695    -0.75055991
 H -3.20215142     2.24577444     0.55922254
 H -1.72409224     3.16108505     0.92003790
 H -2.23830835     2.96148175    -0.74963760
 H -1.54427811    -3.11701451    -0.14633143
```

dmPA-rad-2

22
Stoichiometry = C8H7N2O5

O	-2.07089657	0.12520094	0.11827103
O	-0.51927234	3.21798954	0.90450981
O	-0.22976955	-3.50283803	-0.10022193
O	-1.47710876	2.66965965	-0.94327026
O	-2.02293410	-2.39467035	0.22974998
N	-0.74154668	2.46058934	-0.01285247
N	-0.80812803	-2.45836250	0.04980856
C	1.36453664	-1.25475514	-0.03918319
C	1.37742172	1.21678803	-0.04780353
C	1.96226652	-0.02816166	-0.06563362
C	-0.00631590	1.18540357	-0.00681565
C	-0.04750402	-1.21934547	0.01781061
C	-0.75430639	0.00544527	0.03749339
C	2.23751493	-2.48063378	-0.05626567
C	2.17285307	2.48789976	-0.07177793
H	2.03775216	-3.12095787	0.80161415
H	2.05836529	-3.07702596	-0.94935393
H	3.27803985	-2.16190795	-0.03636086
H	2.17350139	2.94207546	0.91971754
H	3.19740709	2.27815386	-0.37041373
H	1.73660096	3.21097668	-0.76206303
H	-2.44679324	-0.77700241	0.19819369

dmPA-rad-3

22
Stoichiometry = C8H7N2O5

O	2.02623901	-2.39956085	0.06887361
O	-0.43023581	3.30815405	0.69221252
O	-1.61827210	2.54296046	-0.92635131
O	-0.59761493	-3.15224338	1.04657152
O	-1.36033473	-2.76538436	-0.92924237
N	-0.75039247	2.44207344	-0.09025419
N	-0.71138349	-2.48312323	0.05002861
C	1.38286084	1.23176206	0.01489046
C	-0.74658783	-0.01679224	-0.02474129
C	-0.01520390	1.17037109	-0.02623034
C	-0.00524582	-1.18983258	0.02831265
C	1.99562429	0.01116156	0.04296375
C	1.38663564	-1.21914395	0.05787700
C	2.18375207	2.50477056	-0.00096762
C	-2.25048274	-0.05776962	-0.02638407
H	2.14327151	2.98666336	0.97505652
H	3.21950812	2.27991374	-0.24667554
H	1.78914949	3.21091144	-0.73100412
H	-2.61111772	-0.95860708	0.46635687
H	-2.66570249	0.80689823	0.48578016
H	-2.62563447	-0.05333417	-1.04943989
H	2.97879855	-2.25534218	0.08752461

NO_2

3
Stoichiometry = NO_2

O	-1.08970954	0.00000000	0.13602581
O	1.08970954	0.00000000	0.13602581
N	0.00000000	0.00000000	-0.31552988

PA-ket-TS1

```
19
Stoichiometry = C6H3N3O7
 C  0.59835534    -1.60845170    -0.08798796
 C -0.78623540    -1.56428466     0.05814806
 C -1.30964709    -0.30146407     0.22617342
 C -0.33262663     0.65390127     0.32675354
 C  0.73432797     1.07568296    -0.37350895
 C  1.22794085    -0.38599837    -0.07282209
 H  1.17105502    -2.52517539    -0.11032122
 N -1.63247238    -2.74018352    -0.05093698
 H -2.36108980    -0.04766681     0.18404184
 N  2.68440771    -0.37649604     0.22255260
 O  1.35573515     1.99472112    -0.82195787
 H  0.09920786     3.39549782    -0.51768169
 N -1.55207281     2.78589462     0.09060224
 O -0.75769416     3.81207495    -0.28427508
 O -2.62970063     3.12116256     0.38324400
 O  3.10256413     0.53683459     0.88092892
 O  3.31440042    -1.30832369    -0.21005349
 O -2.82326906    -2.57305344     0.07559199
 O -1.07614166    -3.79349953    -0.25322997
```

PA-ket

```
15
Stoichiometry = C6H2N2O5
 O  2.89385995    -2.13625555     0.01129872
 O -2.09254821    -2.24212510    -0.05711687
 O -0.06526888    -2.98453917    -0.03662374
 O  0.59136633     3.61255531     0.04256418
 O -1.51790486     3.17346865    -0.00249021
 N -0.89746436    -2.08974423    -0.03911075
 N -0.35103910     2.85242444     0.01657160
 C  1.03790845    -0.49642267     0.00391257
 C -0.37486399    -0.75723331    -0.01836439
 C  2.01551101    -1.42363773     0.00689143
 C -0.06065609     1.43576635     0.00729779
 C  1.20694611     0.92126439     0.02010718
 C -1.05674559     0.41757669    -0.01693196
 H  2.13054492     1.47404115     0.03834943
 H -2.12435977     0.55641819    -0.03025090
```

PA-aci-TS2

```
19
Stoichiometry = C6H3N3O7
 C  0.66354605     1.45865877     0.16594478
 C -0.78196039     1.43557950     0.14146643
 C -1.44368458     0.26926290     0.06147039
 C -0.71232738    -0.96874962     0.01557580
 C  0.77411662    -0.98370788    -0.10082192
 C  1.39245551     0.33521725     0.07191328
 H  1.16178317     2.41511333     0.25753339
 N -1.51722859     2.69747473     0.23471167
 H -2.52195760     0.21776737     0.06668542
 N  2.85315418     0.43282325     0.16240589
 O  1.43453978    -1.96463569    -0.38342237
 H -0.69527656    -3.72825551    -0.58049727
 N -1.42984284    -2.08861653     0.01109152
 O -0.74602402    -3.25708491     0.26429528
```

```
 O -2.63584328    -2.18735849    -0.10453799
 O  3.41031346    -0.40033973     0.82816234
 O  3.37344552     1.36481627    -0.40704368
 O -2.72290116     2.64059719     0.20311354
 O -0.85698937     3.70497096     0.33667673
```

Aci-PA-2

```
19
Stoichiometry = C6H3N3O7
 O -0.43701357    -2.50016519    -0.26725972
 O  3.38049131    -1.01770441     0.02864304
 O -3.51386168    -0.19322417    -0.60197863
 O  2.09289856    -2.77030414    -0.03538489
 O -2.89784586    -1.73847731     0.76707406
 O  1.56454848     3.38327963     0.06037527
 O -0.56888383     3.65419587     0.05553268
 N  2.24462056    -1.43587714    -0.01161507
 N -2.68905132    -0.79856509     0.04467325
 N  0.42886067     2.97100350     0.04433833
 C  1.12059527    -0.69706334    -0.02557615
 C -1.30321776    -0.31304327    -0.01927820
 C -0.22778320    -1.32553339    -0.10362671
 C  0.23360071     1.51675139     0.00819329
 C  1.31249417     0.71320685     0.01149915
 C -1.10437615     1.01153404    -0.00894011
 H  2.31070228     1.12749289     0.04093705
 H -1.94036036     1.69886719    -0.00402788
 H  3.01215359    -3.09179275     0.00053910
```

PA-ket-TS2

```
19
Stoichiometry = C6H3N3O7
 C -0.01475011    -1.68393344    -0.05223770
 C -1.26040178    -1.05874747     0.00998380
 C -1.22852658     0.31511454     0.08575917
 C  0.03644602     0.82417934     0.18504078
 C  1.24378915     0.67488608    -0.42376660
 C  1.06979710    -0.85122402    -0.05967996
 H  0.11252862    -2.75632021    -0.01758611
 N -2.51232582    -1.78349851    -0.06971153
 H -2.10032651     0.95178443     0.01114101
 N  2.39074061    -1.45559069     0.23631859
 O  2.21851271     1.18554098    -0.86910085
 H  0.04479424     4.88006879     0.15381731
 N -0.51462783     3.09600460     0.03579460
 O  0.46476073     3.99815344     0.07535532
 O -1.60488890     3.52238132     0.10181572
 O  3.15853798    -0.80558549     0.89315992
 O  2.56789704    -2.57323122    -0.18425163
 O -2.44330996    -2.98579732    -0.18109982
 O -3.53327989    -1.13418269    -0.01281968
```

Aci-PA-3

```
19
Stoichiometry = C6H3N3O7
 C -0.89553009     1.03576271    -0.08757895
 C -1.24242165    -0.41016844    -0.03093978
 C -0.26540154    -1.44196165    -0.00437965
 C  1.03621325    -1.09506479    -0.01483058
```

```
 C  1.47531687     0.26475801    -0.03225914
 C  0.56546607     1.24901468    -0.02826945
 O -1.70204409     1.92138539    -0.21435734
 N -2.54597202    -0.73661651    -0.02926551
 O -3.49810021    -0.01080620    -0.04821697
 O -2.80329005    -2.08253748     0.00104215
 H -3.77563708    -2.11440747    -0.00001026
 H -0.54763562    -2.48389581     0.02149986
 N  2.05044900    -2.15529326     0.00808965
 H  2.53416013     0.48868871    -0.03984531
 N  1.05381415     2.63352095     0.03244168
 O  1.66347909    -3.30078871     0.02084458
 O  3.20721009    -1.80395010     0.01246490
 O  0.45687622     3.38458945     0.75913300
 O  2.03675207     2.89820088    -0.62285312
```

PA-ket-TS3

```
19
Stoichiometry = C6H3N3O7
 C  0.44375946     1.14479081     0.24400899
 C -0.82879970     0.57327237     0.13058929
 C -1.51166154    -0.56231806     0.08973227
 C -0.63827416    -1.65060130    -0.01292403
 C  0.72825648    -1.41740071    -0.02484624
 C  1.19920464    -0.13016025     0.04623064
 O  0.88219797     2.25477214     0.42927008
 N -2.04565043     2.66247625    -0.29956531
 O -1.56464734     3.42737914    -1.03559390
 O -1.68397665     2.82742347     1.00502109
 H -0.92873413     3.45660922     1.01507822
 H -2.58792539    -0.66503593     0.14513567
 N -1.19751166    -2.99018020    -0.07632232
 H  1.42973219    -2.23582492    -0.10040172
 N  2.66640902     0.05065014    -0.08362538
 O  3.05877587     1.02244793    -0.66702888
 O  3.34636347    -0.83242321     0.38560772
 O -0.41328694    -3.90576338    -0.15339056
 O -2.40426035    -3.08902682    -0.04888817
```

mPA-ket-TS1

```
22
Stoichiometry = C7H5N3O7
 C  0.40074538    -1.51161537    -0.03371043
 C -0.99539829    -1.31079109     0.07785986
 C -1.40200736    -0.00602621     0.21452668
 C -0.35626207     0.87071094     0.31731046
 C  0.75592201     1.16652268    -0.37197995
 C  1.10662172    -0.32165664    -0.05373899
 C  1.06812248    -2.85320174     0.01331449
 H  0.98714162    -3.32953821    -0.96415796
 H  0.56317789    -3.49885789     0.72673826
 H  2.12008944    -2.76960096     0.26538292
 N -2.00102297    -2.35363772    -0.06136477
 H -2.42740665     0.33110185     0.13869375
 N  2.56512278    -0.33982315     0.22746081
 O  1.49240747     2.01822618    -0.79074552
 H  0.36408882     3.50293881    -0.51283621
 N -1.35591173     3.07237525     0.06428376
 O -0.45095653     4.00668438    -0.29635049
 O -2.39720518     3.51911224     0.33878244
```

```
 O  2.92658867     0.20863881     1.23470585
 O  3.25661444    -0.90064870    -0.58327478
 O -3.14741294    -2.04280871     0.16717268
 O -1.62502604    -3.45244624    -0.40136257
```

mPA-ket

```
22
Stoichiometry = C7H5N3O7
 O  3.14840552    -2.16282935    -0.08139976
 O -1.79597656    -2.44655653    -0.07167242
 O  0.27015918    -3.04967432    -0.09097437
 O  0.87444658     3.50115169     0.04359917
 O -1.24838397     3.15554972     0.04986405
 N -0.61366269    -2.20355795    -0.06973516
 N -0.09700911     2.77754836     0.03483000
 C -0.87339037     0.32716836    -0.01409763
 C -0.16274282    -0.84579022    -0.04125721
 C  0.14131890     1.35110571     0.00392046
 C  2.24377900    -1.48204778    -0.06344119
 C  1.25000924    -0.57320294    -0.04035772
 C  1.40968147     0.83915020    -0.01122511
 C -2.34973494     0.53126884    -0.00597155
 H  2.32931048     1.39940681    -0.00261117
 H -2.87123249    -0.41778154    -0.02516713
 H -2.63878520     1.09807060     0.87871431
 H -2.64308353     1.13558804    -0.86402723
```

mPA-aci-TS2

```
22
Stoichiometry = C7H5N3O7
 C  0.62874861     1.19915952     0.08033934
 C -0.82517030     1.19649171     0.03530791
 C -1.56491069     0.07476539    -0.00274336
 C -0.92655701    -1.19769447    -0.02831566
 C  0.54505239    -1.31371989    -0.12851285
 C  1.21012778    -0.01316477     0.01782481
 C  1.43949387     2.45004631     0.24684052
 N -1.57217902     2.46460153     0.00823845
 H -2.64387785     0.13065212     0.00627357
 N  2.67715146    -0.12033835     0.06772381
 O  1.16605755    -2.32519210    -0.36362777
 H -1.02843493    -3.94994145    -0.60715380
 N -1.72193156    -2.27661114    -0.04918316
 O -1.11676469    -3.47132130     0.23395745
 O -2.91522923    -2.29106253    -0.20103625
 O  3.15284190    -0.49853192     1.10843853
 O  3.28130722     0.18362966    -0.93128073
 O -2.69357127     2.46272794     0.45737543
 O -1.02040477     3.41685548    -0.49405704
 H  2.44947927     2.21230597     0.56941391
 H  0.97925849     3.10999338     0.97891544
 H  1.48607096     2.99521136    -0.69427798
```

Aci-mPA-2

```
22
Stoichiometry = C7H5N3O7
 O -1.26293450    -2.31922225     0.14489625
 O -3.29179049     0.12116850     1.00474437
 O -3.20629558    -0.26916160    -1.11230818
```

```
 O  2.72275594     2.40151092    -0.43350175
 O  1.07635639     3.39477186     0.52304858
 O  2.86411899    -2.31800124     0.04835506
 O  1.03069348    -3.49270211     0.11578507
 N -2.70847740    -0.05105857    -0.03653482
 N  1.60163665     2.42983384     0.01644233
 N  1.65240668    -2.30115565     0.06690161
 C -0.63228834     1.22062218    -0.03419638
 C -1.23861244     0.01999374     0.00653262
 C  0.82135570     1.18310086    -0.01986218
 C -0.60809908    -1.30599257     0.07442993
 C  0.86659109    -1.21437316     0.04154958
 C  1.53340753     0.04271552    -0.00631278
 C -1.41853346     2.49338503    -0.14524152
 H  2.61343627     0.07496705    -0.01923890
 H -2.44498461     2.28691263    -0.43883717
 H -1.41831437     3.01911245     0.80867280
 H -0.96795450     3.15962112    -0.87862056
 H  1.77424674    -4.12254019     0.12022660
```

mPA-ket-TS2

```
22
Stoichiometry = C7H5N3O7
 C  0.03482887    -1.51345897    -0.02162179
 C -1.23946825    -0.89511738     0.04723990
 C -1.24604477     0.47627536     0.10020150
 C -0.00347982     1.04177379     0.16564837
 C  1.19074348     0.91716241    -0.46368645
 C  1.06542691    -0.60809950    -0.09129887
 C  0.26330090    -2.99229214     0.09726700
 N -2.50915401    -1.59430041    -0.03170383
 H -2.14437855     1.07594401     0.02955859
 N  2.45478596    -1.07642640     0.13002603
 O  2.16842705     1.43904836    -0.89770922
 H -0.08468171     5.04129932     0.18219601
 N -0.62273427     3.25245598     0.04637940
 O  0.34268156     4.17040151     0.04553912
 O -1.71254772     3.65478491     0.20194819
 O  3.00355568    -0.68874361     1.12839889
 O  2.91435736    -1.81023760    -0.70819452
 O -2.48508686    -2.78046820    -0.27570492
 O -3.51400542    -0.94057587     0.14595747
 H  1.29943888    -3.21829741     0.32897128
 H  0.00656351    -3.47769358    -0.84436966
 H -0.38746107    -3.41131371     0.86094329
```

Aci-mPA-3

```
22
Stoichiometry = C7H5N3O7
 C  1.25093711     0.74662380     0.05060050
 C -0.01533504     1.50524328     0.04358097
 C -1.27738106     0.85216833     0.00085516
 C -1.33214125    -0.49293672    -0.02663243
 C -0.15628083    -1.34656959    -0.05904733
 C  1.02501643    -0.70178597    -0.02435539
 O  2.35827187     1.22746127     0.10626357
 N  0.04761136     2.84323930     0.09105069
 O  1.01905639     3.54485025     0.13257377
 O -1.16726580     3.47877636     0.09076779
 H -0.91563435     4.41798256     0.12403420
```

```
 H -2.19496892     1.42028740    -0.00003835
 N -2.68198857    -1.07704809     0.01384362
 C -0.22897643    -2.84066845    -0.17841921
 N  2.27670908    -1.47429944    -0.08204852
 O -3.59468948    -0.40762818    -0.41182974
 O -2.79394178    -2.17940940     0.49921227
 O  2.79005046    -1.59028901    -1.16653443
 O  2.68058967    -1.93127975     0.95824834
 H -0.97709256    -3.13076246    -0.91408200
 H -0.52868060    -3.27883185     0.77260354
 H  0.73423613    -3.24971366    -0.47370032
```

mPA-ket-TS3

```
22
Stoichiometry = C7H5N3O7
 C  0.48711974     1.30647733    -0.27366202
 C -0.61613268     0.77186974     0.30586100
 C -1.40935089    -0.32509353     0.20038458
 C -0.71085642    -1.50210249     0.05040457
 C  0.69553165    -1.39144843    -0.06441457
 C  1.14426463    -0.09057697    -0.06443984
 O  1.04838495     2.30470224    -0.61185191
 N -1.92959016     2.71069635     0.10283437
 O -2.35195779     3.22675756    -0.85821647
 O -1.53240529     3.53931717     1.07803502
 H -1.65013741     4.45278278     0.74578428
 H -2.48727719    -0.25815433     0.15713051
 N -1.46389840    -2.73649780    -0.08423304
 C  1.63576919    -2.56231005    -0.06867906
 N  2.59567821     0.16987539     0.11428736
 O  2.93231957     0.66620484     1.15673952
 O  3.31079450    -0.14606751    -0.80212791
 O -0.85739810    -3.73515340    -0.40239170
 O -2.65608575    -2.68319599     0.12665357
 H  2.65579369    -2.25736395     0.14231184
 H  1.61399502    -3.04393465    -1.04593692
 H  1.31396945    -3.30244569     0.65931909
```

dmPA-ket-TS1

```
25
Stoichiometry = C8H7N3O7
 C  0.55174960    -1.54276931    -0.01466594
 C -0.84722238    -1.38593947     0.07804345
 C -1.33565106    -0.08882070     0.17063825
 C -0.30639017     0.80932579     0.25709379
 C  0.86171851     1.10304914    -0.34442609
 C  1.25033037    -0.35093900    -0.06019732
 C  1.24986834    -2.86880820     0.08142221
 N -1.76456701    -2.50460125    -0.06045526
 C -2.75865960     0.37875733     0.06618809
 N  2.70671051    -0.36706491     0.22928896
 O  1.60192248     1.98884334    -0.70462913
 H  0.70093506     3.48890892    -0.43133921
 N -1.08445143     3.23716387    -0.02536954
 O -0.06263075     4.08129606    -0.22943380
 O -2.09647998     3.78061867     0.19945277
 O  3.07117887     0.20744997     1.22033759
 O  3.39465740    -0.96500835    -0.55827028
 O -2.86403672    -2.38497847     0.43518783
 O -1.37384835    -3.47684741    -0.66637991
```

```
 H  2.22432775    -2.76765170     0.55131039
 H  1.39810216    -3.27733994    -0.91812211
 H  0.64833097    -3.57675344     0.64316327
 H -3.27160139    -0.16249208    -0.72574601
 H -2.80381304     1.44827090    -0.11389531
 H -3.26847350     0.14962402     1.00131404
```

dmPA-ket

```
25
Stoichiometry = C8H7N3O7
 O  3.31609335    -1.54714843    -0.09699958
 O -0.08690180     3.56139053     0.03306725
 O -2.07513672     2.75020633    -0.02754704
 O  0.66842475    -2.99333050    -0.02196539
 O -1.47643297    -2.81383615     0.01689912
 N -0.86892627     2.63194783     0.00177173
 N -0.36628311    -2.33803741    -0.00279860
 C  1.03906509     1.05138456    -0.03736587
 C -1.11265980     0.09279701     0.01758301
 C -0.31924690     1.29955048    -0.00378966
 C -0.19273545    -0.92084483    -0.00731562
 C  1.13674204    -0.37418029    -0.04077386
 C  2.28955991    -1.06644304    -0.07146158
 C  2.19853296     1.98579732    -0.06665158
 C -2.59921283    -0.00383145     0.06513380
 H  2.19290111     2.62848054     0.81341266
 H  3.13929180     1.43613428    -0.10349249
 H  2.13655011     2.64640341    -0.93126351
 H -2.91459739    -1.03808010     0.13636722
 H -2.98029034     0.56624365     0.91213350
 H -3.02810613     0.45388043    -0.82703792
```

dmPA-aci-TS2

```
25
Stoichiometry = C8H7N3O7
 C  1.40395656     0.22330375     0.01271935
 C  0.41068485     1.27382613    -0.00517545
 C -0.92985679     1.11139030    -0.01575959
 C -1.39953295    -0.25964747     0.00465337
 C -0.46855704    -1.41783072    -0.08778765
 C  0.93837932    -1.03550024    -0.00402762
 C  2.86169997     0.56657882     0.04361465
 N  0.94696009     2.64614292     0.04111029
 C -1.87256332     2.27632381     0.08436939
 N  1.86435310    -2.17799867    -0.01049947
 O -0.79855207    -2.56105003    -0.31549322
 H -3.38717682    -2.25577999    -0.28259886
 N -2.71501900    -0.50721240    -0.00518200
 O -3.09040316    -1.73279531     0.48063259
 O -3.60964751     0.24130879    -0.31394998
 O  1.94853988    -2.80366156     1.01523060
 O  2.46376655    -2.39668330    -1.03601151
 O  0.78155015     3.34025107    -0.93295390
 O  1.52290783     2.97154451     1.05271049
 H  3.47795492    -0.30520731    -0.15288132
 H  3.11855989     0.98515111     1.01675414
 H  3.08510604     1.32560703    -0.70797058
 H -2.63144582     2.08261994     0.84085224
 H -2.39337516     2.43365299    -0.85887865
 H -1.34219886     3.18667451     0.34636730
```

Aci-dmPA-2

```
25
Stoichiometry = C8H7N3O7
 O -1.21951186    -2.40202195    -0.37603969
 O  1.79256219     2.89694838     0.97317671
 O  0.86364946     3.25853551    -0.93345445
 O -3.31433813    -0.72522890     1.02794557
 O  2.80770607    -2.25879864     0.29386629
 O -3.47359789     0.05370901    -0.97421188
 O  1.02446976    -3.44692768    -0.05997933
 N  1.13000537     2.56433357     0.01966062
 N -2.85431399    -0.27799887     0.00787521
 N  1.61383160    -2.23667507     0.05482315
 C  1.43364931     0.15740028    -0.05261034
 C -0.86594625     1.12402358     0.05168371
 C  0.57763591     1.19814843     0.01638856
 C -1.39504972    -0.10425599    -0.03204033
 C  0.82679051    -1.16513501    -0.08130018
 C -0.64841639    -1.35404544    -0.18951416
 C  2.91595125     0.37219935    -0.18863197
 C -1.68801918     2.36916902     0.18755252
 H  3.42867402     0.15325855     0.74656068
 H  3.32596569    -0.29315158    -0.94473998
 H  3.13124344     1.39892239    -0.46893060
 H -2.70351420     2.14048977     0.49901139
 H -1.23791761     3.04229176     0.91792936
 H -1.72212703     2.89292059    -0.76782706
 H  1.76065226    -4.04928590     0.14951818
```

dmPA-ket-TS2

```
25
Stoichiometry = C8H7N3O7
 C -0.13217145    -1.53470320     0.02871854
 C -1.35770887    -0.83322525     0.03481762
 C -1.31053993     0.55937859     0.03043873
 C -0.02956465     1.00592888     0.12155757
 C  1.22574164     0.74009476    -0.34226485
 C  0.98912358    -0.73940989    -0.03020154
 C -0.02708242    -3.02476185     0.20360397
 N -2.63466586    -1.51079509    -0.07794207
 C -2.45340145     1.51815850    -0.16759783
 N  2.31208766    -1.34927359     0.25121237
 O  2.26910902     1.24159112    -0.65870324
 H  1.90554015     4.16217753     0.30845136
 N  0.31443776     3.32090743    -0.21803963
 O  1.18174765     3.66485542     0.74204083
 O  0.53877891     3.75768505    -1.28077838
 O  2.87523561    -0.99574473     1.25305732
 O  2.70226160    -2.16172370    -0.54916037
 O -2.64814418    -2.60343417    -0.60071283
 O -3.61271405    -0.93713064     0.35522504
 H  0.90943977    -3.29800163     0.68163276
 H -0.06946376    -3.51392274    -0.76859485
 H -0.85660955    -3.39771657     0.79668079
 H -3.13052746     1.13652823    -0.92736096
 H -2.08126298     2.49547650    -0.45544456
 H -3.01463306     1.59675881     0.76191256
```

Aci-dmPA-3

```
25
Stoichiometry = C8H7N3O7
 C -1.51796862     0.24137411     0.23079697
 C -0.89185272    -1.10382040     0.12857241
 C  0.54537406    -1.28672173     0.05150925
 C  1.27202847    -0.15369429    -0.07208651
 C  0.76118560     1.19794861    -0.11649484
 C -0.56507472     1.33136003     0.02165444
 O -2.69201235     0.45247804     0.42312316
 N -1.76333270    -2.11524140     0.02294553
 O -2.95546553    -2.09143923     0.18470274
 O -1.24835918    -3.32265619    -0.38040894
 H -2.03893245    -3.89030621    -0.37557454
 C  1.22271601    -2.62123838     0.23021349
 N  2.74049501    -0.26776834    -0.11216111
 C  1.68444262     2.36204394    -0.31474435
 N -1.17598190     2.66798181    -0.01335597
 O  3.22911066    -0.86597247    -1.04121387
 O  3.35136305     0.25752657     0.78917586
 O -1.72284495     2.98263273    -1.04024335
 O -1.06886533     3.34435681     0.98046772
 H  2.44046229     2.12547207    -1.06373936
 H  2.20124401     2.58707400     0.61794813
 H  1.13780952     3.24446430    -0.63692280
 H  2.25133599    -2.48686936     0.55133583
 H  1.22814185    -3.18632561    -0.70004663
 H  0.70327190    -3.21144085     0.98006235
```

dmPA-ket-TS3

```
25
Stoichiometry = C8H7N3O7
 C  0.54280856     1.33280031     0.14832020
 C -0.59522798     0.73564223    -0.31037808
 C -1.33550634    -0.39461775    -0.16308340
 C -0.51806405    -1.51778441    -0.05047127
 C  0.87896758    -1.31534388    -0.00408318
 C  1.27499267     0.00179385    -0.02920375
 O  1.04746678     2.39311680     0.39694327
 N -1.75229306     2.80082609    -0.19030699
 O -1.47542127     3.69908739    -0.88137933
 O -1.81242832     3.08239141     1.12747665
 H -1.51258735     4.00816643     1.23554429
 C -2.83305231    -0.32918924    -0.02846509
 N -1.11453841    -2.82594110     0.13992653
 C  1.88326477    -2.43382721    -0.05392365
 N  2.70587628     0.31174778    -0.27208291
 O  3.47395060    -0.01655838     0.59704706
 O  2.98013917     0.84760216    -1.31285558
 O -0.47476118    -3.65307862     0.75150086
 O -2.22210985    -3.00895591    -0.32204298
 H  2.80927547    -2.10854699    -0.51962013
 H  1.48340415    -3.28054290    -0.60348656
 H  2.10952524    -2.77211470     0.95633943
 H -3.15067528     0.69071014     0.15973921
 H -3.16063212    -0.97799036     0.77987155
 H -3.28827588    -0.69429221    -0.94737033
```

Cis-HONO

```
4
Stoichiometry = HNO2
```

```
 O -0.09979395     1.11096150     0.07877649
 N  0.50266286    -0.08284017    -0.16252886
 H -0.97821094     0.90614668     0.45587430
 O -0.15556287    -1.00654457     0.13278200
```

Trans-HONO

```
4
Stoichiometry = HNO2
 N -0.47296133     0.18692835    -0.01924289
 O  0.21607556     1.11971157     0.02564280
 O  0.27408145    -0.98365968    -0.02024937
 H -0.39322981    -1.68227788    -0.06031686
```

mPA-aci-TS4

```
22
Stoichiometry = C7H5N3O7
 C  0.99254497    -1.07261198    -0.02708099
 C -0.38760942    -1.31677707    -0.12187996
 C -1.23737038    -0.17221927    -0.16092403
 C -0.73322126     1.17979750    -0.26839902
 C  0.66660059     1.30159183     0.01779093
 C  1.49259305     0.22541702     0.08141527
 N -2.59835057    -0.35963583     0.16493646
 O -3.37004523     0.66866109     0.22796947
 C -1.59523226     2.23210454    -0.58907764
 N  1.30775863     2.61351373     0.14862013
 O  0.63264646     3.52571330     0.57003759
 N  1.93525968    -2.15852138    -0.00742441
 O  3.10720845    -1.91229957     0.09643228
 O -3.04942645    -1.42355754     0.47131796
 O  2.47958327     2.69443234    -0.14097327
 O  1.49473424    -3.31012403    -0.09865883
 H  2.55812836     0.37345590     0.18829691
 O -0.88357214    -2.52160095    -0.17951916
 H -1.25367525     3.24578787    -0.48216046
 H -2.28327099     2.05123756    -1.41130104
 H -2.66667482     1.62207332     0.11079060
 H -0.10969247    -3.14654730    -0.16199135
```

Aci-mPA-4

```
22
Stoichiometry = C7H5N3O7
 C  0.49770108     1.29769022    -0.15452795
 C  1.25668841     0.06758213    -0.16337105
 C  0.58268972    -1.21408273    -0.47502025
 C -0.81524689    -1.23157221    -0.03110624
 C -1.51269330    -0.09521815     0.11456684
 C -0.88710397     1.17197155    -0.05527333
 N  2.54966824     0.11829743     0.20120843
 O  3.22653108     1.09162725     0.37806222
 C  1.16844299    -2.17455681    -1.20472836
 N -1.51538830    -2.49380943     0.20754097
 O -2.71712806    -2.45959625     0.33416051
 N -1.71209470     2.33450606    -0.00631050
 O -1.16344259     3.44574882    -0.08387149
 O -0.84130347    -3.49963214     0.28425169
 O -2.90409967     2.20567314     0.10535427
 O  3.20848682    -1.05332774     0.45986930
 H -2.56400795    -0.13017602     0.36119123
```

```
 O  1.11278137     2.44160048    -0.19523045
 H  0.66968830    -3.10874093    -1.40404016
 H  2.15159021    -2.02563262    -1.63138988
 H  2.54647931    -1.77004262     0.43145400
 H  0.39416270     3.13839145    -0.15602516
```

mPA-hyd-anth

```
22
Stoichiometry = C7H5N3O7
 C -1.04152332     1.00034743    -0.15729331
 C -1.12219624    -0.39191512    -0.20587630
 C -0.03312395    -1.21849712    -0.13136907
 C  1.23379252    -0.65799706    -0.01429803
 C  1.38966318     0.70867970     0.01237285
 C  0.26666791     1.52137560    -0.05715671
 N -2.34423820    -1.13294481    -0.27243142
 O -2.82495833    -1.13011143     1.05669125
 C -0.55254542    -2.62060616    -0.18198845
 N  2.41255990    -1.51603191     0.08751819
 O  3.49697861    -0.98726032     0.12287118
 N  0.48046328     2.96264393    -0.01610481
 O -0.51143229     3.68349048    -0.07136199
 O  2.21070322    -2.71092606     0.13446389
 O  1.60319794     3.37862207     0.06913311
 O -1.91601132    -2.43586634    -0.57834479
 H  2.37291929     1.15005706     0.08752826
 O -2.15270892     1.70716317    -0.20547185
 H -0.07203418    -3.23499815    -0.93950434
 H -0.46362509    -3.11094479     0.79076583
 H -3.78208220    -1.17633515     0.94925642
 H -1.90684339     2.65432112    -0.17209044
```

mPA-H_2Oelim-TS

```
22
Stoichiometry = C7H5N3O7
 C -1.09134927    -1.03277377     0.18281491
 C -1.16937680     0.35947183     0.33432937
 C -0.07081961     1.21308804     0.27260515
 C  1.19549561     0.65879648     0.08857407
 C  1.33782649    -0.70390859     0.00619833
 C  0.21936955    -1.53496783     0.05160288
 C -0.67517041     2.52207207     0.23581736
 O -1.96806451     2.30665792     0.79234360
 N -2.33427060     1.10771857     0.39485020
 O -2.20563299     1.56334646    -1.55179701
 N  2.37057171     1.51713140    -0.00529008
 O  3.45357427     0.98866310    -0.08063460
 N  0.44364998    -2.96645407    -0.05514862
 O -0.54521249    -3.69565676    -0.04095275
 O  2.16690125     2.71221282    -0.00606845
 O  1.56966748    -3.37204493    -0.15009010
 H  2.32100021    -1.14066731    -0.09686831
 O -2.19177611    -1.74250212     0.17937945
 H -0.20637212     3.43997302     0.54858966
 H -1.19032447     2.37457986    -0.92785999
 H -3.06231188     2.00390086    -1.58463213
 H -1.93782858    -2.68594974     0.08101251
```

mPA-anth

19
Stoichiometry = C7H3N3O6
 O -1.91907755   -2.11505297   -0.00366086
 O -2.63330498   1.94230397   -0.14234463
 O 2.98660119   1.84714144   -0.04631364
 O 1.33471568   3.22516247   -0.10332312
 O 2.10981093   -2.82231344   0.09043099
 O 0.12611572   -3.63254034   0.07368877
 N -2.70856369   0.59095184   -0.10203949
 N 1.80834024   2.10807527   -0.06846285
 N 0.91618014   -2.68839688   0.06196074
 C -0.54437478   1.28294392   -0.08318549
 C -1.45912491   0.19216429   -0.06678712
 C 0.85327002   1.00768759   -0.05238081
 C -1.01078703   -1.17638404   -0.01717060
 C 0.36391652   -1.35005373   0.01112333
 C 1.29056831   -0.26651970   -0.00709024
 C -1.37234329   2.36592043   -0.13196259
 H 2.34888320   -0.48140686   0.01594642
 H -1.20904108   3.42766815   -0.16067864
 H -1.44749861   -2.97896789   0.02855308

dmPA-aci-TS4

25
Stoichiometry = C8H7N3O7
 C -1.32259906   -0.01487027   -0.12002531
 C -0.74575703   1.21072616   -0.22937665
 C 0.68222325   1.22796081   -0.21859476
 C 1.48887439   0.02862889   -0.28940828
 C 0.78715950   -1.17865859   0.04751662
 C -0.60980765   -1.21952892   0.07605304
 N 1.30764098   2.42368289   0.14055343
 O 2.59402173   2.50048425   0.15213087
 C 2.84753440   0.13554177   -0.61531360
 N 1.49870553   -2.40903098   0.27839958
 O 2.67767007   -2.37850890   0.51329290
 N -2.78905786   -0.14161966   -0.19009840
 O -3.24378826   -0.61390644   -1.20183064
 O 0.68407587   3.38057667   0.53380968
 O 0.85924307   -3.46821745   0.25510507
 O -3.41738188   0.25525250   0.76066935
 O -1.33099214   -2.29548346   0.26484522
 C -1.60551650   2.42623688   -0.42844226
 H 3.50504059   -0.70432107   -0.49703593
 H 3.06394679   0.78179715   -1.46257297
 H 2.97731247   1.38554634   0.04505916
 H -1.10020626   3.16374893   -1.04487527
 H -1.82541160   2.89336701   0.53085682
 H -2.54472539   2.14532700   -0.90108291
 H -0.70289673   -3.06262347   0.29908021

Aci-dmPA-4

25
Stoichiometry = C8H7N3O7
 C -0.62895540   1.28755302   -0.08012547
 C 0.81555412   1.14961520   0.01928961
 C 1.45073722   -0.13424478   -0.35682533
 C 0.64520750   -1.29649926   0.04306302
 C -0.72363431   -1.17474641   0.14020121
 C -1.31707196   0.12853812   -0.06178275
 N 1.51568018   2.15793556   0.53100047

```
 O  1.09887293     3.24907107     0.86108735
 C  2.58463177    -0.18450740    -1.06963917
 N  1.24551448    -2.56815174     0.26660101
 O  0.50655514    -3.52878577     0.53206541
 N -2.78095340     0.13392077    -0.21042970
 O -3.42211493     0.72320382     0.62634585
 O  2.44600994    -2.68086454     0.20553473
 O -3.22279435    -0.44281043    -1.17305160
 O  2.85443985     2.00211136     0.77746506
 O -1.55733781    -2.13950280     0.42777716
 H  3.05394585    -1.11930207    -1.32850903
 H  3.04534147     0.72846783    -1.42594994
 H  3.06336708     1.06023709     0.63579738
 H -1.00524250    -2.95975154     0.54191560
 C -1.30454863     2.61642343    -0.23599959
 H -0.68264965     3.28990245    -0.82063987
 H -1.45131569     3.07793285     0.74093071
 H -2.27518810     2.49909524    -0.71228373
```

dmPA-hyd-anth

```
25
Stoichiometry = C8H7N3O7
 C -1.26075554     0.78200659    -0.13272560
 C -1.18653661    -0.60458005    -0.17805701
 C -0.00978005    -1.30579242    -0.12390074
 C  1.19286876    -0.62074688    -0.01863338
 C  1.20152690     0.78737660     0.02369637
 C -0.04035512     1.42905882    -0.03056935
 N -2.31415921    -1.49631192    -0.22715244
 O -2.74314791    -1.57819629     1.12434345
 C -0.36049959    -2.75961887    -0.18550289
 N  2.42766735    -1.36979834     0.05229042
 O  3.48476593    -0.74875370     0.06435670
 N -0.03657938     2.89995109     0.03289476
 O -0.49037144     3.48471040    -0.92352516
 O  2.35944208    -2.57239499     0.10045201
 O  0.38827229     3.40561267     1.04013928
 O -1.74039900    -2.72947148    -0.56861222
 O  2.29217001     1.53548543     0.08197410
 C -2.56661781     1.51195139    -0.18694225
 H  0.17634067    -3.30843444    -0.95518507
 H -0.21006342    -3.24971327     0.77955329
 H -3.65104029    -1.89652201     1.05167097
 H  3.06818953     0.94026480     0.08521219
 H -3.38405415     0.83365438     0.03843251
 H -2.71121507     1.93049173    -1.18351121
 H -2.58106085     2.34035372     0.52106490
```

dmPA-H_2Oelim-TS

```
25
Stoichiometry = C8H7N3O7
 C -1.31245113    -0.82182728     0.19958349
 C -1.24859548     0.57015059     0.34721331
 C -0.06925837     1.31101032     0.28974828
 C  1.14033814     0.64574712     0.12960062
 C  1.15216219    -0.75938247     0.04779727
 C -0.08855050    -1.43701335     0.07670608
 C -0.54414824     2.67581125     0.20810401
 O -1.85910308     2.60038127     0.74728273
 N -2.32780478     1.42716048     0.38732520
 O -2.12235389     1.83062392    -1.61959802
```

```
 N  2.36284395     1.40424399     0.05319893
 O  3.42601138     0.79040684     0.00582018
 N -0.05032087    -2.90219071    -0.05877637
 O -0.55053573    -3.54070039     0.83862318
 O  2.28289696     2.60578703     0.03524034
 O  0.44668534    -3.34898171    -1.06035133
 O  2.24661001    -1.48419879    -0.02609966
 C -2.62309219    -1.53824417     0.16473736
 H  0.00447497     3.54985997     0.52052729
 H -1.02033952     2.57164514    -0.94883462
 H -2.91590865     2.37197677    -1.69366751
 H  3.01497075    -0.87200225    -0.03046595
 H -2.58936553    -2.39010694    -0.51254212
 H -3.40513361    -0.85187279    -0.15152772
 H -2.86144034    -1.91674643     1.16039979
```

dmPA-anth

```
22
Stoichiometry = C8H5N3O6
 O -2.32202156     0.90958429    -0.06690049
 O  2.51796137    -2.31447186    -0.06147303
 O -0.89504592     3.10863061     1.11526493
 O -1.57559613    -3.10211059    -0.18505526
 O -0.14463695     3.41239962    -0.88178285
 O -3.05074326    -1.53764166    -0.18172901
 N  2.75188707    -0.98066704    -0.01857799
 N -0.39322102     2.73494807     0.08618336
 N -1.88365958    -1.93462884    -0.15422138
 C  0.52334084    -1.39974143    -0.06858231
 C  1.29551722     0.98574220     0.01341684
 C  1.56238195    -0.42702116    -0.02339915
 C -0.01535239     1.31107362     0.01589395
 C -0.83630793    -0.96913309    -0.08180371
 C -1.11778539     0.37938561    -0.03732838
 C  1.21012216    -2.57612132    -0.09150438
 C  2.42415270     1.96168870     0.03791872
 H  0.92020764    -3.61071235    -0.12695100
 H  2.11853946     2.93496500     0.41545927
 H  3.23670122     1.56508898     0.64501041
 H  2.80466699     2.09323076    -0.97767745
 H -2.96702990     0.16679758    -0.11972575
```

H_2O

```
3
Stoichiometry = H2O
 O  0.00000000     0.00000000    -0.24262832
 H -0.76444774     0.00000000     0.33831415
 H  0.76444774     0.00000000     0.33831415
```

References

[1] E. Aprà, E. J. Bylaska, W. A. de Jong, N. Govind, K. Kowalski, T. P. Straatsma, M. Valiev, H. J. J. van Dam, Y. Alexeev, J. Anchell, V. Anisimov, F. W. Aquino, R. Atta-Fynn, J. Autschbach, N. P. Bauman, J. C. Becca, D. E. Bernholdt, K. Bhaskaran-Nair, S. Bogatko, P. Borowski, J. Boschen, J. Brabec, A. Bruner, E. Cauët, Y. Chen, G. N. Chuev, C. J. Cramer, J. Daily, M. J. O. Deegan, T. H. Dunning Jr., M. Dupuis, K. G. Dyall, G. I. Fann, S. A. Fischer, A. Fonari, H. Früchtl, L. Gagliardi, J. Garza, N. Gawande, S. Ghosh, K. Glaesemann, A. W. Götz, J. Hammond, V. Helms, E. D. Hermes, K. Hirao, S. Hirata, M. Jacquelin, L. Jensen, B. G. Johnson, H. Jónsson, R. A. Kendall, M. Klemm, R. Kobayashi, V. Konkov, S. Krishnamoorthy, M. Krishnan, Z. Lin, R. D. Lins, R. J. Littlefield, A. J. Logsdail, K. Lopata, W. Ma, A. V. Marenich, J. Martin del Campo, D. Mejia-Rodriguez, J. E. Moore, J. M. Mullin, T. Nakajima, D. R. Nascimento, J. A. Nichols, P. J. Nichols, J. Nieplocha, A. Otero-de-la-Roza, B. Palmer, A. Panyala, T. Pirojsirikul, B. Peng, R. Peverati, J. Pittner, L. Pollack, R. M. Richard, P. Sadayappan, G. C. Schatz, W. A. Shelton, D. W. Silverstein, D. M. A. Smith, T. A. Soares, D. Song, M. Swart, H. L. Taylor, G. S. Thomas, V. Tipparaju, D. G. Truhlar, K. Tsemekhman, T. Van Voorhis, Á. Vázquez-Mayagoitia, P. Verma, O. Villa, A. Vishnu, K. D. Vogiatzis, D. Wang, J. H. Weare, M. J. Williamson, T. L. Windus, K. Woliński, A. T. Wong, Q. Wu, C. Yang, Q. Yu, M. Zacharias, Z. Zhang, Y. Zhao, and R. J. Harrison, "NWChem: Past, Present, and Future", *J. Chem. Phys.* **152**, 184102 (2020). DOI: 10.1063/5.0004997

[2] M. Själander, M. Jahre, G. Tufte, and N. Reissmann, "EPIC: An Energy-Efficient, High-Performance GPGPU Computing Research Infrastructure", arXiv:cs.DC/1912.05848, (2019).

[3] R. Cohen, Y. Zeiri, E.Wurzberg, and R. Kosloff. "Mechanism of Thermal Unimolecular Decomposition of TNT (2,4,6-Trinitrotoluene): A DFT Study", *J. Phys. Chem. A* 111 (2007), pp. 11074–11083. DOI: 10.1021/jp072121s

Kristine Wiik

Unimolecular Decomposition Reactions of Picric Acid and its Methylated Derivatives — a DFT Study

NTNU
Norwegian University of
Science and Technology